New algebraic relationships between tight binding models

Jake Mathew Arkinstall

MPhys (Hons)

October 2019

Abstract

In this thesis, we present a new perspective on tight binding models. Utilising the rich algebraic toolkit provided by a combination of graph and matrix theory allows us to explore tight binding systems related through polynomial relationships.

By utilising ring operations of weighted digraphs through intermediate König digraph representations, we establish a polynomial algebra over finite and infinite periodic graphs, analogous to polynomial operations on adjacency matrices.

Exploring the microscopic and macroscopic behaviour of polynomials in a graph-theoretic setting, we reveal elegant relationships between the symmetrical, topological, and spectral properties of a parent graph G and its family of child graphs $p(G)$.

Drawing a correspondence between graphs and tight binding models, we investigate deep-rooted connections between different quantum systems, providing a fresh angle from which to view established tight binding models.

Finally, we visit topological chains, demonstrate how their properties relate to more trivial underlying chains through effective "square root" operations, and provide new insights into their spectral characteristics.

Declaration

This thesis describes work carried out between April 2014 and September 2018 in the Condensed Matter Theory group at the Department of Physics, Lancaster University, under the supervision of Professor Henning Schomerus. The following section of this thesis is included in work that has been published:

- Chapter 4 Arkinstall, J., Teimourpour, M. H., Feng, L., El-Ganainy, R., and Schomerus, H.. "Topological tight-binding models from nontrivial square roots". *Physical Review B*, vol. 95, no. 16, p. 165109, 2017

This thesis is my own work and contains nothing which is the outcome of work done in collaboration with others, except as specified in the text. This thesis has not been submitted in substantially the same form for the award of a higher degree elsewhere. This thesis does not exceed 80,000 words.

Jake Mathew Arkinstall, MPhys (Hons)

Physics Department, Lancaster University

United Kingdom

Contents

Acknowledgements

First and foremost, I would like to express my utmost gratitude to my friend and supervisor Professor Henning Schomerus. If patience is a virtue, then Henning is a very virtuous person indeed. Without his words of guidance and motivation, none of this work would have been possible. I couldn't have asked for a better supervisor, mentor, or role model.

I would also like to extend a big thankyou to my present colleagues in the Condensed Matter Theory group, particularly Simon Malzard, Marcin Szyniszewski, Marjan Famili and Ryan Hunt, as well as my past colleagues Charles Poli and Diana Cosma, for their friendship and for their willingness to be sounding boards for my ideas.

I want to thank my family for the significant emotional support they have provided during this project. To my wife Jessica, who has somehow managed to put up with a nervous wreck of a husband over the past few weeks, thank you for your love, patience, and endless supply of caffeine. To my parents, thank you for restoring my mentality towards my work in the times that I lost motivation.

Finally, thanks to all of the open source communities whose hard work has made this research possible. This particularly includes the C++ and Eigen communities, the SWIG community, the Python, MatPlotLib, NumPy and SymPy communities, and last but not least, the GNU/Linux community.

Introduction

> The mathematical basis of Heisenberg's treatment is the *law of multiplication* of quantum-theoretical quantities, which he derived from an ingenious consideration of correspondence arguments. The development of his formalism, which we give here, is based upon the fact this rule of multiplication is none other than the well-known mathematical rule of *matrix multiplication*
>
> (M. Born and P. Jordan [1]
>
> English translation by B. L. van der Waerden [2])

The importance of the historical introduction of matrices into the quantum mechanical toolkit cannot be understated. More than just the introduction of a new language, matrices have changed the way that physicists think about quantum problems for the better part of a century. After Heisenberg's groundbreaking paper "Über quantentheoretische Umdeutung kinematischer und mechanischer Beziehungen"[3] came a flood of discussion from Born, Jordan[1, 4], Dirac [5, 6], Pauli [7] and others, leading to a reformulation of the bleeding edge physics research of the day.

To this day, the language of matrices dominates condensed matter physics. Typically, a physicist who is looking to analyse a quantum system through a tight binding model will first write it down in the form of a graph; they might, for example, represent vacant atomic orbitals as nodes, and represent interactions between them as edges. They will then usually use this graph to write down the system's hamiltonian, courtesy of the graph's adjacency matrix (section 1.2.1). If the quantum system has translational symmetry, they will first reduce it into translation eigenspaces, under the Bloch formalism[8]. This approach is, of course, not unique to atoms and electrons. Rather, a similar approach is found in a variety of applications, from photonic systems (with atoms replaced by

dielectric pillars and with photons as excitations) to Majorana excitations in strongly correlated systems [9].

The matrix representation provides an easy way of exploring measurable quantities of the system. Eigendecomposition, for example, provides a natural way of extracting the set of single-particle excitation wavefunctions and their corresponding energies from the hamiltonian. Symmetries can be identified through commutation relationships under matrix multiplication, revealing spectral and topological characteristics[10].

In this work, we build a framework under which relationships between different quantum systems can be explored, and from which observable behaviour can be derived. Revolving around matrix algebra recast into a graph-theoretic approach, this framework provides a map between any tight binding system $\mathcal{S}$ and a child system $p(\mathcal{S})$, with any polynomial p. It explains how microscopic and macroscopic characteristics from $\mathcal{S}$ are manifested in $p(\mathcal{S})$, how trivial topological properties of $p(\mathcal{S})$ can result from non-trivial topological properties of $\mathcal{S}$, and how the spectral properties of defects in $\mathcal{S}$ can be can be explained by analysis of $p(\mathcal{S})$. We also provide methods for finding a suitable polynomial p which transforms a known $\mathcal{S}$ into a child system $p(\mathcal{S})$ with required microscopic properties, where possible.

To this end, we present the duality between matrices and graphs in chapter 1, utilising König digraphs[11] for exploration of the underlying matrix and vector algebra along the way. This algebra provides a mechanism for applying matrix methods to graphs, under which we place particular focus on polynomial evaluation. In section 1.5 we then demonstrate that that the spectral properties from one "parent" graph can be mapped onto those of a "child" polynomial graph. Having explored the ramifications of these

relationships, we move on to develop an understanding of the microscopic behaviour of graph polynomials in chapter 2, and expand the algebra to graphs with infinite periodicity.

With this graph-theoretical toolkit at hand, we are able to explore the properties of quantum tight-binding models in a new light. In chapter 3, we take a fresh look at some well-known quantum toy models, deriving properties from polynomial relationships with simpler systems, with the primary aim of developing a more concrete understanding of the applications of the new graph algebra in a theoretical condensed matter context. Chapter 4 takes our algebra further, exploring topological chains and the deep ancestral relationship of topological properties with underlying symmetries of child polynomial systems. Starting with the Su-Schrieffer–Heeger (SSH) model of Polyacetylene, we find properties rooted in the trivial monatomic chain. We then look at the Rice-Mele model, identifying a polynomial relationship with the SSH chain, and observe the impact of defects on the structure of the underlying system. Finally, we examine the rich topological properties of the Bowtie chain, relating midgap states to those of underlying systems, substantiating our findings with those of established methods by exploring the topological indices in the context of the concrete model.

Full analysis of the bowtie chain, as well as a photonic realisation of the model, is provided in our seminal published work on topologically nontrivial square root systems[12]. Section 4.3 is based on this work, which was written in collaboration with Mohammad H. Teimourpour, Liang Feng and Ramy El-Ganainy.

Units, notation, and terminology

Units

Although some parts of this thesis describe realisations of the theory contained within, the majority of the content is concerned with quantum systems and their observables as abstract entities. The theory applies to atomic systems, photonic systems, or any other linear system that can be reduced, to some reasonable approximation, to a "ball and stick" model.

We shall thus use natural units throughout.

Notation

In the programming world, "syntactic sugar" refers to syntax which makes code easier to read and write, either by making it more visually appealing, more consistent with human language, or by simply reducing the character count of a command.

The same concept applies to physics and mathematics. Indeed, the use of natural units is a fantastic way to make equations simpler to write, easier to understand, and allows for generalisations. There are other uses of syntactic sugar in this thesis, and to avoid confusion they are listed here.

- Appropriate identity matrices and graphs are implied. When adding a complex number $c \in \mathbb{C}$ to a square matrix $H \in \mathbb{C}^{n \times n}$, a formal expression could be $H + c\mathbf{1}_n$, where $\mathbf{1}_n$ is the identity matrix of dimension n. Given the frequency that we will be manipulating matrices in this manner, we will write this simply as $H + c$, and $\mathbf{1}_n$ is to be implied.

- Graph edges are left unlabelled if their weight is unity, or otherwise provided with

a value in the surrounding text. A symmetric pair of directed edges may be represented with a single line with arrowheads on both sides.

A note on terminology

This work presents a new algebra in the context of graphs, and later applies the key principles to quantum tight binding models. Although these subjects are deeply connected, they don't share common terminology. For example, *bonds* in tight binding models are named *edges* in graph theory, *sites* are called *vertices*, amplitudes become *weights*, and the tight-binding *hamiltonian* is analogous to the *adjacency matrix* of the corresponding graph.

In this thesis, we shall use a consistent terminology. As the first half of this thesis focuses on graphs, graph-theoretical terminology is used throughout, rendering the later sections accessible to readers from a background other than condensed matter. Readers from a condensed matter background should thus be prepared for a tactical avoidance of significant conversation about such concepts as Bloch momenta and energy levels, for example, except when necessary. Instead, we refer to the Bloch formalism through eigenspaces of translation graphs, and refer to energy levels more generally as eigenvalues, by virtue of the time-independent Schrödinger equation.

Glossary

	Description	Defined
adj(graph)	The adjacency matrix of the input graph	section 1.2.1
∇(graph)	The incidence matrix of the input graph	section 1.2.3
δ(graph)	The laplacian matrix of the input graph	section 1.2.4
Coates(matrix)	A graph representation of a matrix	section 1.3.1
graph(matrix)	The coates graph of the input matrix's transpose	section 1.3.1
König(matrix)	A digraph representation of a matrix	section 1.3.2
walk(graph)	A digraph representation of a graph via König(adj(graph))	section 1.3.2
graph $\oplus$ graph	The disjoint union of two graphs	section 1.2.5
graph$^{\oplus N}$	The disjoint union of N clones of the input graph	section 2.6

Chapter 1

Graph-Matrix Duality

Introduction

Graph theory is a mathematical framework which provides an abstract setting in which one can describe plethora of problems, with applications in data science, game theory, computer science and the natural sciences. Although they are an intuitive language in their own right, graphs have a duality with matrices, allowing a wide array of operations to be performed on graphs and matrices which extend beyond their native capabilities.

This thesis has a strong focus on some such operations which are pertinent to condensed matter theory. As such, we begin with a light introduction into the relevant areas of graph theory.

1.1 Basic Definitions

1.1.1 Graphs

A *graph* $G(V, E)$ comprises a set of *vertices* V and a set of *edges* E that connect pairs of vertices. A vertex is said to be of *degree* k if there are k edges that connect to it. As an abstract object, a graph's vertices and edges have a contextual underlying meaning, though it is common for vertices to represent a set of distinct entities and for edges to represent a relationship between them, such as a shared property or the existence of a process for some stateful object to transfer from one such entity to the other.

A *labelling* of a graph assigns a unique index to each vertex $v \in V$, typically $0 \ldots |V|$. In a labelled graph, one can refer to a vertex of label a with the notation $v_a \in V$, and one can refer to an edge $e \in E$ from $v_a \in V$ to $v_b \in V$ with the notation $e = \{a, b\}$.

A *weighted* graph equips its edges with a numerical weight. The meaning of this weight is context-dependent: as an example, edges may represent roads between a collection of cities (represented by vertices) and their weight may represent the average fuel cost or travel time along these roads, such as in the famous "travelling salesman" problem.

A *digraph* (or *directed* graph) is a generalisation of a graph, in which edges are given a direction. Rather than stating that an edge e exists *between* two vertices i and j, we state for clarity that e exists *from i to j*, or name i and j the *head* and *tail*, respectively, of e. The existence of such an edge is free of any implication that an edge e^* exists *from j to i*. It is, however, possible for two edges to connect i and j, in opposite directions. If

the digraph is weighted, the weights of these two edges may differ.

Two labelled graphs G_1, G_2 with the same number of vertices are considered equivalent iff, for every edge $\{a, b\}$ in G_1, there exists an edge $\{a, b\}$ of the same weight in G_2; we shall use $G_1 = G_2$ to describe this equivalence. If there exists some permutation f such that each edge $\{a, b\} \in G_1$ has an equivalent edge $\{f(a), f(b)\} \in G_2$, then G_1 and G_2 are *isomorphic*, which we denote with $G_1 \cong G_2$. If, instead, G_1 and G_2 were unlabelled, they are considered equivalent if any labelling exists that renders them equivalent. In a graphical representation, if two graphs are equivalent then the nodes of one can be rearranged to produce the other, as in

$$\tag{1.1}$$
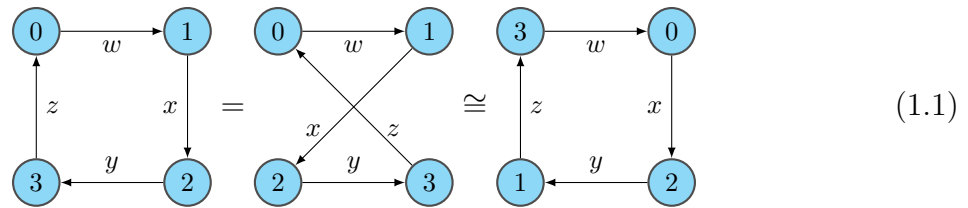
A *walk* from $x \in V$ to $y \in V$ is an alternating sequence of vertices and edges, starting with x and ending with y, such that each edge connects the vertices either side of it. It is said to have *length* l if the number of edges in the sequence is l. A walk's *additive weight* is the sum of the weights of the edges along the walk, and its *multiplicative weight* is the product of the weights of the edges along the walk. The minimum number of edges required to get from a vertex $x \in V$ to another vertex $y \in V$ is called the *distance* $d_G(x, y)$.

We shall introduce a generalised version of distance, which we will call a *distance-set* $\tilde{d}_G(x, y) \subset \mathbb{N}$, comprising all $k \in \mathbb{N}$ for which there exists a walk of length k vertex x to vertex y. By definition, $d_G(x, y) \equiv \min\left(\tilde{d}_G(x, y)\right)$.

A graph is *connected* if, for each pair $x, y \subset V$, $\tilde{d}_G(x, y) \neq \varnothing$. A digraph is *weakly*

connected if it isn't connected but the undirected graph produced by stripping each edge of a direction is connected. Any graph in which there exists a pair of vertices with no path between them is *disconnected*, and can be separated into two or more connected subgraphs.

1.2   Matrix representations of graphs

The dual relationship between graphs and matrices can be exploited both to solve graph-related problems using matrix theory, and to solve matrix-related problems using graph theory. There exist graph transformations that do not have a direct analogue in matrices (such as removing edges to eliminate cycles), and there exist transformations in matrices that do not have a direct analogue in graphs (such as multiplication). Through the duality, it is possible to manipulate matrices in a graph-theoretic manner through their graph representation, and it is possible to manipulate graphs in a matrix-theoretic manner through their matrix representation. This property is of central importance to this thesis.

This section will cover three matrix representations of graphs (the adjacency matrix, the incidence matrix, and the laplacian), and provide a motivating example of describing a graph-theoretic operation (the disjoint union) through the matrix representation. Due to the wide variety of graphs, the definitions of the matrix representations are often inconsistent between different areas of research. For example, directed edges are sometimes represented as negative matrix elements in mixed graphs[13], but sometimes the sign is direction-dependent[14]. The definitions presented in this section will be consistent throughout this thesis.

1.2.1 The adjacency matrix

A graph G of N vertices can be represented as a matrix through its $N \times N$ *adjacency matrix* $\mathrm{adj}(G)$. A labelled graph has a single adjacency matrix, with each row and each column corresponding to a vertex, such that each matrix element (a, b) (at row b and column a) is assigned the weight of the edge b, a. It follows that two equivalent graphs have the same adjacency matrix, and that an unlabelled graph has $N!$ adjacency matrices resulting from the different possible labelling permutations. Consider a labelled graph

$$G = \qquad\qquad\qquad\qquad\qquad\qquad (1.2)$$

Then

$$\mathrm{adj}(G) = \begin{pmatrix} 0 & 0 & 0 & 1 \\ 1 & 0 & 0 & 0 \\ 1 & 1 & 0 & 0 \\ 0 & 0 & 1 & 0 \end{pmatrix} \qquad (1.3)$$

In the absence of an edge between two vertices, the corresponding matrix elements are set to a token value, typically zero or infinity depending on the context*; for our purposes, we shall use zero. *Loop edges*, for which the head and tail are the *same* vertex are thus represented along the diagonal of the adjacency matrix.

---

*If the graph represents a series of electronic components with edge weights corresponding to electrical resistance, infinity would be a suitable placeholder for disconnected components, because a wire of infinite resistance is equivalent to the absence of a wire. On the other hand, if the edge weights instead correspond to conductance, the placeholder would be zero.

1.2.2 Biadjacency matrices

If a graph's vertices can be arranged into $V = V_A \cup V_B$, where no edge exists between any two vertices in V_A or any two vertices in V_B, it is called *bipartite.* For such a graph, we can choose three labelling schemes: one for the whole graph with indices $0 \ldots |V_A| + |V_B| - 1$, one for V_A with indices $0 \ldots |V_A| - 1$, and one for $|V_B|$ with indices $0 \ldots |V_B| - 1$.

We can then form two *biadjacency matrices* $\text{biadj}_{A,B}(G)$ and $\text{biadj}_{B,A}(G)$, such that $\text{biadj}_{X,Y}(G)$ comprises elements (i,j) assigned by the weight of the edge which has the head $v_j \in V_X$ and the tail $v_i \in V_Y$.

It is often useful to choose the labelling scheme for the whole graph such that

$$v_i \in \begin{cases} V_A & i < |V_A| \\ \\ V_B & i >= |V_A| \end{cases}, \tag{1.4}$$

allowing for the useful representation

$$\text{adj}(G) = \begin{pmatrix} \mathbf{0} & \text{biadj}_{B,A}(G) \\ \text{biadj}_{A,B}G & \mathbf{0} \end{pmatrix}. \tag{1.5}$$

Take, as an example,

$$G_{bi} = \qquad \tag{1.6}$$
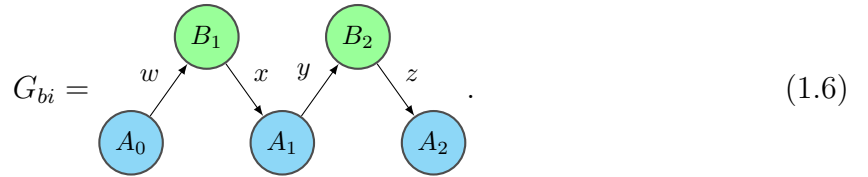
In this case,

$$\text{biadj}_{B,A}(G) = \begin{pmatrix} 0 & 0 \\ x & 0 \\ 0 & z \end{pmatrix}, \qquad \text{biadj}_{A,B}(G) = \begin{pmatrix} w & 0 & 0 \\ 0 & y & 0 \end{pmatrix}, \tag{1.7}$$

$$\text{adj}(G) = \left(\begin{array}{ccc:cc} 0 & 0 & 0 & 0 & 0 \\ 0 & 0 & 0 & x & 0 \\ 0 & 0 & 0 & 0 & z \\ \hdashline w & 0 & 0 & 0 & 0 \\ 0 & y & 0 & 0 & 0 \end{array}\right) \tag{1.8}$$

1.2.3 The incidence matrix

The *incidence matrix* $\nabla(G)$ of an unweighted graph $G(V, E)$ is an $|E| \times |V|$ matrix that describes the connectivity between vertices and edges. Each row and column corresponds to an edge and vertex respectively, and each element is assigned the value

$$\nabla(G)_{a,b} = \begin{cases} 1 & b = \text{head}(a) \\ -1 & b = \text{tail}(a) \\ 0 & \text{otherwise,} \end{cases} \tag{1.9}$$

such that each row has exactly two non-zero values[†]. For example, labelling edges as well as vertices,
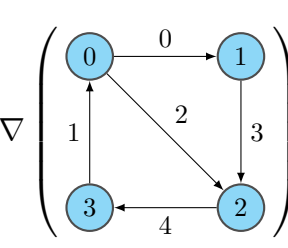
$$\nabla \left(\begin{array}{c} \end{array} \right) = \left(\begin{array}{cccc} 1 & -1 & 0 & 0 \\ 1 & 0 & -1 & 0 \\ -1 & 0 & 0 & 1 \\ 0 & 1 & -1 & 0 \\ 0 & 0 & 1 & -1 \end{array}\right) \tag{1.10}$$

The canonical incidence matrix application is that of electrical circuits, whereby if the graph represents a circuit with edges as wires, solutions to $\nabla^{\dagger}(G)\vec{x} = \vec{0}$ provide the electrical currents along the wires that satisfy Kirchhoff's current law [15, 16]. It also

---

[†]In the case of a *hypergraph*, which contains *hyper-edges* that are connected to more than two vertices, each column can have more than two non-zero values.

provides a reasonable representation of hypergraphs, where representation through an adjacency tensor may be non-trivial to write[17], and provides an efficient computational representation of graphs in which the number of edges is fewer than the number of vertices.

The values $1, -1$ given here are generally used when the graph is unweighted, or when the weights are otherwise not important for some stage of a calculation. There exist a variety of different protocols for creating an incidence matrix for a weighted graph, and these are designed for specific situations.

1.2.4 The laplacian

Let $D(G)$ be the diagonal degree matrix

$$D(G)(i,i) = \sum_{k \in V} \text{weight}\{k,i\}, \qquad G = G(V,E). \tag{1.11}$$

The laplacian of a graph is then defined as

$$\Delta(G) = D(G) - \text{adj}(G), \tag{1.12}$$

for example

$$\Delta \begin{pmatrix} \cdots \end{pmatrix} = \begin{pmatrix} 1 & 0 & 0 & -1 \\ -1 & 1 & 0 & 0 \\ -1 & -1 & 2 & 0 \\ 0 & 0 & -1 & 1 \end{pmatrix}. \tag{1.13}$$
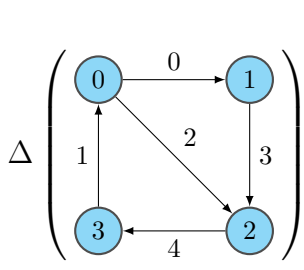
The laplacian is of great interest in spectral graph theory[18][‡] because of its connections to geometry and topology. Indeed, the laplacian acts as a discrete analogy of the continuous laplacian operator, and the number of zero-valued eigenvalues of $\Delta(G)$ corresponds to the number of connected components in G[19].

[‡]The adjacency matrix is also a common representation of interest in spectral graph theory, but does not receive as much attention as the laplacian.

The laplacian of an undirected, unweighted graph be calculated with the incidence matrix ∇ through

$$\Delta(G) = \nabla^\dagger(G) \cdot \nabla(G) \tag{1.14}$$

Such that, with the undirected equivalent of the graph above,

$$\Delta \left(\begin{array}{c} \text{graph} \end{array} \right) = \begin{pmatrix} 1 & 1 & -1 & 0 & 0 \\ -1 & 0 & 0 & 1 & 0 \\ 0 & -1 & 0 & -1 & 1 \\ 0 & 0 & 1 & 0 & -1 \end{pmatrix} \begin{pmatrix} 1 & -1 & 0 & 0 \\ 1 & 0 & -1 & 0 \\ -1 & 0 & 0 & 1 \\ 0 & 1 & -1 & 0 \\ 0 & 0 & 1 & -1 \end{pmatrix} \tag{1.15}$$

$$= \begin{pmatrix} 3 & -1 & -1 & -1 \\ -1 & 2 & -1 & 0 \\ -1 & -1 & 3 & -1 \\ -1 & 0 & -1 & 2 \end{pmatrix}. \tag{1.16}$$

1.2.5 Graph unions

Two graphs $G_1(V_1, E_1), G_2(V_2, E_2)$ can be unified into one graph through one of two types of union. Under a disjoint union, vertices and edges from each are considered unique and are combined into one graph of two disjoint parts,

$$G_1 \oplus G_2 = G_3(V_3, E_3) \tag{1.17}$$

$$V_3 = V_1 \oplus V_2, \qquad E_3 = E_1 \oplus E_2 \tag{1.18}$$

In another form of union, there can be common vertices in V_1 and V_2, and the resulting graph merges G_1 and G_2 to form

$$G_1 \cup G_2 = \tilde{G}_3(\tilde{V}_3, \tilde{E}_3) \tag{1.19}$$

$$\tilde{V}_3 = V_1 \cup V_2, \qquad \tilde{E}_3 = E_1 \cup E_2 \tag{1.20}$$

For the purposes of this thesis, only the disjoint union will be considered. The result of the disjoint union has a rather simple effect on all of the matrix representations of graphs that we have looked at thus far,

$$\text{adj}(G_1 \oplus G_2) = \text{adj}(G_1) \oplus \text{adj}(G_2) \tag{1.21}$$

$$\nabla(G_1 \oplus G_2) = \nabla(G_1) \oplus \nabla(G_2) \tag{1.22}$$

$$\Delta(G_1 \oplus G_2) = \Delta(G_1) \oplus \Delta(G_2), \tag{1.23}$$

as demonstrated graphically with

$$\text{adj}(G_1) = \begin{pmatrix} 0 & x & 0 \\ x & 0 & y \\ 0 & y & 0 \end{pmatrix} \qquad \text{adj}(G_2) = \begin{pmatrix} 0 & z \\ z & 0 \end{pmatrix} \tag{1.25}$$

$$\text{incidence}(G_1) = \begin{pmatrix} 1 & 0 \\ -1 & 1 \\ 0 & -1 \end{pmatrix} \qquad \text{incidence}(G_2) = \begin{pmatrix} 1 \\ -1 \end{pmatrix} \tag{1.26}$$

$$\text{laplacian}(G_1) = \begin{pmatrix} 1 & -1 & 0 \\ -1 & 2 & -1 \\ 0 & -1 & 1 \end{pmatrix} \qquad \text{laplacian}(G_2) = \begin{pmatrix} 1 & -1 \\ -1 & 1 \end{pmatrix} \tag{1.27}$$

$$G_1 \oplus G_2 = \quad$$

$$\mathrm{adj}(G_1 \oplus G_2) = \begin{pmatrix} 0 & x & 0 & 0 & 0 \\ x & 0 & y & 0 & 0 \\ 0 & y & 0 & 0 & 0 \\ 0 & 0 & 0 & 0 & z \\ 0 & 0 & 0 & z & 0 \end{pmatrix} \tag{1.29}$$

$$\mathrm{incidence}(G_1 \oplus G_2) = \begin{pmatrix} 1 & 0 & 0 \\ -1 & 1 & 0 \\ 0 & -1 & 0 \\ 0 & 0 & 1 \\ 0 & 0 & -1 \end{pmatrix} \tag{1.30}$$

$$\mathrm{laplacian}(G_1 \oplus G_2) = \begin{pmatrix} 1 & -1 & 0 & 0 & 0 \\ -1 & 2 & -1 & 0 & 0 \\ 0 & -1 & 1 & 0 & 0 \\ 0 & 0 & 0 & 1 & -1 \\ 0 & 0 & 0 & -1 & 1 \end{pmatrix} \tag{1.31}$$

1.3 Graph representations of matrices

1.3.1 Coates digraphs of matrices

For most intents and purposes, an adjacency matrix can be used to fully describe a graph[§]. Indeed, the *Coates digraph* $\mathrm{Coates}(M)$ of any square matrix M provides a graph whose adjacency matrix is M^T, and thus

$$\mathrm{Coates}(\mathrm{adj}(G)^T) \equiv G. \tag{1.32}$$

This concept will be used heavily throughout this thesis, but we instead wish to remove the transpose requirement and work directly on graphs whose adjacency matrix satisfies M directly. For clarity, let us define

$$\mathrm{graph}(M) \equiv \mathrm{Coates}(M^T), \tag{1.33}$$

such that adj $\odot$ graph forms an identity over matrices and graph $\odot$ adj forms an identity over square matrices.

1.3.2 König digraphs of matrices

The *König digraph* $\mathrm{König}(M)$ of a matrix M is a directed bipartite graph with two layers of vertices (henceforth referred to as the *input* and *output* layers) V_0 and V_1 corresponding to the rows and columns of M respectively, with matrix elements represented by edges directed from the input layer to the output layer[11].

Let $\mathrm{walk}(G) = \mathrm{König}(\mathrm{adj}(G))$ of a graph G be the König digraph of its adjacency matrix. As $\mathrm{adj}(G)$ is a square matrix, $\mathrm{walk}(G)$ comprises two sets of clones of G's vertices,

---

[§]A common method of storing a graph in memory is through the matrix representation, so long as the matrix is not sufficiently sparse as to justify an alternative pointer-based representation.

and edges from G exist in walk(G) with the head and tail replaced with the corresponding vertices in the input and output layers respectively. This is then a bipartite graph with biadj$_{V_0,V_1}$(walk(G)) = adj(G), as shown in the following example.

$$G = \quad \overset{A}{\circlearrowright} \quad \overset{B}{\circlearrowright} \quad \overset{C}{\circlearrowright} \; , \qquad \text{adj}(G) = \begin{pmatrix} A & x & 0 \\ 0 & B & 0 \\ 0 & 0 & C \end{pmatrix} \qquad (1.34)$$

$$\text{walk}(G) = \quad A \; B \qquad C \qquad \text{adj}(\text{walk}(G)) = \begin{pmatrix} \mathbf{0}_3 & \mathbf{0}_3 \\ \text{adj}(G) & \mathbf{0}_3 \end{pmatrix} \qquad (1.35)$$

The inverse, unwalk, merges the input and output layers, such that unwalk(walk(G)) = G.

The separation of the input and output layers makes the König representation an extremely powerful representation of matrices, allowing for the representation of rectangular matrices and, thus, vectors and dual vectors, which have no direct analogue in graphs.

A (column) vector v of dimension N can be represented in a König digraph by a sole *source* vertex in the input layer, and N *sink* vertices in the output layer, such that the edge from the source vertex to sink vertex i is weighted v_i, as in

$$v = \begin{pmatrix} 1 \\ 2 \\ 3 \end{pmatrix} \qquad \text{walk}(v) = \qquad (1.36)$$

Conversely, a dual (i.e. row) vector of dimension N be represented in a König digraph by N source vertices in the input layer and a single sink vertex in the output layer, as in

$$u = \begin{pmatrix} 4 & 5 & 6 \end{pmatrix} \qquad \mathrm{walk}(u) = \qquad\qquad\qquad (1.37)$$

Finally, a scalar can be represented by a single source vertex and a single sink vertex, with edge weight equal to the scalar value, as in

$$t = 7 \qquad\qquad \mathrm{walk}(t) = \; 7 \qquad\qquad (1.38)$$

1.3.3   Concatentation of König digraphs

Consider the multiplication of two matrices $A \in \mathbb{C}^{p \times q}$ and $B \in \mathbb{C}^{q \times r}$, such that $AB \in \mathbb{C}^{p \times r}$. It is possible to represent the multiplication of A and B through the König digraphs of A and B by merging the output layer of König(A) with the input layer of König(B).

For example, let K be the permutation matrix

$$K = \begin{pmatrix} 0 & 1 & 0 \\ 1 & 0 & 0 \\ 0 & 0 & 1 \end{pmatrix}, \qquad \mathrm{König}(K) = \qquad\qquad\qquad (1.39)$$

and let v be a vector in three dimensions, and u be a dual vector in three dimensions

$$v = \begin{pmatrix} 1 & 2 & 3 \end{pmatrix}^T \qquad\qquad u = \begin{pmatrix} 3 & 4 & 5 \end{pmatrix}$$

$$V = \mathrm{König}(v) \qquad\qquad\qquad U = \mathrm{König}(u)$$

$$= \qquad\qquad\qquad\qquad\qquad = $$

Then the digraph corresponding to the multiplication KV is the graph formed by merging the three output vertices of König(V) with the three input matrices of König(K),

König(K) × König(V) =
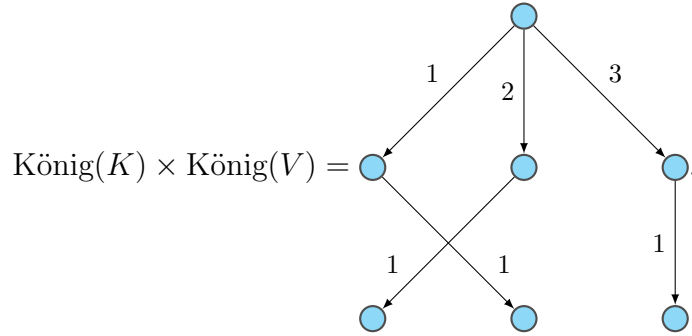
We are now left with a graph with *three* layers of vertices: an input layer, an intermediate layer, and an output layer. We can now define a reduction operation

$$\text{reduce} : \text{König}(A) \times \text{König}(B) \to \text{König}(AB) \tag{1.40}$$

that performs the graph analogue of matrix multiplication: for each vertex in the intermediate layer, connect the head of each incoming edge e_i with the tail of each outgoing edge e_o with an edge of weight weight(e_i) × weight(e_o). It is clear that this is simply a graph analogue of the matrix product $(AB)_{i,j} = \sum_k A_{i,k} B_{k,j}$.

We will be using this concept heavily for the remainder of this thesis so, for brevity, let the reduction operation be implicit whenever a König digraph is compared with a multi-layer digraph, such that we may write

König(KV) = König(K) × König(V)
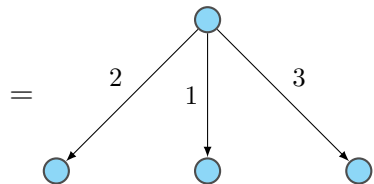
This represents a vector with components

$$\text{biadj}_{\text{sink,source}}(KV) = \begin{pmatrix} 2 & 1 & 3 \end{pmatrix}^T, \tag{1.41}$$

in agreement with

$$\begin{pmatrix} 0 & 1 & 0 \\ 1 & 0 & 0 \\ 0 & 0 & 1 \end{pmatrix} \begin{pmatrix} 1 \\ 2 \\ 3 \end{pmatrix} = \begin{pmatrix} 2 \\ 1 \\ 3 \end{pmatrix}. \tag{1.42}$$

We may then consider multiplication on the left by U,
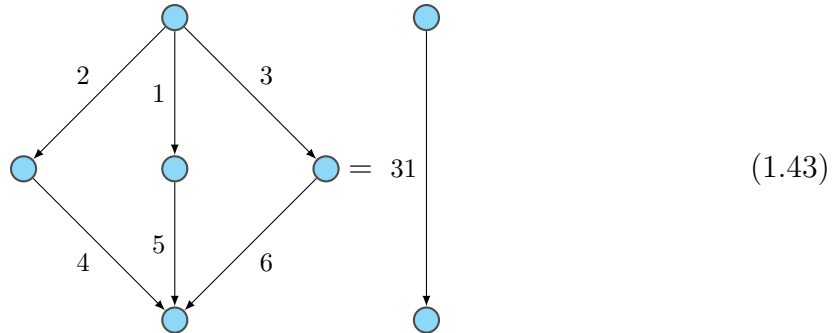
in agreement with

$$\begin{pmatrix} 4 & 5 & 6 \end{pmatrix} \begin{pmatrix} 0 & 1 & 0 \\ 1 & 0 & 0 \\ 0 & 0 & 1 \end{pmatrix} \begin{pmatrix} 1 \\ 2 \\ 3 \end{pmatrix} = \begin{pmatrix} 4 & 5 & 6 \end{pmatrix} \begin{pmatrix} 2 \\ 1 \\ 3 \end{pmatrix} = 31 \tag{1.44}$$

1.4   Matrix-theoretic operations on graphs

So far we have seen how graphs can be represented as matrices and how matrices can be represented as graphs. We have seen that a graph-theoretic operation can be implemented through a matrix representation, and that a matrix-theoretic operation can be implemented through a graph representation. This is established literature, and is used heavily in a variety of different fields, including electronics, artificial intelligence, and condensed matter physics.

In this thesis, the duality between graphs and matrices is taken one step further. Specifically, we will be looking closely at transforming graphs with polynomials, in a manner such that their adjacency matrices will be transformed by the same polynomials.

The set of square matrices of equal size forms a *ring*, such that they form a group under element-wise *addition*

$$(A + B)_{i,j} = A_{i,j} + B_{i,j}, \tag{1.45}$$

and also have a defined *multiplication*

$$(AB)_{i,j} = \sum_{n=0}^{N-1} A_{i,k} B_{k,j}. \tag{1.46}$$

which is

- *left distributive* $A * (B + C) = A * B + A * C,$

- *right distributive* $(A + B) * C = A * C + B * C,$ and

- *associative* $A * (B * C) = (A * B) * C.$

A general function comprising such operations is a polynomial

$$p : x \rightarrow \sum_k c_k x^k. \tag{1.47}$$

We can extend this algebra to graphs with a few simple steps. Consider two graphs G, H on the same set of vertices. Addition is trivial: $G + H$ is simply a graph on the same vertices with edges from both G and H, adding weights of common edges. For example,

$$H = \quad , \qquad \mathrm{adj}(H) = \begin{pmatrix} D & 0 & 0 \\ y & 0 & 0 \\ 0 & z & F \end{pmatrix} \tag{1.48}$$

$$\mathrm{walk}(H) = \qquad \mathrm{adj}(\mathrm{walk}(H)) = \begin{pmatrix} \mathbf{0}_3 & \mathbf{0}_3 \\ \mathrm{adj}(H) & \mathbf{0}_3 \end{pmatrix} \tag{1.49}$$

24

$$\mathrm{walk}(G + H) = \mathrm{walk}(G) + \mathrm{walk}(H)$$

$$= \quad A + D \qquad B \qquad C + F \qquad\qquad (1.50)$$

$$G + H = \mathrm{unwalk}(\mathrm{walk}(G + H))$$

$$= \qquad\qquad\qquad\qquad\qquad\qquad (1.51)$$
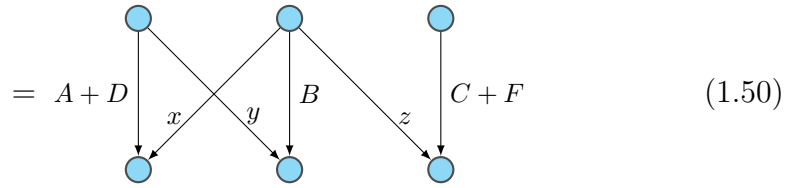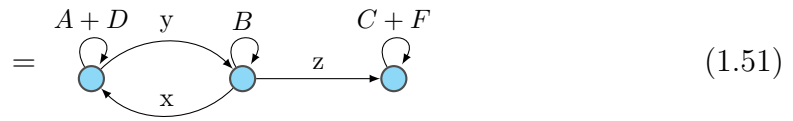
Their multiplication GH can be obtained from $\mathrm{graph}(\mathrm{adj}(G)\mathrm{adj}(H))$ or, equivalently, through

$$\mathrm{unwalk}(\mathrm{walk}(G) \times \mathrm{walk}(H)). \qquad\qquad (1.52)$$

. For example,

$$\mathrm{walk}(H) \times \mathrm{walk}(G) = \qquad\qquad\qquad\qquad (1.53)$$

$$= \qquad + \qquad + \qquad$$

$$+ \qquad + \qquad + \qquad , \qquad\qquad (1.54)$$

$$= \begin{pmatrix} & AD & \\ & & \end{pmatrix} + \begin{pmatrix} & xD & \\ & & \end{pmatrix} + \begin{pmatrix} & Bz & \\ & & \end{pmatrix}$$

$$+ \begin{pmatrix} & Ay & \\ & & \end{pmatrix} + \begin{pmatrix} & xy & \\ & & \end{pmatrix} + \begin{pmatrix} & CF & \\ & & \end{pmatrix} \qquad (1.55)$$

$$= \qquad \overset{Dx \quad Bz}{\underset{AD \quad xy \quad CF}{\underset{Ay}{}}} \qquad . \qquad (1.56)$$

$$HG = \mathrm{unwalk}(\mathrm{walk}(H) \times \mathrm{walk}(G))$$

$$= \qquad \overset{AD \quad Ay \quad xy \qquad CF}{\underset{Dx}{ \xrightarrow{Bz} }} \qquad . \qquad (1.57)$$

Multiplication of more than two graphs, for example a graph power[20], can either be performed through repeated walks and unwalks or, due to the associativity of rings, by concatenating the walk graphs of each operand and reducing the final many-layer graph in any order.

Although the approach of applying matrix operations on the adjacency matrices of the operands and drawing a graph on the same vertices, the graphical approach through König digraphs is a useful book-keeping tool which provides a deeper insight into the operations. This will make itself clear later in this thesis, when we graphically demonstrate the logic behind the appearance of topological characteristics in the polynomial of a graph.

The multiplicative identity of a walk graph simply joins vertices in the input layer with the corresponding vertices in the output layer, with edges of unit weight. For example, the identity walk graph of four vertices is

$$\mathbf{1}_4 = \begin{array}{cccc} \bullet & \bullet & \bullet & \bullet \\ 1\downarrow & 1\downarrow & 1\downarrow & 1\downarrow \\ \bullet & \bullet & \bullet & \bullet \end{array} . \tag{1.58}$$

Multiplying a multiple $x\mathbf{1}_N$ of the N-dimensional identity walk graph with an N-dimensional walk vector v is equivalent to multiplying v by the scalar x, as we expect from matrix algebra. Although this result alone is trivial, we will see a useful generalisation in section 1.5.2. For example,

$$(x\mathbf{1}_4) \times \text{walk} \begin{pmatrix} v_1 \\ v_2 \\ v_3 \\ v_4 \end{pmatrix} = \qquad \tag{1.59}$$

$$= \qquad \tag{1.60}$$

$$= \qquad \tag{1.61}$$

1.5 Eigendecomposition

An *eigenvalue* λ of a *diagonalisable* matrix $M \in \mathbb{C}^{N \times N}$ is a scalar value which is a solution to the *characteristic polynomial* of M

$$\det(M - \lambda) = 0.$$

As a single variable polynomial of order N, the fundamental theorem of algebra states that there are N such eigenvalues $\lambda_0, \lambda_1, \ldots, \lambda_N$ such that

$$\det(M - \lambda) = (\lambda_0 - \lambda)(\lambda_1 - \lambda) \ldots (\lambda_N - \lambda).$$

Eigenvalues need not be distinct; any eigenvalue which occurs q times in the expansion is said to have an *algebraic multiplicity* of q, such that the sum of algebraic multiplicities of each unique eigenvalue is N. An eigenvalue with algebraic multiplicity $q > 1$ is called *degenerate*.

For each eigenvalue with algebraic multiplicity q, there are $\tilde{q} \in [1 \mathrel{..} q]$ linearly independent *eigenvectors*, which are nonzero vectors v for which

$$(M - \lambda)\,v = 0 \tag{1.62}$$

$$Mv = \lambda v. \tag{1.63}$$

$\tilde{q}$ is called the *geometric multiplicity* of λ in M, and any non-zero linear combination of corresponding eigenvectors also has eigenvalue λ. For example, let

$$Mv = \lambda v, \qquad\qquad Mu = \lambda u$$

then

$$M(av + bu) = aMv + bMu$$

$$= a\lambda v + b\lambda u$$

$$= \lambda(av + bu). \tag{1.64}$$

Such eigenvectors thus span an *eigenspace* of M, or a space in which every point except for the zero vector is an eigenvector with eigenvalue λ.

If, for every eigenvalue λ of M, the geometric multiplicity and algebraic multiplicity of λ are equal, then M is said to be *diagonalisable*. All diagonalisable matrices can be written as a diagonal matrix $\Lambda = \mathrm{diag}\left(\{\lambda_0, \ldots, \lambda_n\}\right)$ in the basis of a complete set of linearly independent and normalised eigenvectors, or eigenstates, $Q = \{v_o, \ldots, v_n\}$ through the transformation

$$M = Q\Lambda Q^{-1}. \tag{1.65}$$

The process of finding a Q and Λ is called *eigendecomposition*. Λ is unique up to a permutation, which must also be applied to Q. However, Q is not unique: it depends on a choice of phase[¶] and a choice of basis for each eigenspace. Different diagonalisation techniques may produce different, but nonetheless valid, Q and different permutations of Λ and Q.

From this point onwards, we will only be considering diagonalisable matrices.

1.5.1 Eigendecomposition of polynomials of matrices

All eigenstates of a matrix M are also eigenstates of $P(M)$, where P is some polynomial, and their corresponding eigenvalues λ transform as $P(\lambda)$. More formally, for any eigendecomposition of M into an eigenvalue matrix Λ and an eigenstate matrix Q, there exists an eigendecomposition of $P(M)$ into an eigenvalue matrix $P(\Lambda)$ and the same eigenstate matrix Q.

[¶]each eigenstate maintains unit magnitude and linear independence from other eigenstates when multiplied by any complex number on the unit circle

We can show this by first analysing integer powers of M

$$M^N = (Q\Lambda Q^{-1})^N \tag{1.66}$$

$$= Q\Lambda\left(Q^{-1}Q\right)\Lambda Q^{-1}\dots \tag{1.67}$$

$$= Q\Lambda\Lambda\dots Q^{-1} \tag{1.68}$$

$$= Q\Lambda^N Q^{-1}. \tag{1.69}$$

Expressing the polynomial P of order A, through its action on an indeterminate X as

$$P : X \to \sum_{a=0}^{A} C_a X^n \tag{1.70}$$

then allows us to write

$$P(M) = \sum_{a=0}^{A} C_a M^a \tag{1.71}$$

$$= \sum_{a=0}^{A} C_a Q\Lambda^a Q^{-1} \tag{1.72}$$

$$= Q\left(\sum_{a=0}^{A} C_a \Lambda^a\right) Q^{-1} \tag{1.73}$$

$$= Q P(\Lambda) Q^{-1}. \qquad \square \tag{1.74}$$

$P(\Lambda)$ is a diagonal matrix obeying $P(\Lambda)_{n,n} = P(\Lambda_{n,n})$. Thus $P(M)$ shares the same eigenstates of M, with eigenvalues $\{P(\lambda_n)\}$.

In the special case of hermitian matrices this provides a trivial proof of the Cayley-Hamilton theorem [21], which states that a diagonalisable matrix satisfies its own characteristic equation $P(X) = \det(M - X) = 0$. As the individual elements of the diagonal matrix Λ solve $P(X)$ by definition, $P(\Lambda)$ is the $N \times N$ zero matrix, hence $P(M)$ is also

the $N \times N$ zero matrix.

As a result, properties of $P(M)$ may be viewed as being rooted in its *ancestry* from M. By extension, if a polynomial Q exists such that $M = Q(M')$, for some matrix M', the properties of M, along with all $P(M)$, might stem from those of M'.

The converse does not generally hold. Consider two distinct eigenvalues λ_1, λ_2 of M, with algebraic multiplicities α_1, α_2 and eigenspaces $\mathcal{E}_1, \mathcal{E}_2$ respectively. Now consider some polynomial such that $P(\lambda_1) = P(\lambda_2) = \tilde{\lambda}$.

In $P(M)$, the eigenvalue $\tilde{\lambda}$ then has algebraic multiplicity $\tilde{\alpha} = \alpha_1 + \alpha_2$. As $P(M)$ is diagonalisable, the geometric multiplicities accumulate likewise, and its corresponding eigenspace $\tilde{E} = E_1 \oplus E_2$ is the orthogonal direct sum of the eigenspaces of λ_1 and λ_2.

Any point $z \in \tilde{\mathcal{E}}$ is an eigenvector of $P(M)$ with eigenvalue $\tilde{\lambda}$, but z need not exist within either $\mathcal{E}_1$ or $\mathcal{E}_2$. Thus, while it is *possible* to choose a basis for $\tilde{\mathcal{E}}$ for which each basis vector belongs in either $\mathcal{E}_1$ or $\mathcal{E}_2$, it is not *necessary* to do so. Thus there exist eigendecompositions of $P(M)$ for which $P(\Lambda)$ and $\tilde{Q}$ are not a valid eigendecomposition of M.

Let us now demonstrate this with the matrix

$$M = \frac{1}{\sqrt{2}} \begin{pmatrix} 0 & 0 & 1 \\ 0 & 0 & 1 \\ 1 & 1 & 0 \end{pmatrix}, \qquad M^2 = \frac{1}{2} \begin{pmatrix} 1 & 1 & 0 \\ 1 & 1 & 0 \\ 0 & 0 & 2 \end{pmatrix}.$$

M may be eigendecomposed into the eigenstates and eigenvalues

$$u = \frac{1}{2} \begin{pmatrix} 1 & 1 & \sqrt{2} \end{pmatrix}^T \qquad \lambda_u = 1, \tag{1.75}$$

$$v = \frac{1}{2} \begin{pmatrix} 1 & 1 & -\sqrt{2} \end{pmatrix}^T \qquad \lambda_v = -1, \qquad (1.76)$$

$$w = \frac{1}{\sqrt{2}} \begin{pmatrix} 1 & -1 & 0 \end{pmatrix}^T \qquad \lambda_w = 0. \qquad (1.77)$$

Multiplying these eigenstates through M^2, where $x \xrightarrow{A} y$ implies $Ax = y$,

$$u \xrightarrow{M} u \xrightarrow{M} u$$

$$v \xrightarrow{M} -v \xrightarrow{M} v$$

$$w \xrightarrow{M} 0 \xrightarrow{M} 0$$

we see that, while they are indeed eigenstates of M^2, both u and v have eigenvalue 1 in M^2. As per eq. (1.64), the eigenstates found by directly decomposing M^2 may be any two orthonormal linear combinations of u and v.

As M^2 is separable into a direct sum of two matrices

$$M^2 = \frac{1}{2} \begin{pmatrix} 1 & 1 \\ 1 & 1 \end{pmatrix} \oplus \begin{pmatrix} 1 \end{pmatrix},$$

$$= m_1 \oplus m_2$$

a natural decomposition of M^2 would be a symmetric and anti-symmetric pair of vectors in the space of m_1 and a unit vector in the space of m_2,

$$\tilde{u} = \begin{pmatrix} 0 & 0 & 1 \end{pmatrix}^T \qquad \lambda_{\tilde{u}} = 1$$

$$\tilde{v} = \frac{1}{\sqrt{2}} \begin{pmatrix} 1 & 1 & 0 \end{pmatrix}^T \qquad \lambda_{\tilde{v}} = 1$$

$$\tilde{w} = \frac{1}{\sqrt{2}} \begin{pmatrix} 1 & -1 & 0 \end{pmatrix}^T \qquad \lambda_{\tilde{w}} = 0,$$

The degenerate pair are not eigenstates of M,

$$M\tilde{u} = \tilde{v} \qquad\qquad\qquad M\tilde{v} = \tilde{u},$$

but they are of course linear combinations of u and v,

$$\left(\begin{array}{c|c} \tilde{u} & \tilde{v} \end{array}\right) = \frac{1}{\sqrt{2}} \left(\begin{array}{c|c} u & v \end{array}\right) \begin{pmatrix} 1 & 1 \\ -1 & 1 \end{pmatrix}. \tag{1.78}$$

There is also another matrix, L which squares to the same M^2,

$$L = \frac{1}{\sqrt{2}} \begin{pmatrix} 1 & 1 & 0 \\ 1 & 1 & 0 \\ 0 & 0 & 2 \end{pmatrix}, \tag{1.79}$$

$$L^2 = M^2, \tag{1.80}$$

and this decomposes in the same way as M^2, and we might say that M^2's properties are inherited from its alternative square root L. This would, however, be a tautology, because L is itself a scalar multiple of M^2.

1.5.2 Eigenstates and graphs

Just as an eigenstate v of a matrix M obeys $Mv = \lambda_v v$ for some scalar λ, we can describe an eigenstate V of a graph G as one which multiplies through walk(G) to produce a scalar multiple of V, such that

$$\tag{1.81}$$
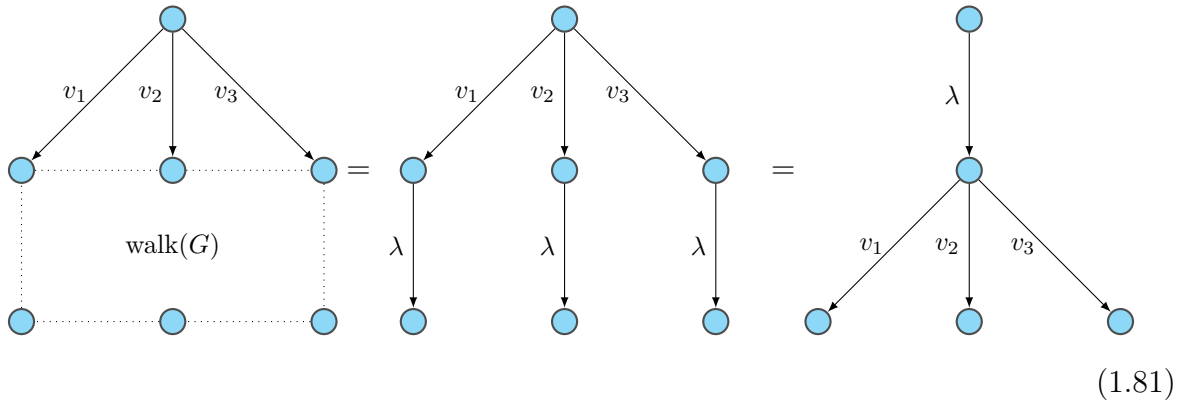
The latter representation is particularly useful for reasoning about a set of eigenstates u, v, w with eigenvalues $\lambda_1, \lambda_2, \lambda_3$, as we can then write

$$\tag{1.82}$$
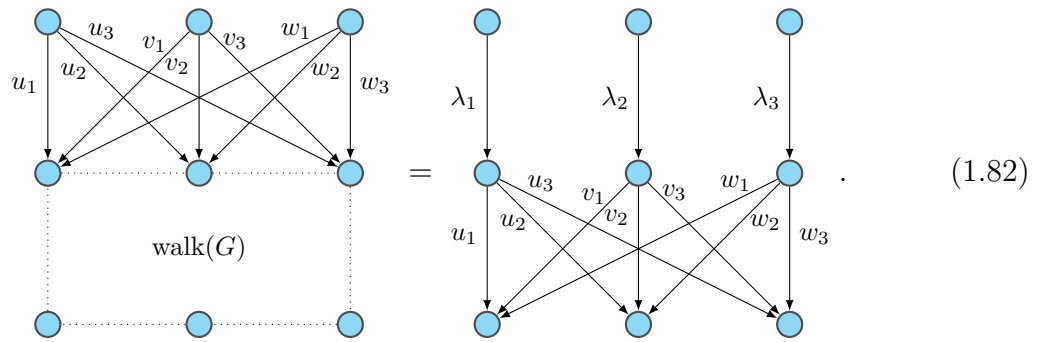
As an eigenstate is invariant, except for a scale factor λ^n, when multiplied through the finite graph G^n, it follows that the properties of each eigenstate are dependent not just on the structure of G, but on that of all powers of G.

Consider two vertices x, y in a graph and recall that we have defined their distance set $\tilde{d}_G(x, y)$ as the set of all $k \in \mathbb{N}$ for which there exists at least one walk from of length k from x to y. If there is any $k \in \tilde{d}_G(x, y)$ such that the multiplicative weights of all such walks of length k do not sum to zero$^{\parallel}$, then G^k connects vertices x and y.

As an eigenstate v of G is also an eigenstate of G^k, the components v_x, v_y corresponding to vertices x and y must necessarily take this connectivity into account. Any modification

---

$^{\parallel}$If the multiplicative walk weights do indeed mutually cancel, this is a graph analogue of destructive interference

to an edge attached to vertex y would then modify v_x, thus the eigendecomposition of G is *macroscopic*, depending on the entire structure of G rather than the neighbourhood of each vertex alone.

If, for every $k \in \tilde{d}_G(x,y)$, the set of walks of length k between vertices x and y are mutually destructive, it is possible for v_x and v_y to be unrelated, and for modifications of the neighbourhood of vertex y to have no effect on v_x.

Let us now demonstrate the nature of destructive and constructive interference in the language of graphs. Let $a \in R$ be a varying parameter, and consider the graphs

$$G_c = \qquad \qquad \qquad \qquad \qquad \qquad \qquad \qquad \qquad \qquad (1.83)$$

$$G_d = \qquad \qquad \qquad \qquad \qquad \qquad \qquad \qquad \qquad , \qquad (1.84)$$
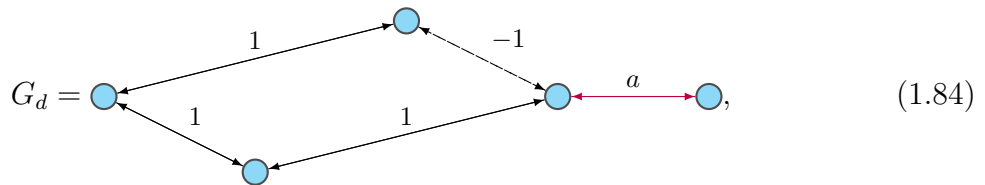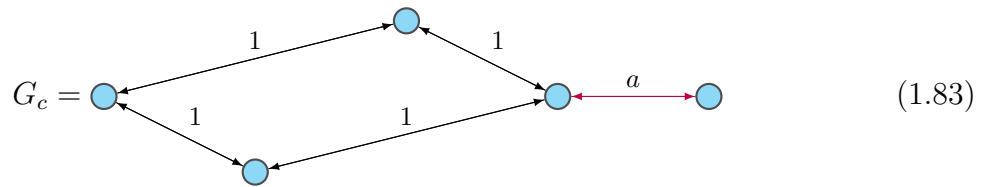
where any edge with weight dependent on a is coloured purple for the benefit of the reader. The vertices of interest are the leftmost vertex and the vertex immediately to the left of the rightmost vertex, which we shall denote Q and R respectively. There are two walks of length 2 from Q to R in both graphs, but the multiplicative weights of these paths are 1 and 1 in G_c, whereas they are 1 and -1 in G_d. Thus, we expect that G_c^2 contains an edge of weight 2 between Q and R due to the constructive interference of the two possible paths, but in G_d^2 such an edge is absent due to the destructive interference of the two paths. This edge provides the avenue through which vertex Q gains a direct dependence on the parameter a in higher powers of G_c.

We shall now demonstrate this behaviour directly through König digraphs. Starting from G_c, let us first look at its square and the formation of the edge between Q and R.

$$\mathrm{walk}(G_c) = \qquad\qquad\qquad\qquad\qquad , \tag{1.85}$$

$$\mathrm{walk}(G_c^2) = \qquad\qquad\qquad\qquad\qquad , \tag{1.86}$$

$$= \qquad\qquad\qquad\qquad\qquad , \tag{1.87}$$

$$\Rightarrow G_c^2 = \qquad\qquad\qquad\qquad\qquad . \tag{1.88}$$

We can see that there will be some power of G_c that will contain an edge connected to Q that depends upon a by inspection: The path QRR in G_c^2 has a multiplicative weight of $2(a^2 + 2)$, which will contribute to the edge between Q and R in G_c^4. However, we need

36

look no further than G_c^3 to find the first a-dependent edge incident on Q, as

$$G_c^3 = \quad (1.89)$$
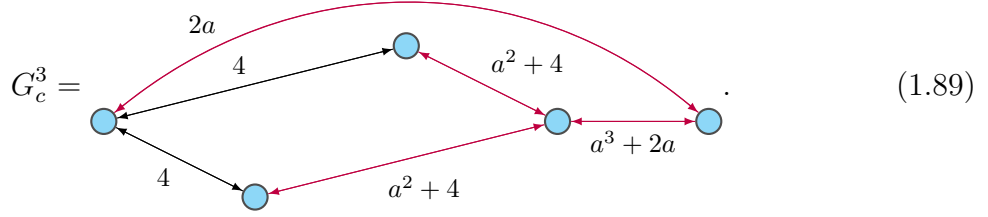
The eigenstates and eigenvalues of G_c are given by

$$\gamma = \sqrt{a^4 + 16}$$

$$\beta_\pm = a^2 - \gamma \pm 4, \qquad \delta_\pm = a^2 + \gamma \pm 4$$

$$v_{c,1} = \begin{pmatrix} 0 & -\frac{1}{\sqrt{2}} & \frac{1}{\sqrt{2}} & 0 & 0 \end{pmatrix} \qquad \lambda_{c,1} = 0 \qquad (1.90)$$

$$v_{c,2} \propto \begin{pmatrix} \frac{\delta_-}{\sqrt{\beta_+}} & \frac{-2\gamma_-}{\beta_+} & \frac{-2\gamma_-}{\beta_+} & \frac{-\sqrt{\beta_+}}{\sqrt{2}} & a \end{pmatrix} \qquad \lambda_{c,2} = -\sqrt{2\beta_+} \qquad (1.91)$$

$$v_{c,3} \propto \begin{pmatrix} \frac{-\delta_-}{\sqrt{\beta_+}} & \frac{-2\gamma_+}{\beta_+} & \frac{-2\gamma_-}{\beta_+} & \frac{\sqrt{\beta_+}}{\sqrt{2}} & a \end{pmatrix} \qquad \lambda_{c,3} = \sqrt{2\beta_+} \qquad (1.92)$$

$$v_{c,4} \propto \begin{pmatrix} \frac{-\beta_-}{\sqrt{\delta_+}} & \frac{2\gamma_+}{\delta_+} & \frac{2\gamma_+}{\delta_+} & \frac{\sqrt{\delta_+}}{\sqrt{2}} & a \end{pmatrix} \qquad \lambda_{c,4} = -\sqrt{2\gamma_+} \qquad (1.93)$$

$$v_{c,5} \propto \begin{pmatrix} \frac{\beta_-}{\sqrt{\delta_+}} & \frac{2\gamma_+}{\delta_+} & \frac{2\gamma_+}{\delta_+} & \frac{-\sqrt{\delta_+}}{\sqrt{2}} & a \end{pmatrix} \qquad \lambda_{c,5} = \sqrt{2\gamma_+}. \qquad (1.94)$$

The zero eigenstate solely occupies the two middle vertices due to their symmetry: G_c is invariant under a swapping of them. However, in all other eigenstates, the (0th) component corresponding to vertex Q have components that are all functions of a.

Let us now divert our attention to C_d. No power of G_d (and, by extension, no polynomial of G_d) ever connects the vertices Q and R, demonstrated with

$$\text{walk}(G_d) = \quad , \quad (1.95)$$

37

$$\text{walk}(G_d^2) = \tag{1.96}$$

$$= \tag{1.97}$$

$$G_d^2 = \tag{1.98}$$

$$G_d^3 = \tag{1.99}$$

$$G_d^4 = \tag{1.100}$$
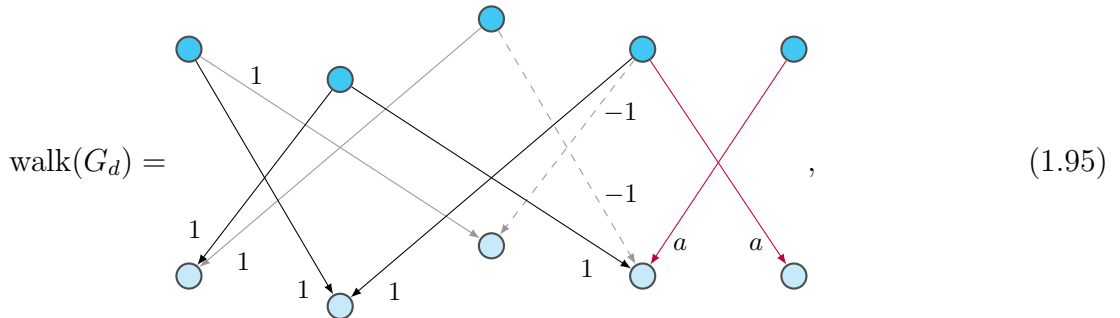
$$G_d^5 = \quad , \tag{1.101}$$

Clearly the even powers, which are simply integer powers of G_d^2, leave vertex Q isolated from the rest of the graph. Upon multiplying these by G, each contribution of a into an edge connected to Q is cancelled out by an alternate path. The opposing signs between the intermediate vertices and vertex R on every power of G_d prohibit any interactions between Q and R, thus any eigenstate with amplitude on Q must be entirely independent of a.

Indeed, the eigenstates and eigenvalues of G_d are

$$v_1 = \frac{1}{2}\begin{pmatrix} -\sqrt{2} & 1 & 1 & 0 & 0 \end{pmatrix} \qquad \lambda_1 = -\sqrt{2} \tag{1.102}$$

$$v_2 = \frac{1}{2}\begin{pmatrix} \sqrt{2} & 1 & 1 & 0 & 0 \end{pmatrix} \qquad \lambda_2 = \sqrt{2} \tag{1.103}$$

$$v_3 = \frac{1}{\sqrt{2a^2(a^2-1)+4}}\begin{pmatrix} 0 & a & -a & a^2-2 & a^2 \end{pmatrix} \qquad \lambda_3 = -\sqrt{a^2+2} \tag{1.104}$$

$$v_4 = \frac{1}{\sqrt{2a^2(a^2-1)+4}}\begin{pmatrix} 0 & a & -a & a^2+2 & a^2 \end{pmatrix} \qquad \lambda_4 = \sqrt{a^2+2} \tag{1.105}$$

$$v_5 = \frac{1}{\sqrt{2a^2+4}}\begin{pmatrix} 0 & -a & a & 0 & 2 \end{pmatrix} \qquad \lambda_5 = 0 \tag{1.106}$$

Chapter 2

Microscopic viewpoint

Introduction

As shown in section 1.5, eigendecomposition generally explores *macroscopic* properties of a system: a perturbation of an edge can have an impact on eigenstate components corresponding to vertices far away. We have also seen that a *parent* graph's macroscopic properties can be linked to those of a *child* graph, such that the child is achieved through some polynomial of the parent*.

One key property of our graph algebra is that it can provide an intuitive graphical insight into how *microscopic* properties of a graph can impact those of its polynomials; we have already seen a glimpse of this with the destructive interference demonstrated in section 1.5.2, where even powers G^{2n} exhibit a disconnect between some of the neighbouring vertices in G.

Of course, G was chosen specifically for this reason. How, then, does one construct a

---

*There exist polynomials $p(G) = G$, such as $p = 1$ and $p = f + 1$, where f is G's characteristic polynomial. Our terminology thus implies that G is its own child and its own parent. The terminology is nonetheless rather useful in most situations.

G for which $p(G)$ has some required local properties?

This section takes a pedagogical approach to introducing a toolkit which can be used for such a purpose, starting from the simplest graphs and working up to those with more complexity.

2.1 Polynomials and loop edges

Consider a graph $S_1(A)$ comprising a single vertex with a loop edge of weight A

$$S_1 = \quad \overset{A}{\circlearrowright} \quad , \qquad \text{walk}(S_1) = \quad A \quad , \qquad \text{adj}(S_1) = (A) . \qquad (2.1)$$

This graph admits a single eigenstate $v = (1)$ with eigenvalue $\lambda = A$.

We can trivially see that the following properties are obeyed:

$$S_1(A) + S_1(B) = S_1(A + B) \qquad (2.2)$$

$$a S_1(A) = S_1(aA) \qquad (2.3)$$

$$S_1(A)^n = S_1(A^n) , \qquad (2.4)$$

thus the polynomial is directly applied to the loop edge weight

$$P(S_1(A)) = S_1(P(A)) \qquad (2.5)$$

A graph with multiple disjoint vertices is impacted in the same way: such a graph can be expressed as the outer sum

$$S(A, B, \ldots) = S_1(A) \oplus S_1(B) \oplus \ldots$$

41

and the polynomial $P(S)$ operates on the component graphs independently as

$$P(S(A, B, \ldots)) = P(S_1(A) \oplus S_1(B) \oplus \ldots) \tag{2.6}$$

$$= P(S_1(A)) \oplus P(S_1(B)) \oplus \ldots \tag{2.7}$$

$$= S_1(P(A)) \oplus S_1(P(B)) \oplus \ldots \tag{2.8}$$

$$= S(P(A), P(B), \ldots) \tag{2.9}$$

$$(2.10)$$

Thus, if a polynomial $P(G)$ of any graph G exists which reduces it into a set of disconnected vertices, then any child $\tilde{P}(P(G))$ for some polynomial $\tilde{P}$ is also disconnected, and the loop edges are directly modified by $\tilde{P}$.

2.2 Edge modification

Consider a graph $S_2(A, B; t_{AB}, t_{BA})$ comprising two vertices with loop edges of weight A and B, an edge from the first vertex to the second with weight t_{AB}, and from the second to the first with weight t_{BA}.

$$(2.11)$$

The two eigenvalues $\lambda_\pm$ of $S_2(A, B; t_{AB}, t_{BA})$ satisfy

$$\lambda_\pm = \mu \pm \sqrt{\Delta^2 + t_{AB} t_{BA}} \qquad \mu = \frac{1}{2}(A + B) \qquad \Delta = \frac{1}{2}(A - B). \tag{2.12}$$

The trivial addition and scalar multiplication goes along the same lines as in section 2.1

$$S_2(A, B; t_{AB}, t_{BA}) + S_2(A', B'; t'_{AB}, t'_{BA}) = S_2(A + A', B + B'; t_{AB} + t'_{AB}, t_{BA} + t'_{BA})$$

$$(2.13)$$

$$aS_2(A, B; t_{AB}, t_{BA}) = S_2(aA, aB; at_{AB}, at_{BA}),$$ (2.14)

but multiplication is somewhat more involved. Let us begin with a squaring operation

$$(2.15)$$

$$(2.16)$$

$$S_2(A, B; t_{AB}, t_{BA})^2 = S_2\big(A^2 + t_{BA}t_{AB}, B^2 + t_{AB}t_{BA}; (A + B)t_{AB}, (A + B)t_{BA}\big).$$

$$(2.17)$$

As in section 2.1, the weight of the loop edges is modified through the polynomial $p : x \to x^2$, but an extra term $t_{AB}t_{BA}$ is introduced. The weight of the edge linking the two vertices has also been changed. From the walk graph approach, the new loop edges correspond to the sum of the walks

- Remaining in place for two steps

- Walking to the other vertex and back

and the new edges correspond to the walks

- Remaining in place, then walking to the other vertex.

- Walking to the other vertex, then remaining in place.

An important special case of this result is that of $A + B = 0$, where the edge between vertices A and B reduces in S_2^2, separating the resulting graph into two independent graphs of a single vertex each.

$$\left(\begin{array}{c} \beta \quad \overset{t_{AB}}{\underset{t_{BA}}{\rightleftarrows}} \quad -\beta \end{array} \right)^2 = \begin{array}{cc} \beta^2 + t_{BA}t_{AB} & \beta^2 + t_{AB}t_{BA} \end{array} \tag{2.18}$$

$$= \begin{array}{cc} \beta^2 + t_{AB}t_{BA} & \oplus & \beta^2 + t_{AB}t_{BA} \end{array}, \tag{2.19}$$

or, equivalently,

$$S_2(\beta, -\beta; t_{AB}, t_{BA})^2 = S_2\big(\beta^2 + t_{BA}t_{AB}, \beta^2 + t_{AB}t_{BA}; 0, 0\big) \tag{2.20}$$

$$= S_1\big(\beta^2 + t_{AB}t_{BA}\big) \oplus S_1(\beta^2 + t_{AB}t_{BA}) \tag{2.21}$$

All configurations of S_2 can be brought into this form through a subtraction by the mean loop edge weight, and thus there exists a second order polynomial for each S_2 which eliminates the edge between the two vertices

$$S_2(A, B; t_{AB}, t_{BA}) - \mu = S_2(\Delta, -\Delta; t_{AB}, t_{BA}) \tag{2.22}$$

$$(S_2(A, B; t) - \mu)^2 = S_2(A, B; t_{AB}, t_{BA})^2 - 2\mu S_2(A, B; t_{AB}, t_{BA}) + \mu^2 \qquad (2.23)$$

$$= S_2\big(\Delta^2 + t_{AB}t_{BA}, \Delta^2 + t_{AB}t_{BA}; 0, 0\big) \qquad (2.24)$$

Thus, given

$$P : X \to X^2 - 2\mu X + \mu^2,$$

$$P : S_2(A, B; t_{AB}, t_{BA}) \to S_1(\Delta^2 + t_{BA}t_{AB}) \oplus S_1(\Delta^2 + t_{AB}t_{BA}). \qquad (2.25)$$

$S_1(\Delta^2 + t_{AB}t_{BA})$ has a single eigenvalue $\Delta^2 + t_{AB}t_{BA}$, and the direct sum of two such graphs thus has two eigenvalues of the same value $\Delta^2 + t_{AB}t_{BA}$. As we have seen, we can solve

$$P(\lambda) = \Delta^2 + t_{AB}t_{BA}$$

to retrieve the eigenvalues $\lambda_\pm$ of S_2

$$0 = \lambda^2 - 2\mu\lambda + \mu^2 - \Delta^2 - t_{AB}t_{BA}$$

$$\lambda = \mu \pm \frac{1}{2}\sqrt{4\mu^2 - 4\mu^2 + 4\Delta^2 + 4t_{AB}t_{BA}}$$

$$= \mu \pm \sqrt{\Delta^2 + t_{AB}t_{BA}},$$

in agreement with eq. (2.12).

This should come as no surprise, because (through the Cayley-Hamilton theorem) a graph G solves its own characteristic equation C_G

$$C_G(G) = 0, \qquad (2.26)$$

and, in this case,

$$P(G) = C_G(G) + \Delta^2 + t_{AB}t_{BA}. \qquad (2.27)$$

45

This graph demonstrates our second principle: polynomials can act to remove edges between connected vertices. In two-vertex graphs, this is always achievable through some polynomial, though larger graphs might exhibit more complex interactions that cannot be broken down in this manner. The distinguishing feature is whether or not the graph is what we shall call *pseudo-bipartite*, that is, whether the vertices can grouped into two sets such that no vertex in one set has an edge to any other vertex in the same set *other than itself*, and such that the loop edge weights of all vertices in such a set are identical. In this case, subtracting the mean μ of the two sets' loop edge weights from the graph G provides a graph $G - \mu$ in which the two vertex sets have equal but opposite loop edge weights.

Through the mechanism described in this section the square $(G - \mu)^2$ of such a graph is devoid of edges between vertices of different sets, such that the sets can be separated.

In some graphs, then, simple polynomials can result in multiple independent graphs which can be analysed in isolation to build a picture of the original graph, as we shall exploit in section 3.4. In some other graphs, a child system may exhibit topological defects, as explored in chapter 4, with signatures of topological behaviour appearing in the eigenspectrum of the parent system.

2.3   Joining next-nearest neighbours

As well as eliminating an edge between *nearest* neighbours (those reachable with a walk of length 1), we can introduce an edge between *next-nearest* neighbours (those reachable with a walk of length 2). At least three vertices are needed, so we begin with a quick overview of three-vertex graphs and move on to a chain.

Let us extend S_2 by adding a new vertex C and connecting it to both A and B, and

let us call this graph $S_3(A, B, C; t_{AB}, t_{AC}, t_{BA}, t_{BC}, t_{CA}, t_{CB})$, comprising three vertices, A, B, C with loop edges of weight A, B, C, connected through edges t_{ij} (where i, j are distinct vertices labelled by their weight A, B, C)

$$(2.28)$$
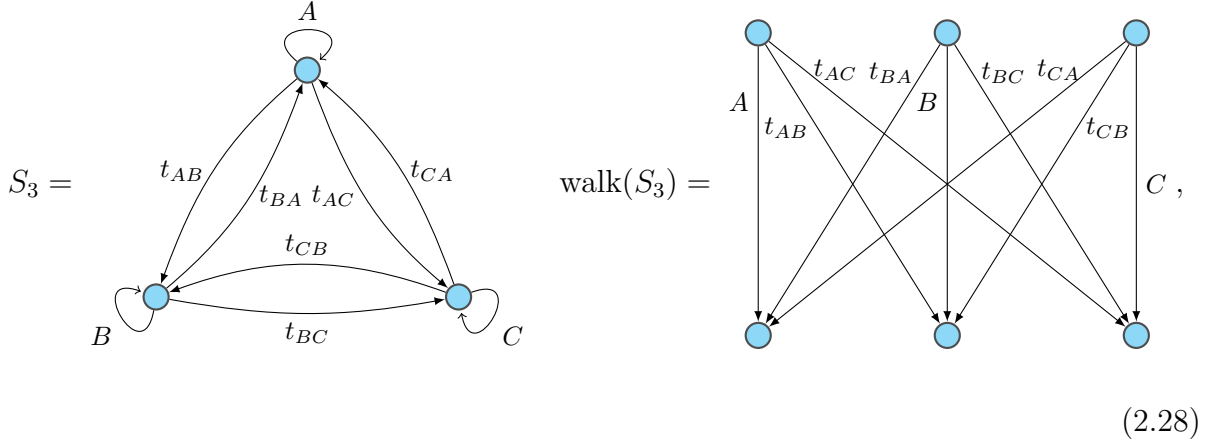
$$\text{adj}(S_3) = \begin{pmatrix} A & t_{BA} & t_{CA} \\ t_{AB} & B & t_{CB} \\ t_{AC} & t_{BC} & C \end{pmatrix}. \qquad (2.29)$$

S_3 squares as
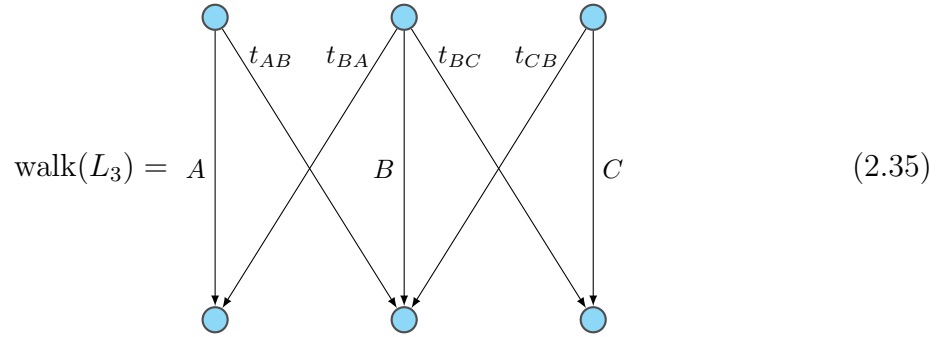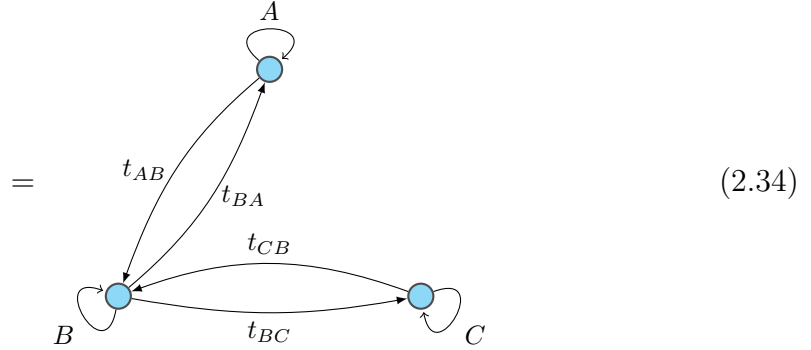
$$S_3(A, B, C, t_{AB}, \ldots)^2 = S_3(A', B', C', t'_{AB}, \ldots) \qquad (2.30)$$

with

$$X' = X^2 + t_{XY}t_{YX} + t_{XZ}t_{XZ} \qquad (2.31)$$

$$t'_{XY} = t_{XY}(X + Y) + t_{XZ}t_{ZY} \qquad (2.32)$$

for all $X, Y, Z \in \{A, B, C\}, X \neq Y \neq Z$

Now we shall move on to a special case: the chain $L_3(A, B, C, t_{AB}, t_{BA}, t_{BC}, t_{CB})$ formed by removing the edges between A and C,

47

$$L_3 = S_3(A, B, C, t_{AB}, 0, t_{BA}, t_{BC}, 0, t_{CB}) \tag{2.33}$$

$$= \tag{2.34}$$

$$\text{walk}(L_3) = \tag{2.35}$$

Although L_3 has a disconnect between A and C, they become connected in $(L_3)^2$ by edges of weight $t_{AB}t_{BC}, t_{CB}t_{BC}$.

$$(L_3(A, B, C))^2 = \qquad , \tag{2.36}$$
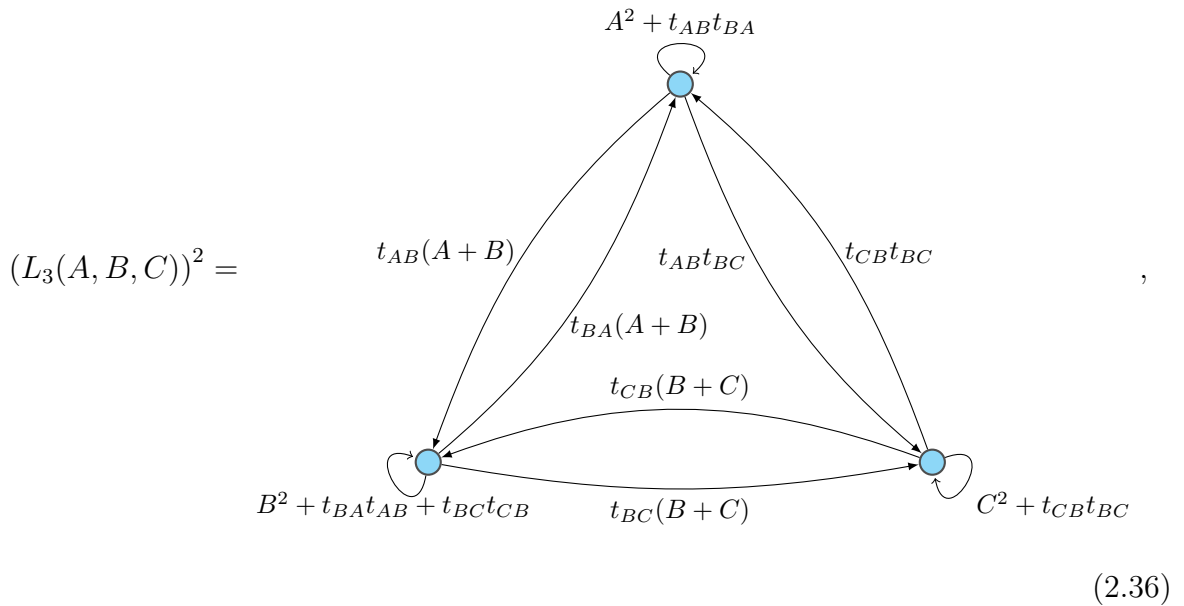
As these edges are single term multiples of existing bonds, there does not exist a configuration of L_3 which does not exhibit an edge between A and C in its square, apart from those with at least one absent edge. Furthermore, the edges between A and B can be eliminated in the square if $A + B = 0$ and those between B and C if $B + C = 0$
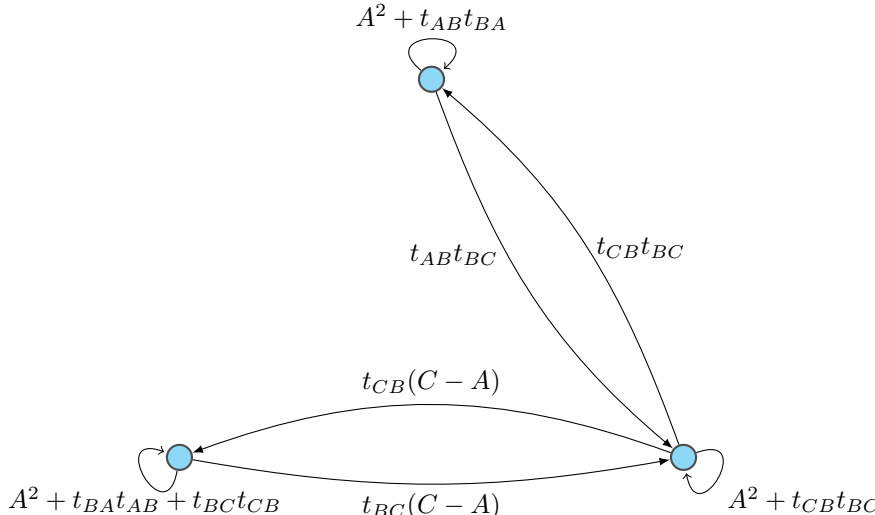
$$
(L_3(A, -A, C))^2 = \quad
\begin{array}{c}
A^2 + t_{AB}t_{BA} \\[2pt]
\bullet \\[4pt]
t_{AB}t_{BC} \qquad t_{CB}t_{BC} \\[6pt]
t_{CB}(C - A) \\
\bullet \longleftrightarrow \bullet \\
A^2 + t_{BA}t_{AB} + t_{BC}t_{CB} \qquad t_{BC}(C - A) \qquad A^2 + t_{CB}t_{BC}
\end{array}
\tag{2.37}
$$

If $A = C, B = -A$, then both of these conditions are met and the only remaining edges will be between A and C
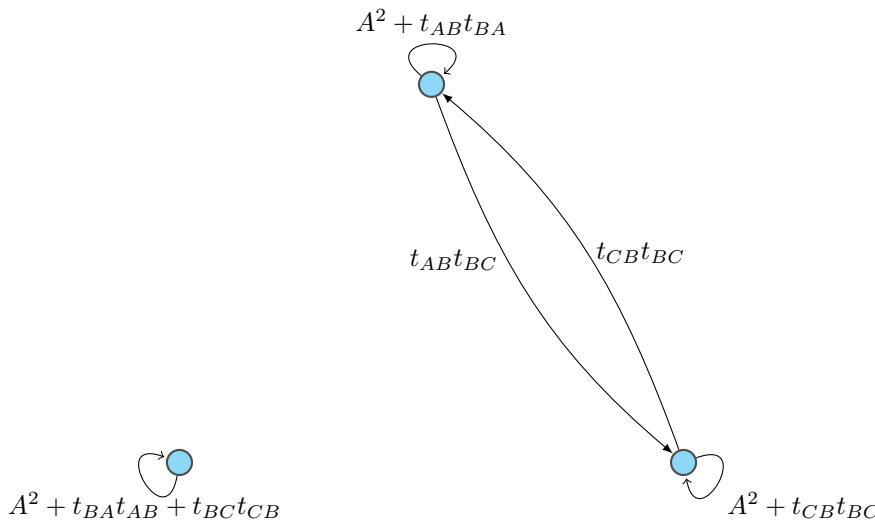
$$
(L_3(A, -A, A))^2 = \quad
\begin{array}{c}
A^2 + t_{AB}t_{BA} \\[2pt]
\bullet \\[4pt]
t_{AB}t_{BC} \qquad t_{CB}t_{BC} \\[6pt]
\bullet \qquad\qquad\qquad \bullet \\
A^2 + t_{BA}t_{AB} + t_{BC}t_{CB} \qquad\qquad A^2 + t_{CB}t_{BC}
\end{array}
\tag{2.38}
$$

Note that $L_3(A, -A, C)^2$ is also a chain, and upon swapping the labelling of B and C we find another L_3

$$L_3(A, -A, C) \sim L_3\Big(A^2 + t_{AB}t_{BA}, \ A^2 + t_{CA}t_{AC}, \ A^2 + t_{BA}t_{AB} + t_{BC}t_{CB};$$

$$t_{AB}t_{BC}, \ t_{CB}t_{BC}, \ t_{CB}(C - A), \ t_{BC}(C - A)\Big) \qquad (2.39)$$

2.4 Interference

We have now seen that next nearest neighbours can become connected by an edge under a second power, and that this is unavoidable in a three-site chain without absent edges. It is, however, possible to produce a graph in which the second power does not exhibit next-nearest edges, as we have seen in section 1.5.2. The trick is to introduce an additional intermediate vertex with edges chosen such that the multiplicative path between two next-nearest neighbours cancels out through destructive interference.

Consider, then, a graph C_4 in the form of a square

$$C_4 = \qquad\qquad\qquad\qquad \mathrm{adj}(C_4) = \begin{pmatrix} A & t_{BA} & t_{CA} & 0 \\ t_{AB} & B & 0 & t_{BD} \\ t_{AC} & 0 & C & t_{DC} \\ 0 & t_{BD} & t_{CD} & D \end{pmatrix}$$

$$\mathrm{walk}(C_4) = \qquad\qquad\qquad\qquad\qquad\qquad\qquad\qquad\qquad\qquad\qquad (2.40)$$

50

Squaring C_4 results in a new graph with edges

$$A' = A^2 + t_{BA}t_{AB} + t_{CA}t_{AC} \qquad (2.41)$$

$$B' = B^2 + t_{DB}t_{BD} + t_{AB}t_{BA} \qquad (2.42)$$

$$C' = C^2 + t_{CA}t_{AC} + t_{DC}t_{CD} \qquad (2.43)$$

$$D' = D^2 + t_{CD}t_{DC} + t_{DB}t_{BD} \qquad (2.44)$$

$$t'_{XY} = t_{XY}(X + Y), \qquad (2.45)$$

where t_{XY} are existing edges in C_4, and four additional edges connecting the next nearest neighbours

$$t'_{AD} = t_{BD}t_{AB} + t_{CD}t_{AC} \qquad (2.46)$$

$$t'_{DA} = t_{BA}t_{DB} + t_{CA}t_{DC} \qquad (2.47)$$

$$t'_{BC} = t_{AC}t_{BA} + t_{DC}t_{BD} \qquad (2.48)$$

$$t'_{CB} = t_{AB}t_{CA} + t_{DB}t_{CD} \qquad (2.49)$$

We can cancel out the vertex between the next nearest neighbours by restricting edges such that the terms above cancel. For example, with

$$t_{AB} = -\alpha \qquad\qquad t_{BD} = \frac{t_{CD}t_{AC}}{\alpha} \qquad (2.50)$$

$$t_{BA} = -\beta \qquad\qquad t_{DB} = \frac{t_{CD}t_{AC}}{\beta} \qquad (2.51)$$

the edges t'_{AD} (through eq. (2.50)) and t_{BA} (through eq. (2.51)) are cancelled out. We can also cancel out the edges t'_{BC} and t'_{CB} simply by choosing

$$t_{CD} = \gamma \qquad\qquad\qquad t_{DC} = \frac{\alpha\beta}{\gamma}$$

such that

Left graph (raised to the power 2): vertices A, B, C, D with edges labelled $-\alpha$, $-\beta$ (between A and B); t_{CA}, t_{AC} (between A and C); $\frac{t_{CA}\alpha}{\gamma}$, $\frac{t_{AC}\gamma}{\alpha}$ (between B and D); γ, $\frac{\alpha\beta}{\gamma}$ (between C and D).

$=$

Right graph: vertices with self-loops A^2, B^2, C^2, D^2; edges labelled $-\alpha(A+B)$, $-\beta(A+B)$ (between A^2 and B^2); $t_{CA}(A+C)$, $t_{AC}(A+C)$ (between A^2 and C^2); $\frac{\alpha t_{CA}}{\gamma}(B+D)$, $\frac{\gamma t_{AC}}{\alpha}(B+D)$ (between B^2 and D^2); $\gamma(C+D)$, $\frac{\alpha\beta}{\gamma}(C+D)$ (between C^2 and D^2).

$$+\ (t_{AC}t_{CA} + \alpha\beta), \tag{2.52}$$

where for notational ease we imply the final term multiplies with the identity.

Thus, along with a choice of A, B, C, D, t_{AC} and t_{CA}, we have the choice of three free parameters α, β, δ from which to produce a graph which exhibits destructive interference between (A and D) and (B and C), resulting in another C_4, after raising to the power 2.

As we have seen in section 2.2, we can separate neighbouring vertices by providing them with opposing loop weights. For example,

- $A = \Delta, B = -\Delta$ separates A and B,

- $A = \Delta, B = -\Delta, C = \Delta, D = -\Delta$ separates A and B and C and D, resulting in a separable graph of two S_2 subgraphs.

- $A = \Delta, B = -\Delta, C = -\Delta, D = \Delta$ separates all four sites, resulting in four isolated vertices of self-loop weight Δ^2.

2.5 Connecting distant neighbours

We have so far looked at graphs with a small number of vertices, and it is clear that general graphs can become rather complex under a polynomial unless they obey specific requirements, such as presenting destructive interference at walks of a certain length, or unless the polynomial is specifically chosen to exploit the Cayley-Hamilton theorem. Graphs that do not obey such requirements, particularly connected graphs with edges of strictly positive weight, increase their number of edges until their maximum number of edges $M(M+1)/2$ (for a graph with M vertices) is reached.

For this subsection, we will look at a simpler graph, the *cycle graph* C_N, with N vertices, arranged as an N-gon such that each vertex has two neighbours, with undirected edges of unit weight, e.g

$$\text{(2.53)}$$
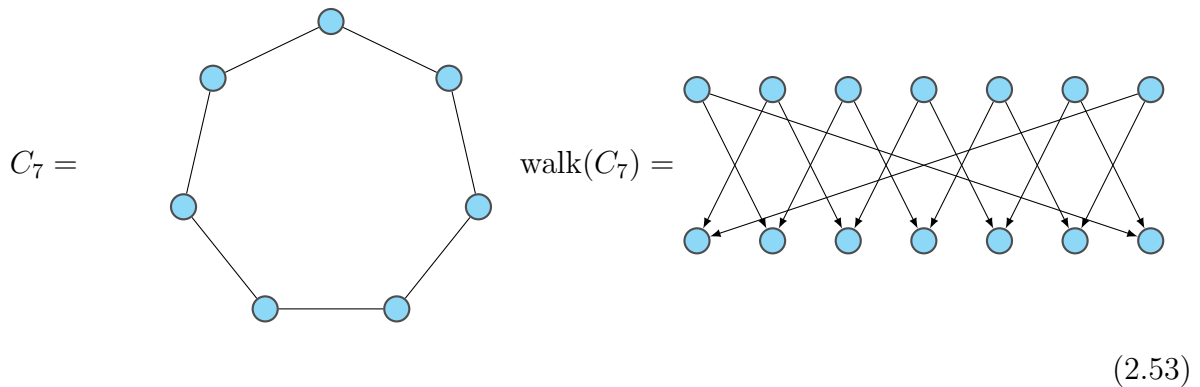
As there are no self-loops in C_7, C_7^2 will lose all edges between those that are neighbours in C_7 (as the sum of self-loops between nearest neighbours always sums to zero), but will exhibit edges between the next nearest neighbours of unit weight and new vertex loops of weight $1^2 + 1^2 = 2$.

$$\left(\begin{array}{c} \\ \\ \\ \\ \end{array} \right)^2 = \qquad\qquad\qquad\qquad (2.54)$$

Let

$$p_0 : x \to 1 \qquad\qquad (2.55)$$

$$p_1 : x \to x \qquad\qquad (2.56)$$

$$p_2 : x \to x^2 - 2 \qquad\qquad (2.57)$$

be polynomials which map C_7 to a graph with only loop edges, a graph with only nearest neighbour edges and a graph with only next-nearest neighbour edges respectively. Can we find a polynomial p_3 which maps C_7 to a graph with only 3rd nearest neighbour edges?

$$\left(\begin{array}{c} \\ \\ \\ \\ \end{array} \right)^3 = \qquad\qquad\qquad\qquad (2.58)$$

$$= p_3(C_7) + 3C_7 \qquad\qquad (2.59)$$

$$\Rightarrow p_3 : x \to x^3 - 3x. \qquad\qquad (2.60)$$

54

We now have three polynomials that can generate a 7-vertex cycle with required n^{th}-neighbour edge weights

$$wp_0(C_7) + xp_1(C_7) + yp_2(C_7) + zp_3(C_7) = \qquad\qquad (2.61)$$
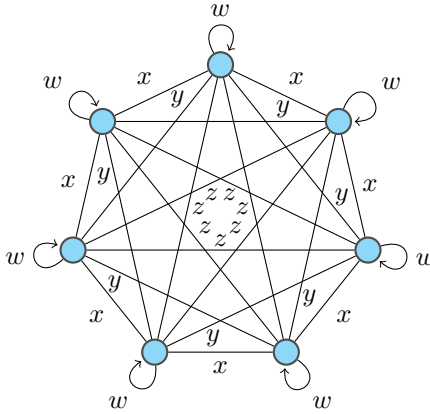
such that we can generate the *complete* graph
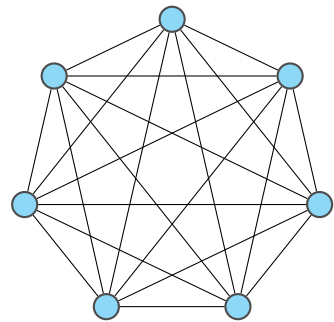
$$\sum_{i=1}^{3} p_i(C_7) = \qquad\qquad (2.62)$$

with knowledge that

$$\left(\sum_{i=1}^{3} p_i\right) : \lambda \to \tilde{\lambda} \qquad\qquad (2.63)$$

maps each eigenvalue of C_7 to that of its complete equivalent.

This is not, of course, a feature specific to C_7. The polynomials p_i are a result of the local structure of cycle graphs, and they extend as

$$p_0 : x \to 1$$

$$p_1 : x \to x$$

$$p_2 : x \to x^2 - 2$$

$$p_k : x \to x p_{k-1}(x) - p_{k-2}(x) \qquad (i > 2). \qquad (2.64)$$

We can prove the form of p_k by induction. Imagine some C_N with large N, and assume p_{k-2} and p_{k-1} are polynomials that map C_N to a graph with only the $(k-2)^{\text{th}}$ and $(k-1)^{\text{th}}$ neighbours connected with unit edge weight respectively $(k > 2)$. Then we can look at the local neighbourhood of some vertex V_i by multiplying $p_{k-1}(C_N)$ with a walk vector $v_j = \delta_{ij}$

$$(2.65)$$

$$(2.66)$$
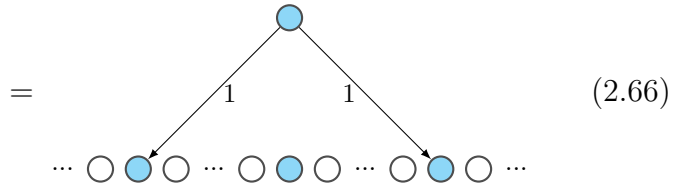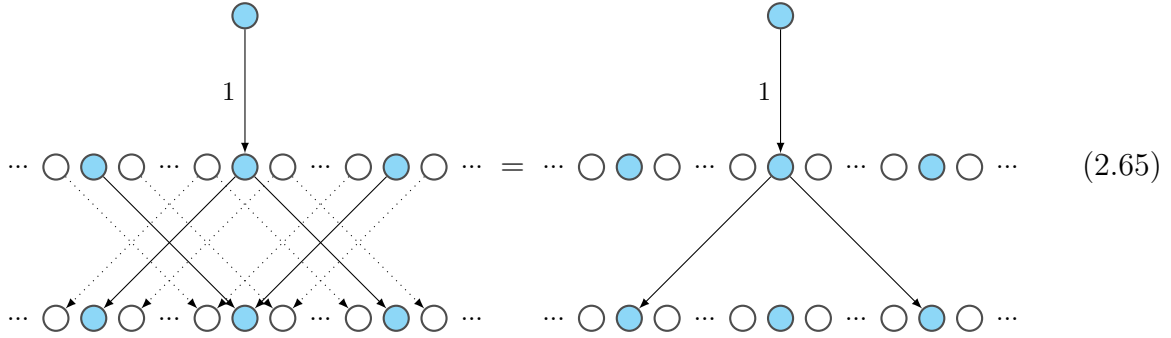
Now we can multiply by C_N

$$(2.67)$$
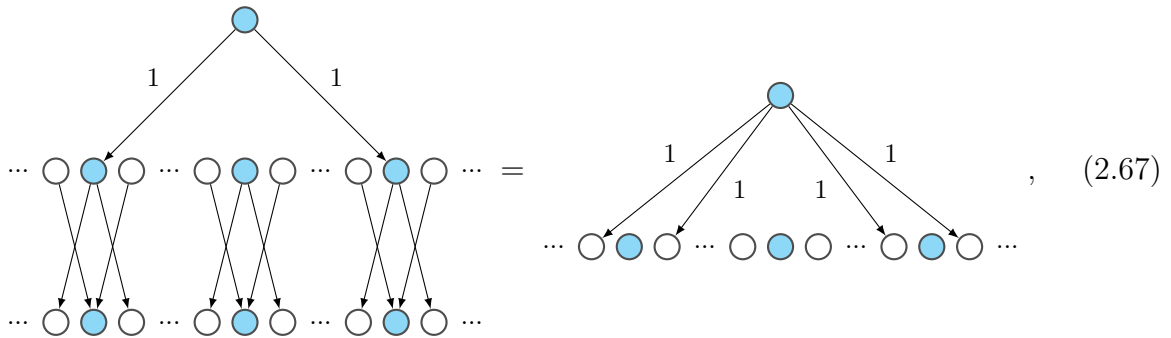
thus

$$C_N p_{k-1}(C_N) = p_k(C_N) + p_{k-2}(C_N)$$

$$p_k : x \rightarrow x p_{k-1}(x) - p_{k-2}(x) \qquad \square \qquad (2.68)$$

Through this, we can describe a cycle graph $f(C_N)$ equipped with arbitrarily weighted n^{th}-neighbour edges through the polynomial

$$f = a p_0 + b p_1 + c p_2 + d p_3 + \ldots \qquad (2.69)$$

such that each eigenstate and eigenvalue pair (v, λ) obeying

$$C_N v = \lambda v \qquad (2.70)$$

will also obey

$$f(C_N) v = f(\lambda) v. \qquad (2.71)$$

The polynomials p_k described here are related to the Chebyshev polynomials of the first kind[22],

$$T_0(x) = 1 \qquad (2.72)$$

$$T_1(x) = x \qquad (2.73)$$

$$T_k(x) = 2x T_{k-1}(x) - T_{k-2}(x). \qquad (2.74)$$

The kth Chebyshev polynomial indeed maps the nearest-neighbour cycle with edge weights $^1\!/_2$ to the kth nearest-neighbour cycle with edge weights $^1\!/_2$. This distinction manifests itself in the trigonometric transformations provided by the polynomials,

$$T_k(\cos(x)) = \cos(kx), \qquad\qquad p_k(2\cos(x)) = 2\cos(kx), \qquad (2.75)$$

which becomes particularly useful in section 3.1, where we will relate the eigenspectra of general chains of infinite length to the eigenspectrum of the unit nearest-neighbour infinite chain.

2.6 Periodic Systems

M disconnected copies of a graph G can be written as a direct sum of G with itself M times or, equivalently, a tensor product of $\mathbf{1}_M$ and G. Such an operation will be used heavily in this section, so let us introduce the shorter notation

$$G^{\oplus M} \equiv \mathbf{1}_M \otimes G, \tag{2.76}$$

and let us denote the M copies of G as $g_0, ..., g_{M-1}$.

For example, if

$$\text{walk}(\tilde{G}) = \tag{2.77}$$

then

$$\text{walk}(\tilde{G}^{\oplus 3}) = \tag{2.78}$$

where readers with a colour copy will see the vertices of each copy g_0, g_1, g_2 in blue (left), red (centre), and green (right) respectively.

For such a repeating graph, we can introduce connectivity between components with use of a *translation* graph, comprising edges directed from every vertex in each g_m to the corresponding vertex in $g_{(m+1 \mod M)}$. Let T be the translation graph of $G^{\oplus 3}$, then

$$\text{walk}(T) = \qquad\qquad\qquad\qquad\qquad\qquad\qquad\qquad (2.79)$$

$$\text{walk}(T^{-1}) = \qquad\qquad\qquad\qquad\qquad\qquad\qquad , \qquad (2.80)$$
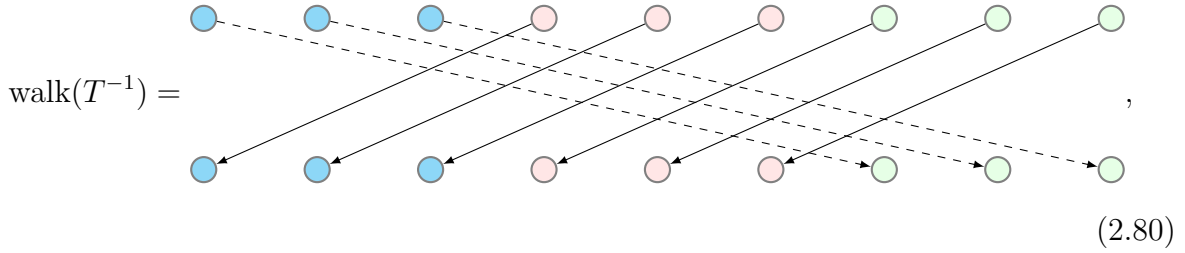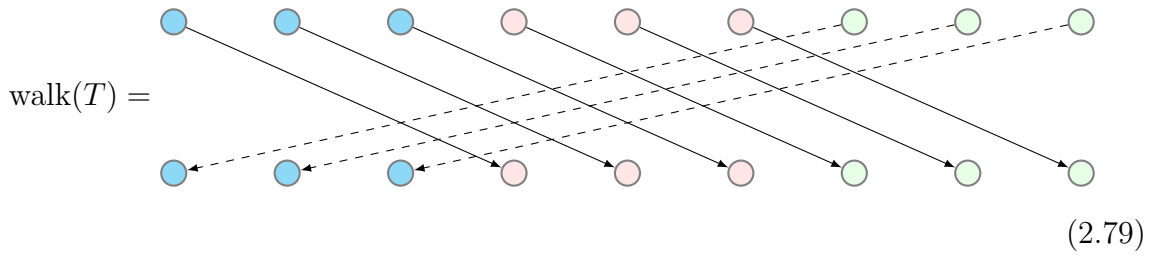
where the dashed lines are used as a visual aid to highlight the wrap-around effect of the modulus operation.

Consider that we want an edge from a vertex u in each g_m to a vertex v in $g_{m+1 \mod M}$. We can represent this inter-cell connectivity with two pieces of information: a graph R in which there exists an edge from the vertex corresponding to u to the vertex corresponding to v, and a translation. As an example, consider the graph $\tilde{R}$ with

$$\text{walk}(\tilde{R}) = \qquad\qquad\qquad\qquad\qquad\qquad\qquad (2.81)$$

then

$$\text{walk}\left(\tilde{R}^{\oplus 3}\right) = \qquad\qquad\qquad\qquad\qquad\qquad\qquad\qquad , \tag{2.82}$$

which we can multiply by the translation graph to obtain

$$\text{walk}\left(T\tilde{R}^{\oplus 3}\right) = \qquad\qquad\qquad\qquad\qquad\qquad\qquad\qquad \tag{2.83}$$

$$= \qquad\qquad\qquad\qquad\qquad\qquad\qquad\qquad . \tag{2.84}$$

Thus $T\tilde{R}^{\oplus M}$ describes connectivity with neighbours to the right. We can also form a graph $\tilde{L}$ and use it to describe connectivity with neighbours to the left with $\tilde{L}T^{-1}$. Consider the graph $\tilde{L}$ with

$$\text{walk}(\tilde{L}) = \qquad\qquad\qquad\qquad\qquad\qquad \tag{2.85}$$

then

$$\text{walk}(T^{-1}\tilde{L}^{\oplus 3}) = \quad$$

$$(2.86)$$

We can now describe a periodic graph F, constructed from the unit cell $\tilde{G}$, with inter-cell edges to graphs on the right defined by $\tilde{R}$ and on the left defined by $\tilde{L}$, through the expression

$$F = \tilde{G}^{\oplus M} + T\tilde{R}^{\oplus M} + T^{-1}\tilde{L}^{\oplus M} \qquad (2.87)$$

such that

$$\text{adj}(F) = \begin{pmatrix} \text{adj}(\tilde{G}) & \text{adj}(\tilde{L}) & \mathbf{0} & \dots & \mathbf{0} & \text{adj}(\tilde{R}) \\ \text{adj}(\tilde{R}) & \text{adj}(\tilde{G}) & \text{adj}(\tilde{L}) & \ddots & \mathbf{0} & \mathbf{0} \\ \mathbf{0} & \text{adj}(\tilde{R}) & \text{adj}(\tilde{G}) & \ddots & \mathbf{0} & \mathbf{0} \\ \vdots & \ddots & \ddots & \ddots & \ddots & \vdots \\ \mathbf{0} & \mathbf{0} & \mathbf{0} & \ddots & \text{adj}(\tilde{G}) & \text{adj}(\tilde{L}) \\ \text{adj}(\tilde{L}) & \mathbf{0} & \mathbf{0} & \dots & \text{adj}(\tilde{R}) & \text{adj}(\tilde{G}) \end{pmatrix}. \qquad (2.88)$$

As T obeys $T^M = 1$, its eigenvalues $\lambda_{T,m}$ are M^{th} roots of unity

$$\lambda_{T,m} = \exp\left(\frac{2i\pi m}{M}\right), \qquad m \in [0 .. M-1]. \qquad (2.89)$$

Consider some graph X on the same vertices as G, such that $X^{\oplus M}$ comprises only edges between vertices within in the same cell.

$$X = \quad$$

$$(2.90)$$

Then $TX^{\oplus M}$ is a graph comprising edges from the same input layer as $X^{\oplus M}$, to edges from the output layer translated by one unit cell,

$$TX^{\oplus M} = \quad\quad\quad\quad\quad\quad\quad\quad\quad\quad\quad\quad\quad\quad\quad\quad\quad\quad (2.91)$$

$$= \quad\quad\quad\quad\quad\quad\quad\quad\quad\quad\quad\quad\quad\quad\quad\quad\quad\quad\quad . \quad (2.92)$$

Likewise,

$$X^{\oplus M}T = \quad\quad\quad\quad\quad\quad\quad\quad\quad\quad\quad\quad\quad\quad\quad\quad\quad\quad (2.93)$$

$$= \quad\quad\quad\quad\quad\quad\quad\quad\quad\quad\quad\quad\quad\quad\quad\quad\quad\quad\quad . \quad (2.94)$$
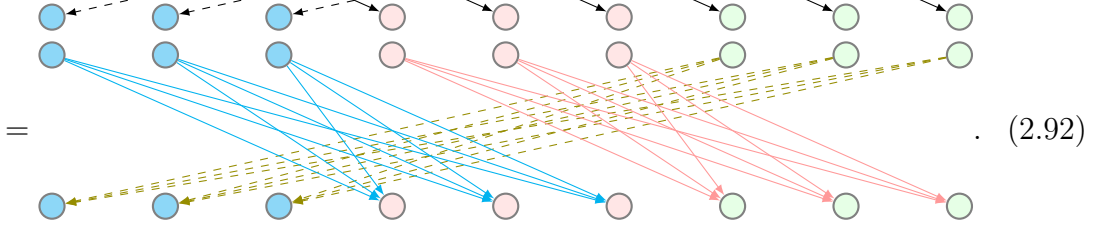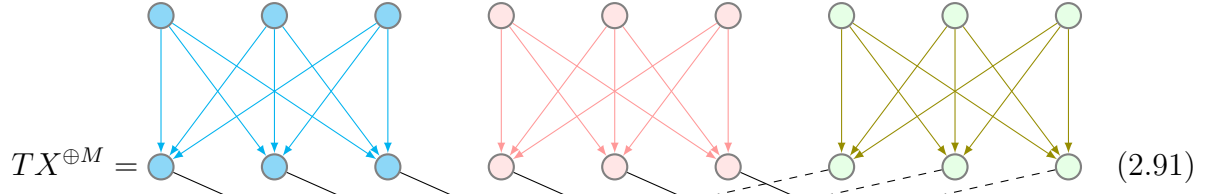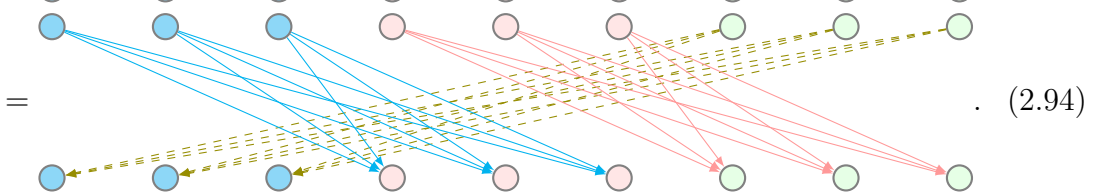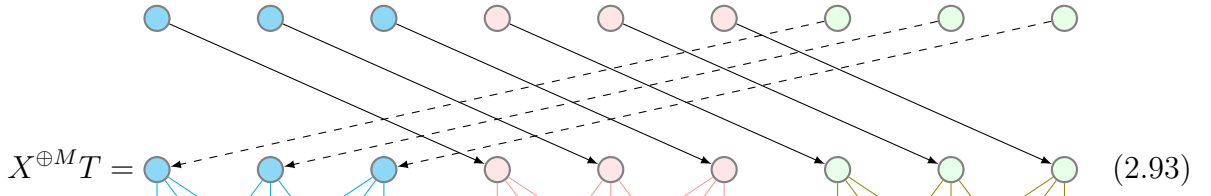
Thus T commutes with any such unit graph, including $G^{\oplus M}$, $R^{\oplus M}$ and $L^{\oplus M}$. It thus commutes with F, which is a linear combination of these unit graphs and T itself. Because of this, we can separate the Hilbert space $\mathcal{F}$ acted on by F into the eigenspaces $\mathcal{F}_n$ of T, such that

$$\mathcal{F} = \bigoplus_{m=0}^{M-1} \mathcal{F}_m, \quad\quad\quad\quad\quad (2.95)$$

where T has eigenvalue $\lambda_{T,m}$ throughout $\mathcal{F}_m$. In each such eigenspace, we can project F into a graph $\tilde{F}(\lambda_{T,m}) \in \mathcal{F}_m$ by substituting the operator T with its eigenvalue $\lambda_{T,m}$,

$$\tilde{F}(\lambda_{T,m}) = \tilde{G}^{\oplus M} + \lambda_{T,m}\tilde{R}^{\oplus M} + \lambda_{T,m}^{-1}\tilde{L}^{\oplus M}, \tag{2.96}$$

$$= \tilde{f}_0(\lambda_{T,m}) \oplus \ldots \oplus \tilde{f}_{M-1}(\lambda_{T,m}) \tag{2.97}$$

where

$$\tilde{f}_n(\lambda_{T,m}) = \tilde{G} + \lambda_{T,m}\tilde{R} + \lambda_{T,m}^{-1}\tilde{L}. \tag{2.98}$$

Even though each subgraph $\tilde{f}_n(\lambda_{T,m})$ is independent from its neighbours, the total algebraic multiplicity of $\tilde{F}(\lambda_{T,m})$ is N: $\mathcal{F}_m$ enforces a translation eigenvalue of $\lambda_{T,m}$. As such, we can eigendecompose $\tilde{f}_0(\lambda_{T,m})$ and expand each of its eigenstates

$$\tilde{f}_0(\lambda_{T,m})v = \lambda v \tag{2.99}$$

into a full eigenstate V of F through

$$V = v \oplus \left(\lambda_{T,m}^1 v\right) \oplus \ldots \oplus \left(\lambda_{T,m}^{M-1} v\right) \tag{2.100}$$

$$\tilde{F}(\lambda_{T,m})V = \lambda V \tag{2.101}$$

As a result, we can fully eigendecompose F through analysis of the smaller subgraphs f formed as a superposition of its unit cell $\tilde{G}$ and its neighbour connection matrices $\tilde{R}$ and $\tilde{L}$. An example of this process is provided in example 1.

If we take the number of repetitions to infinity, we can represent an infinite, periodic graph. The translation eigenvalues are thus the rational[†] roots of unity

$$\lambda_{T,\theta} = \exp\left(2\pi i \theta\right) \qquad\qquad \theta \in \mathbb{Q} \tag{2.102}$$

[†]The number of repetitions is *countable*, thus the number of translation eigenspaces must also be countable. As such, this method does not extend to irrational eigenvalues of the translation graph.

and we can separately analyse translation eigenspaces through the graphs $\tilde{f}(\theta)$. This result is one that condensed matter theorists are particularly familiar with: it is nothing less than Bloch's Theorem[8].

It is important to use caution when dealing with infinite systems. So far we have only looked at generating infinite graphs that are nonetheless *locally finite*, meaning that although there are an infinite number of vertices, each vertex has a finite number of neighbours. As a result, each row and column of the adjacency matrix has a finite number of nonzero elements, as does each row and column of any finite-degree polynomial of the adjacency matrix, which is well defined. In this formalism, it is valid to calculate the eigenspectra of finite degree polynomials of locally finite periodic systems[‡].

If, instead, we wish to use polynomials of infinite degree, we may end up with a *locally infinite* child graph, such that each vertex has an infinite number of neighbours. The adjacency matrix of a locally infinite hermitian graph has an infinite number of nonzero elements in each row and column, and multiplication with such matrices is undefined in general[24]. Validity of such multiplications is continent on the convergence of the summation used for calculating each element of the result. Examples of the valid and an invalid cases are provided in section 3.1.

Example 1 (*Translation eigenspace projection*)**.** Let us use the graphs $\tilde{G}, \tilde{L}, \tilde{R}$ from above

$$\text{walk}(\tilde{G}) = \qquad\qquad\qquad\qquad (2.103)$$

[‡]An in-depth discussion of the eigendecomposition of locally finite graphs can be found in [23]

$$\text{walk}(\tilde{L}) = \qquad\qquad\qquad\qquad\qquad\qquad\qquad\qquad (2.104)$$

$$\text{walk}(\tilde{R}) = \qquad\qquad\qquad\qquad\qquad\qquad\qquad\qquad (2.105)$$

and create a periodic graph by

$$F = \tilde{G}^{\oplus 3} + T\tilde{R}^{\oplus 3} + T^{-1}\tilde{L}^{\oplus 3} \qquad\qquad\qquad\qquad (2.106)$$

$$\text{walk}(F) = \qquad\qquad\qquad\qquad\qquad\qquad\qquad\qquad , $$

$$(2.107)$$

which we may visualise in a wrapped-around form as

$$F = \qquad\qquad\qquad\qquad\qquad\qquad\qquad\qquad . \qquad (2.108)$$
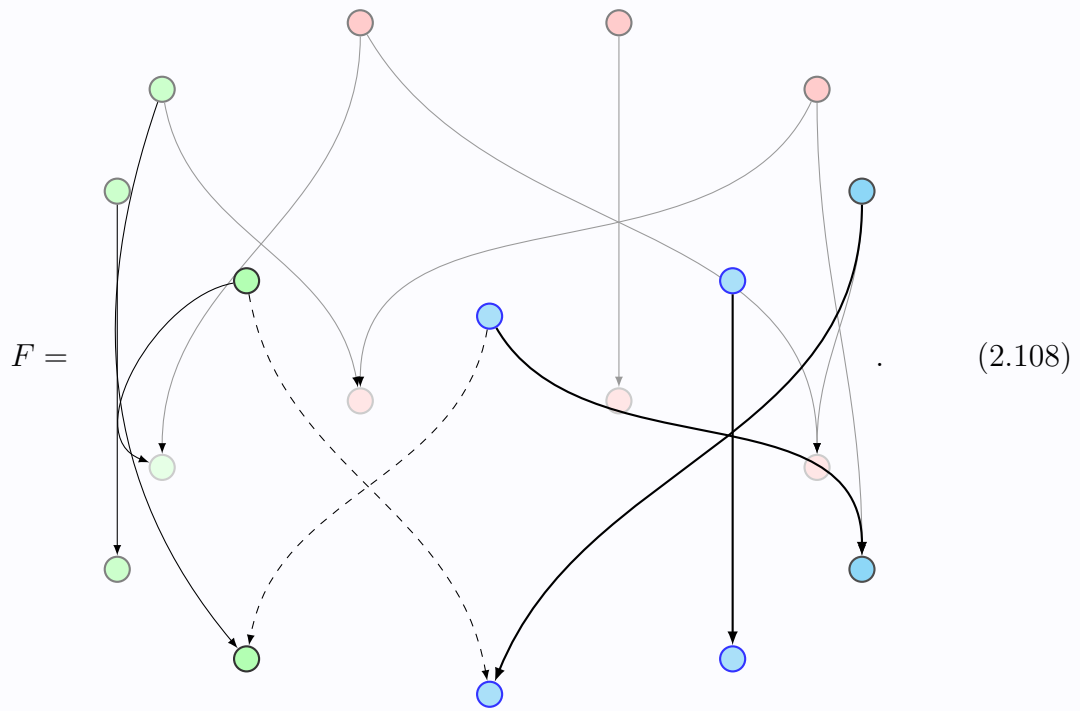
We can easily verify that F and T commute, through

$$\text{walk}(FT) =$$

$$(2.109)$$

66

$$= \text{walk}(TF) = $$

(2.110)

$$=$$

,

(2.111)
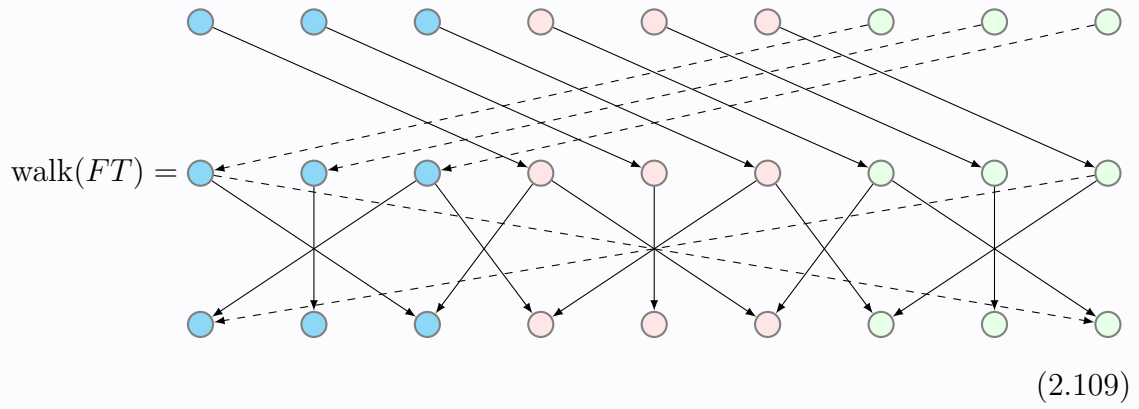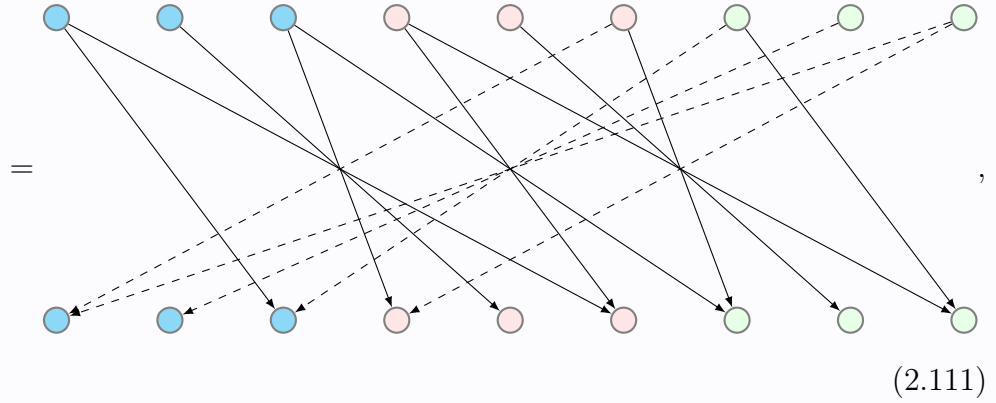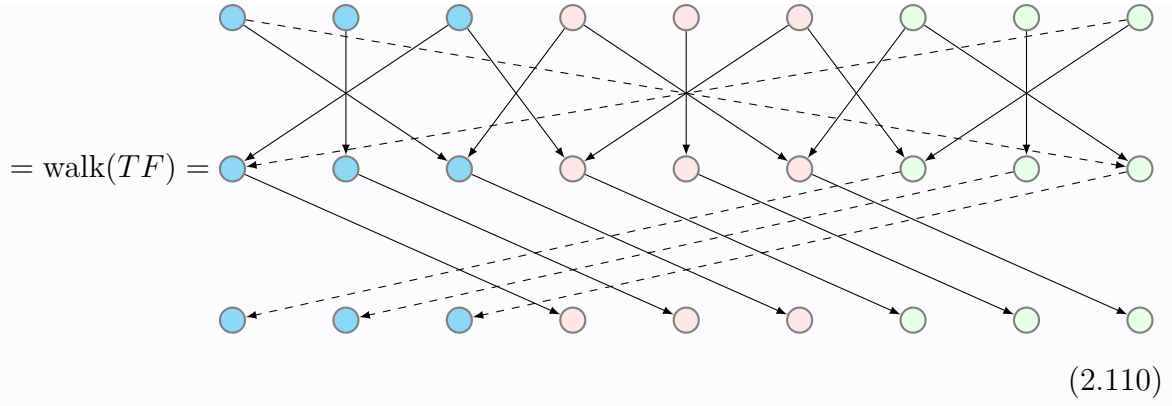
Let us now look at the three $\tilde{F}(\lambda_{T,n})$, formed from the translation eigenvalues

$$\lambda_{T,n} = \exp\left(\frac{2\pi i n}{3}\right), \qquad n \in \{0, 1, 2\} \tag{2.112}$$

$$\text{walk}(\tilde{F}(\lambda_{T,n})) = \begin{pmatrix} 0 & 0 & 1 + \exp\left(\frac{2\pi i n}{3}\right) \\ 0 & 1 & 0 \\ 1 + \exp\left(\frac{-2\pi i n}{3}\right) & 0 & 0 \end{pmatrix}. \tag{2.113}$$

$\tilde{F}(\lambda_{T,n})$ has eigenvalues and corresponding eigenvectors

$$\tilde{v}_{n,0} = \begin{pmatrix} 0 & 1 & 0 \end{pmatrix} \qquad \lambda_{H,n,0} = 1 \tag{2.114}$$

$$\tilde{v}_{n,1} = \frac{1}{\sqrt{2}} \begin{pmatrix} \exp\left(\frac{n\pi i}{3}\right) & 0 & -1 \end{pmatrix} \qquad \lambda_{H,n,1} = -2\cos\left(\frac{n\pi i}{3}\right) \tag{2.115}$$

$$\tilde{v}_{n,2} = \frac{1}{\sqrt{2}} \begin{pmatrix} \exp\left(\frac{n\pi i}{3}\right) & 0 & 1 \end{pmatrix} \qquad \lambda_{H,n,2} = 2\cos\left(\frac{n\pi i}{3}\right) \tag{2.116}$$

and thus its corresponding eigenstates in the Hilbert space $\mathcal{F}$ are

$$\lambda_{F,n,0} = 1 \qquad \lambda_{F,n,1} = -2\cos\left(\frac{n\pi i}{3}\right) \qquad \lambda_{F,n,2} = 2\cos\left(\frac{n\pi i}{3}\right)$$

$$v_{n,0} = \frac{1}{\sqrt{3}}\begin{pmatrix} 0 & 1 & 0 & 0 & e^{\left(\frac{2n\pi i}{3}\right)} & 0 & 0 & e^{\left(\frac{4n\pi i}{3}\right)} & 0 \end{pmatrix}$$

$$v_{n,1} = \frac{1}{\sqrt{6}}\begin{pmatrix} e^{\left(\frac{n\pi i}{3}\right)} & 0 & -1 & e^{\left(\frac{3n\pi i}{3}\right)} & 0 & -e^{\left(\frac{2n\pi i}{3}\right)} & e^{\left(\frac{5n\pi i}{3}\right)} & 0 & -e^{\left(\frac{4n\pi i}{3}\right)} \end{pmatrix}$$

$$v_{n,2} = \frac{1}{\sqrt{6}}\begin{pmatrix} e^{\left(\frac{n\pi i}{3}\right)} & 0 & 1 & e^{\left(\frac{3n\pi i}{3}\right)} & 0 & e^{\left(\frac{2n\pi i}{3}\right)} & e^{\left(\frac{5n\pi i}{3}\right)} & 0 & e^{\left(\frac{4n\pi i}{3}\right)} \end{pmatrix},$$

where the phase factors have been written explicitly in elements 4 to 9 to demonstrate the translation property. We can trivially see that the eigenstates generated by the different subspaces are orthonormal, and that they are eigenstates of F. As there are 9 such eigenstates, and because $\dim \mathcal{F} = 9$, and because F is hermitian, we have found all eigenstates of F.

Chapter 3

Tight Binding Toy Models

Introduction

So far, we have looked at a graph algebra, describing a method of generating polynomials of graphs, and observing that eigendecomposition of a child graph $P(G)$ can be indirectly performed through its parent graph G. In this chapter, we will move away from abstract matters and into those of some practicality in condensed matter physics.

In this setting, graphs are used to describe a discrete set of basis states (vertices), and the complex probability amplitudes of transitioning between them (weighted edges), such that their adjacency matrices correspond to the hamiltonian of the represented system. As such, graphs for closed systems are hermitian, such that each edge has a corresponding conjugate transpose edge.

In the tight binding model, the basis states correspond to an electron's occupation of atomic orbitals in a material, such that it is assumed that all possible electronic states are in a superposition of occupation of a set of orbitals. Transition probabilities are determined by the properties of the material itself, which are assumed to be uninfluenced

by the electronic state, and by the properties of the environment in which the material is in. The hamiltonian describes the dynamics of a state as it evolves over time.

In coupled-mode theory of photonic crystals[25], basis states correspond to optical excitations in dielectric nanostructures. These states are governed by the Helmholtz equation, the optical analogue of the Schr̈odinger equation, defining dynamics along the length of a waveguide rather than through time.

In both of these types of system, the tight binding model serves as an approximation to the behaviour of independent particles. In some cases, the approximation is a good representation of the true behaviour of a quantum system, and in others it serves as a useful initial step, to be used as a basis for further exploration with more advanced methods. For our purposes, it serves as a unifying model, enabling us to look upon condensed matter systems as a collection of "sticks and balls", without concerning ourselves with setting-dependent behaviours such as spin-orbit coupling or loss and gain.

This chapter begins by analysing a collection of simple tight binding models, demonstrating, along the way, how the polynomial algebra presented in this thesis can be used to simplify calculations and obtain a deeper insight into their algebraic properties.

The terminology used throughout the previous sections of this thesis will continue throughout: tight binding systems will be presented as graphs, and their corresponding hamiltonians as adjacency matrices.

As previously stated, analysing periodic systems through the Bloch formalism is analogous to the decomposition of periodic graphs into translation eigenspaces. Although the mathematical underpinning is identical, the Bloch formalism concerns itself with geometrical properties: the translation eigenvalue $\lambda_T(\theta) = \exp(2\pi i\theta)$ is viewed as the exponential $\exp(i\vec{k}.\vec{r})$, containing an inner product between momentum, a vector in reciprocal space,

and translation vectors in real space. Graphs, on the other hand, are viewed through a topological, rather than geometrical, lens; a vertex has no concept of a physical position. Whilst it is certainly possible to embellish vertices with a position, we shall stick to the language of translation eigenspaces and discuss any geometrical properties in commentary.

3.1   The Monatomic Chain

The monatomic chain M is the simplest infinite system, comprising a single vertex in each repeating cell, with translational symmetry along a single axis, and a unit weighted edge connecting each vertex to both of its neighbours, depicted as

$$M = \ldots \qquad \ldots \qquad (3.1)$$

$$\text{walk}(M) = \ldots \qquad \ldots \qquad (3.2)$$

Following section 2.6, we can represent the chain as a single-vertex graph $\tilde{G}$, with connection graphs $\tilde{R}$ and $\tilde{L}$, with

$$\text{walk}(\tilde{G}) = \qquad \text{walk}(\tilde{R}) = 1 \qquad \text{walk}(\tilde{L}) = 1 \qquad (3.3)$$

$$\text{adj}(\tilde{G}) = \begin{pmatrix} 0 \end{pmatrix} \qquad \text{adj}(\tilde{R}) = \begin{pmatrix} 1 \end{pmatrix} \qquad \text{adj}(\tilde{L}) = \begin{pmatrix} 1 \end{pmatrix} \qquad (3.4)$$

71

Figure 3.1: The eigenspectrum of the reduced monatomic chain $m(\theta)$ for varying θ

and we can project the chain into translation eigenspaces with

$$\tilde{m}(\theta) = \boxed{\begin{matrix} \bullet \\ \big| \; 2\cos\left(2\pi\theta\right) \\ \bullet \end{matrix}} \qquad \mathrm{adj}(\tilde{m}(\theta)) = \left(\, 2\cos(2\pi\theta)\,\right), \qquad (3.5)$$

for which the sole eigenvector is trivially (1) with eigenvalue $2\cos(2\pi\theta)$.

In section 2.5 we saw that we can apply a polynomial p_n (described in eq. (2.64)) to a cycle graph, generating a graph with n^{th}-neighbour edges. We can describe a monatomic chain with arbitrary n^{th}-neighbour edges t_n with

$$p' = \sum_n t_n p_n, \qquad (3.6)$$

$$M' = p'(M) \qquad (3.7)$$

$$= \dots \qquad (3.8)$$

such that each eigenvalue $2\cos(2\pi\theta)$ of M has a corresponding eigenvalue $p'(2\cos(2\pi\theta))$

in M'. Conveniently, the polynomials described in eq. (2.64) satisfy the trigonometric relationship

$$p_n : 2\cos(2\pi\theta) \to 2\cos(2n\pi\theta) \tag{3.9}$$

Thus the corresponding eigenvalue of M' is

$$\lambda(\theta) = \sum_n 2t_n \cos(2n\pi\theta). \tag{3.10}$$

This result in itself seems remarkably simple: the eigenspectrum is simply a sum over the eigenspectra formed from each individual n^{th} neighbour edge configuration. This clearly isn't the case in all systems, though, and relies on each of the nth neighbour edge graphs commuting with one another. As each nth neighbour interaction chain is simply a polynomial of the nearest-neighbour chain within our framework, this property cleary holds for the monatomic chain.

In some scenarios, one may wish to model a monatomic chain with edge weights calculated as a function of vertex distance: this function need not have finite extent, taking us back to the discussion in section 2.6. For example, consider an infinite chain with loop edges 1 and edge weights halving for each subsequent neighbour. The elements t_n in eq. (3.10)are then given by $t_n = 2^{-n}$, and the eigenspectrum of such a system is presented in fig. 3.2. A sum over a finite distance of q vertices provides the eigenspectrum

$$\sum_{n=0}^{q} \frac{2\cos(2\pi nk)}{2^n} = \frac{4\cos(2\pi k) - 8 + 2^{1-q}(2\cos(2\pi k(1+q)) - \cos(2\pi kq))}{4\cos(2\pi k) - 5}, \tag{3.11}$$

converging in the infinite limit to

$$\sum_{n=0}^{\infty} \frac{2\cos(2\pi nk)}{2^n} = \frac{4\cos(2\pi k) - 8}{4\cos(2\pi k) - 5}. \tag{3.12}$$

73

In this circumstance, the adjacency matrix of this graph is locally infinite but multiplication is still well-defined. There are models which may, at first glance, seem like reasonable interaction models, but which are nonetheless problematic due to sums that do not converge. Take, for example, an inverse relationship between edge weight and distance, not including any loop edges, such that $t_n = n^{-1}, n \geq 1$. The eigenspectrum for such a system with large, but not infinite, maximum edge distance is presented in fig. 3.3. However, the sum $\sum_{n=1}^{\infty} n^{-1}$ does not converge, thus the zero-momentum eigenvalue for such a system with infinitely extending edges is undefined. A modified interaction model with $t_n = n^{-s}, s > 1$, converges: it is the definition of $\zeta(s)$, where ζ is the Riemann zeta function.
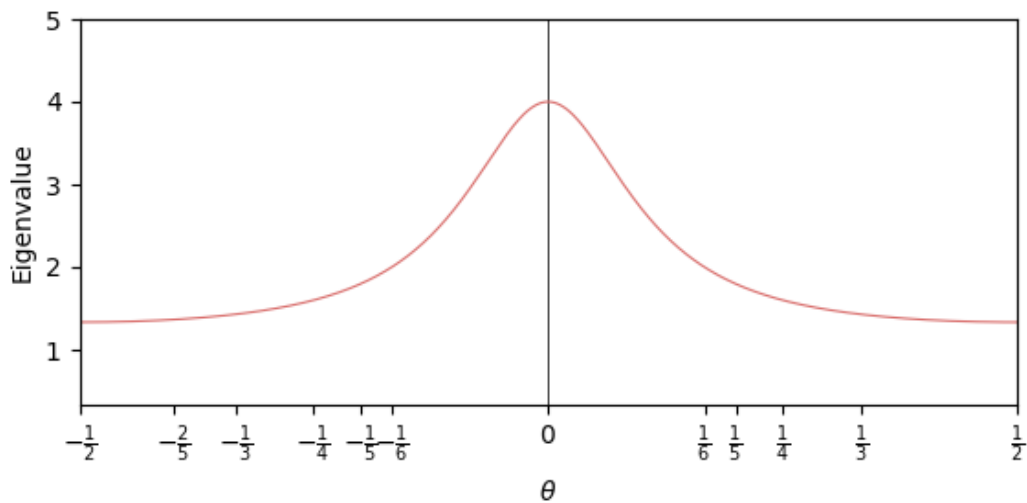
Figure 3.2: The eigenspectrum of $\sum_{n=0}^{\infty} 2^{-n} M^n$, representing a monatomic chain with a edge weight that halves each unit distance.
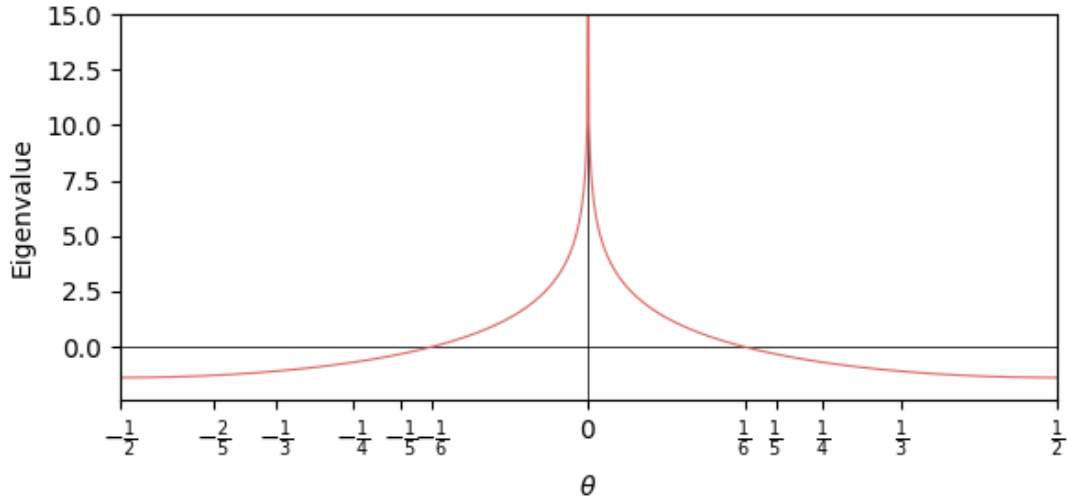
Figure 3.3: The eigenspectrum of $\sum_{n=1}^{\infty} \frac{1}{n} M^n$, which represents a monatomic chain with an inverse relationship between site distance and edge weight.

3.2 Time evolution and the square root of The Aharonov-Bohm Effect

The time-dependent Schrödinger equation

$$\partial_t \psi(t) = -iH\psi(t) \tag{3.13}$$

describes how a state ψ evolves through time under the influence of the hamiltonian H. We can describe the state at time t by as compared with an initial state $\psi(0)$ through

$$\psi(t) = \exp(-iHt)\psi(0). \tag{3.14}$$

As an exponential can be described by the Maclaurin series

$$\exp(x) = \sum_{n=0}^{\infty} \frac{x^n}{n!}, \tag{3.15}$$

75

we can write

$$\psi(t) = \left(\sum_{n=0}^{\infty} \frac{(-iHt)^n}{n!} \right) \psi(0) \tag{3.16}$$

In our framework, H corresponds to a graph, and ψ as a walk vector. As we have defined a polynomial algebra over graphs, we can describe a graph corresponding to the "time evolution operator" U, where

$$U(H, t) = \sum_{n=0}^{\infty} \frac{(-iHt)^n}{n!} \tag{3.17}$$

such that

$$U(H, t)\psi(0) = \psi(t) \tag{3.18}$$

The dynamics of a state are thus determined by its initial configuration and a power series of the hamiltonian. This allows us to project our understanding of polynomials of various graphs into analysis of an evolving system, with observable implications.

The Aharonov-Bohm effect[26] is a particularly useful physical phenomenon which we can explore directly in this setting. The effect was discovered by consideration of a charged particle travelling through a multiply-connected surface: Starting at an initial position, it has two topologically-inequivalent paths by which it can reach a point on the other side of a hole in the surface. A magnetic vector potential due to a solenoid centred at the hole multiplies each path by a different phase, such that the superposition of both paths causes interference, and when the two paths are out of phase by π radians, this interference is destructive and the particle never appears at the final position. The same effect can be achieved in the absence of a magnetic potential by introducing a resonant scattering site between two vertices, enabling a realisation in a photonic setting[27].

We can model this system with the graph

$$G(a,b) = \quad\quad\quad\quad \mathrm{adj}(G(a,b)) = \begin{pmatrix} 0 & a & b & 0 \\ a & 0 & 0 & b \\ b & 0 & 0 & -a \\ 0 & b & -a & 0 \end{pmatrix} \quad (3.19)$$

We can then demonstrate that there is destructive interference between the leftmost vertex and rightmost vertex under any walk length in G by observing the powers of G. These take the simple forms, for $n \in \mathbb{N}$,

$$G(a,b)^{2n} = (a^2 + b^2)^n \mathbf{1}_4 \quad = \quad (a^2+b^2)^n$$

$$(3.20)$$

$$G(a,b)^{2n+1} = (a^2 + b^2)^n G(a,b) \quad = \quad\quad\quad\quad (3.21)$$

Thus no power, polynomial, or power series of $G(a,b)$ has an edge from the left vertex to the right vertex. Indeed, any power, polynomial or power series of G resolves to a

77

linear combination $xG + y$, for some x and y. Let ψ and ϕ be states that fully occupy the leftmost and rightmost vertices respectively,

$$\psi = \begin{pmatrix} 1 & 0 & 0 & 0 \end{pmatrix}^T \tag{3.22}$$

$$\phi = \begin{pmatrix} 0 & 0 & 0 & 1 \end{pmatrix}^T \tag{3.23}$$

then

$$\phi^\dagger p(G(a,b))\psi = 0 \tag{3.24}$$

for all polynomials p, and thus

$$\phi^\dagger U(G,t)\psi = 0 \tag{3.25}$$

for all t, as demonstrated in fig. 3.4.

The time evolution operator $U(G(a,b),t)$ is a power series of $G(a,b)$ in which the coefficients of all even powers are real, and those of all odd powers are imaginary. A graph $F(a,b)$ obeying

$$F^2 = \tilde{P}(G), \tag{3.26}$$

where P is some polynomial, can never have an edge from vertex A to vertex D in its even powers. As a result, the time evolution of a state that initially solely occupies vertex A will always have an imaginary amplitude on D.

We can demonstrate this with the graph
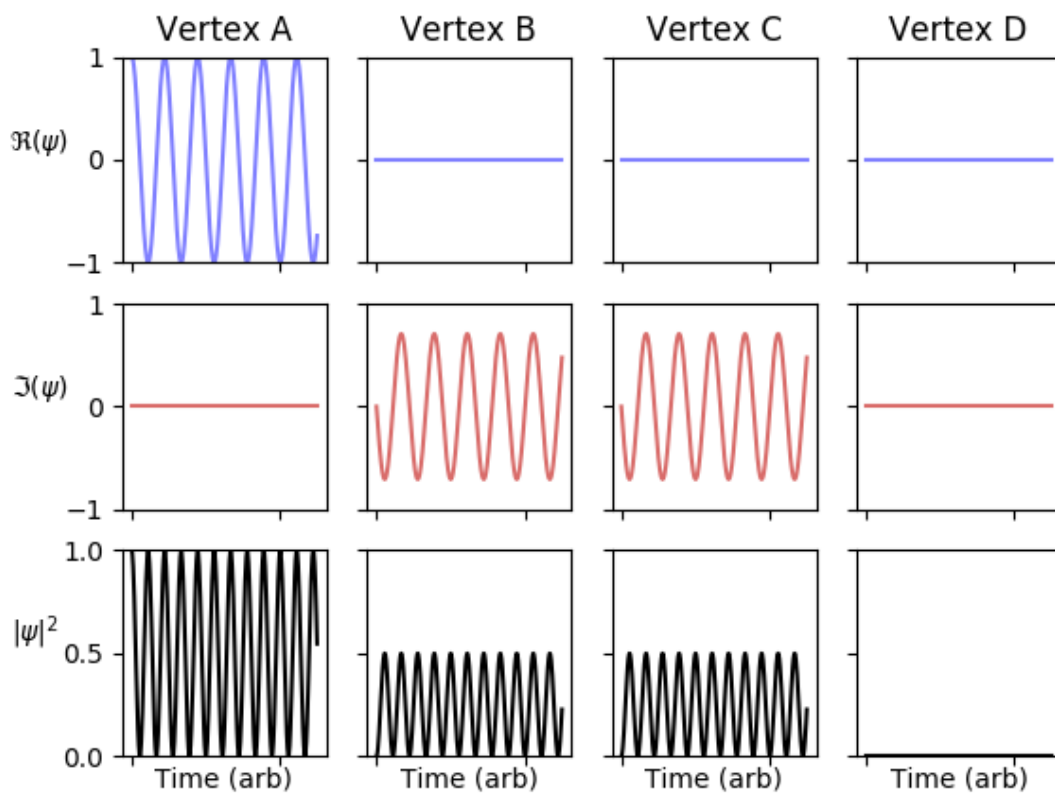
Figure 3.4: The components of a state $\psi = U(G(1,1),t)\psi_0$ for varying times t, where the initial state ψ_0 fully occupies the leftmost vertex A with amplitude 1. The amplitude of the evolving state is always zero at the rightmost vertex D.

$$F = \qquad\qquad\qquad\qquad\qquad\qquad\qquad\qquad\qquad\qquad\qquad\qquad\qquad (3.27)$$

such that

$$F^2 = 2 \quad \text{(3.28)}$$
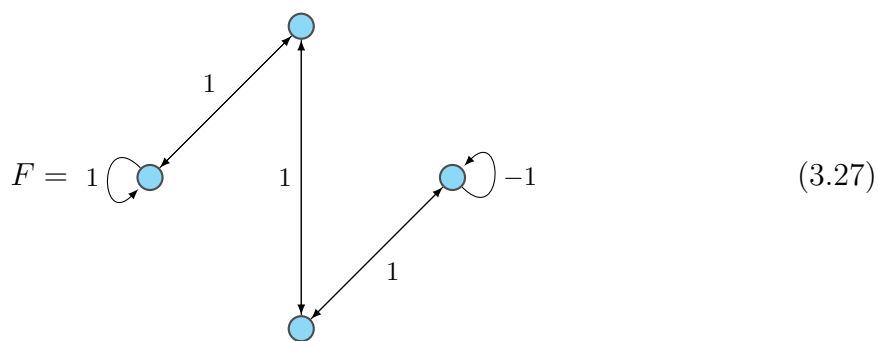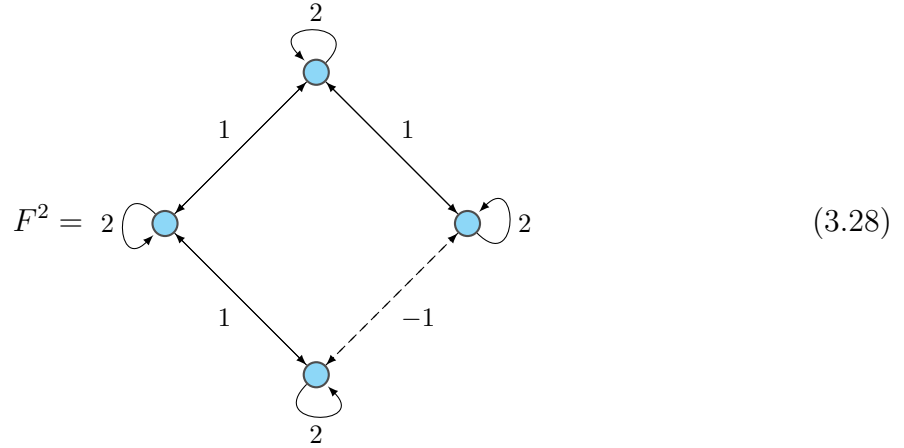
$$= G(1,1) + 2, \quad \text{(3.29)}$$

such that we can call F a "square root" of the Aharonov-Bohm loop $G(1,1) + 2$. Obeying eq. (3.26), we expect the time evolution operator overlap between the A and D sites to be imaginary, or

$$\Re(\phi^* U(F,t)\psi) = 0 \quad \text{(3.30)}$$

This is indeed the case, as demonstrated by the time evolution simulation fig. 3.5 of F, starting with unit amplitude on site A.
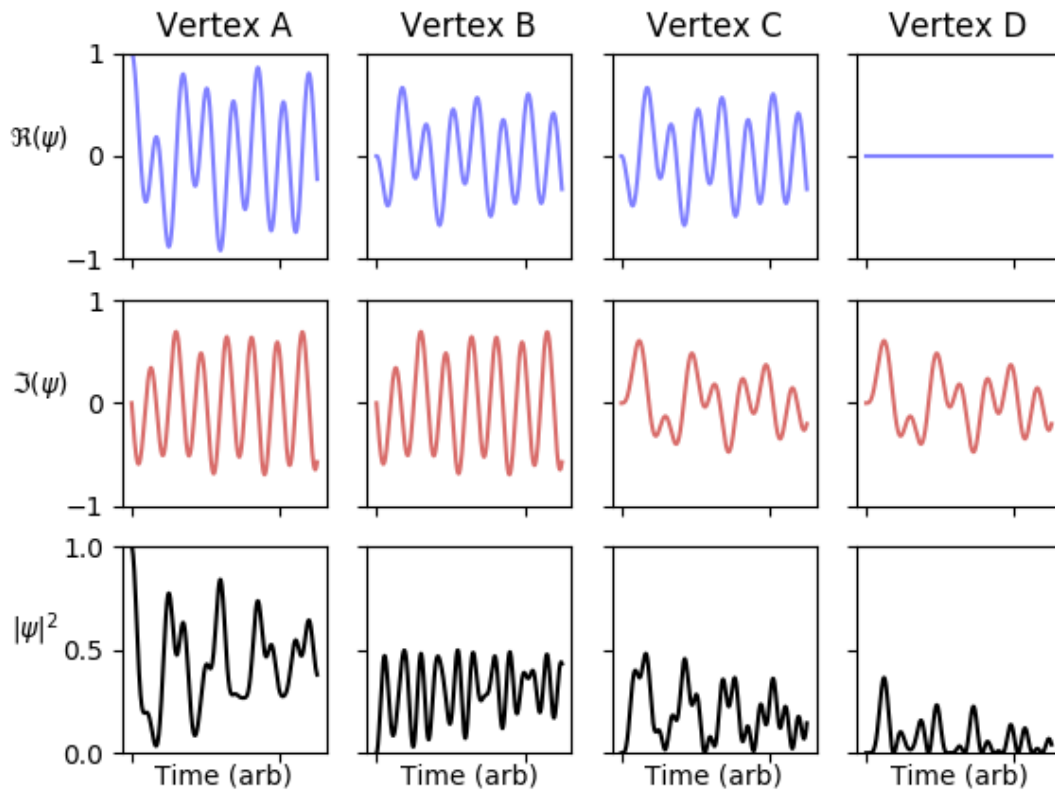
Figure 3.5: The components of a state $\psi = U(F,t)\psi_0$ for varying times t, where the initial state ψ_0 fully occupies vertex A with amplitude 1. Because only odd powers of F can have an edge between vertex A and vertex D, the amplitude on D is always imaginary.

3.3   The Square Lattice and The Hofstadter Butterfly

Although we have so far looked at graphs with translation symmetry in a single direction, two-dimensional systems can be built in a similar manner. Let

$$\text{walk}(\tilde{G}) = \qquad\qquad \text{walk}(\tilde{C}) = {}_1 \qquad\qquad (3.31)$$

Let where $X^{\oplus\infty,\infty}$ describe a graph X copied infinitely across two orthogonal directions $\hat{x}$ and $\hat{y}$, forming a 2 dimensional grid. We also need to introduce translation graphs acting in these directions, so let

$$\text{walk}(T_x) = $$

$$(3.32)$$

$$\text{walk}(T_y) = $$

$$(3.33)$$

Then we can describe a square lattice through the sum

$$S = \tilde{G}^{\oplus\infty,\infty} + \left(T_x + T_x^{-1} + T_y + T_y^{-1}\right) \tilde{C}^{\oplus\infty,\infty}, \tag{3.34}$$

$$= \qquad\qquad\qquad\qquad\qquad\qquad\qquad\qquad\qquad\qquad \tag{3.35}$$
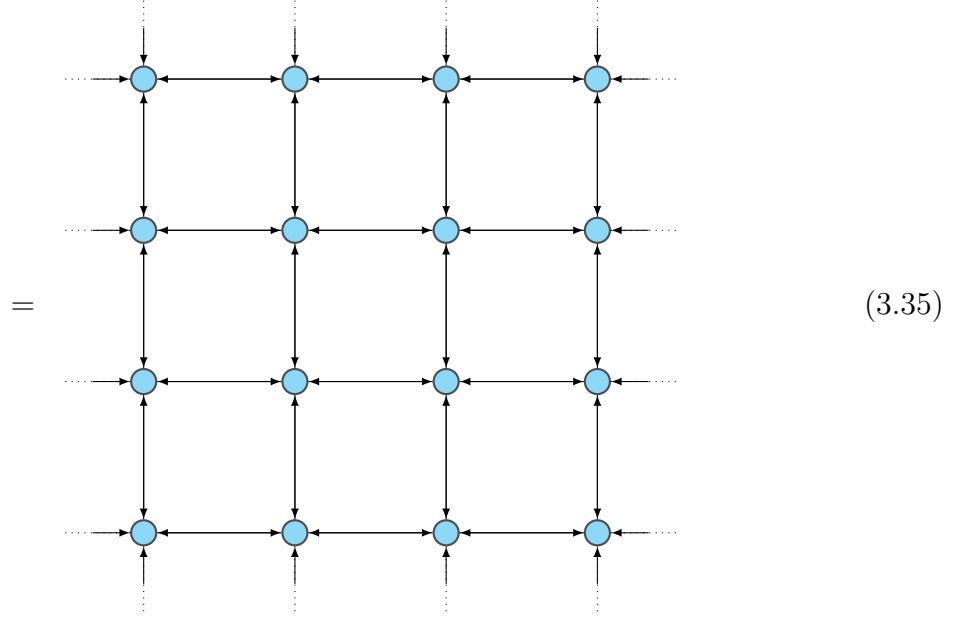
The translation operators T_x and T_y are independent, yet commute with one another and thus with S. As such, we can project S into eigenspaces of T_x and T_y, which have eigenvalues

$$\lambda_x(\theta_x) = \exp(2i\pi\theta_x)\,, \tag{3.36}$$

$$\lambda_y(\theta_y) = \exp(2i\pi\theta_y)\,, \tag{3.37}$$

such that we may reduce S into the reduced graph $\tilde{s}(\theta_x, \theta_y)$ in the eigenspace θ_x of T_x and θ_y of T_y, with

$$\mathrm{walk}\big(\tilde{s}(\theta_x, \theta_y)\big) = \quad \bigg| \; 2\cos\left(2\pi\theta_x\right) + 2\cos\left(2\pi\theta_y\right) \tag{3.38}$$

with eigenspectrum

$$E(\theta_x, \theta_y) = 2\cos(2\pi\theta_x) + 2\cos(2\pi\theta_y) \tag{3.39}$$

83
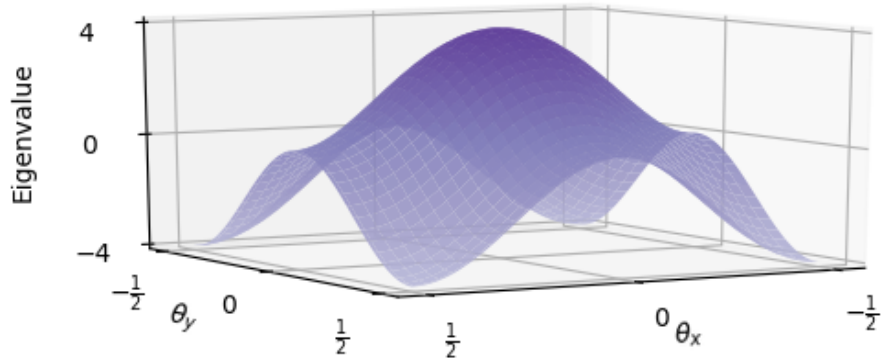
Figure 3.6: Eigenspectrum of a unit square lattice

plotted in fig. 3.6.

At a first glance, the introduction of a second dimension complicates the polynomial algebra. After all, a walk of m steps along the graph is no longer restricted to a single dimension, and there are now many routes from one vertex to another. Consider, for example, S^2,

$$S^2 = \qquad , \qquad (3.40)$$
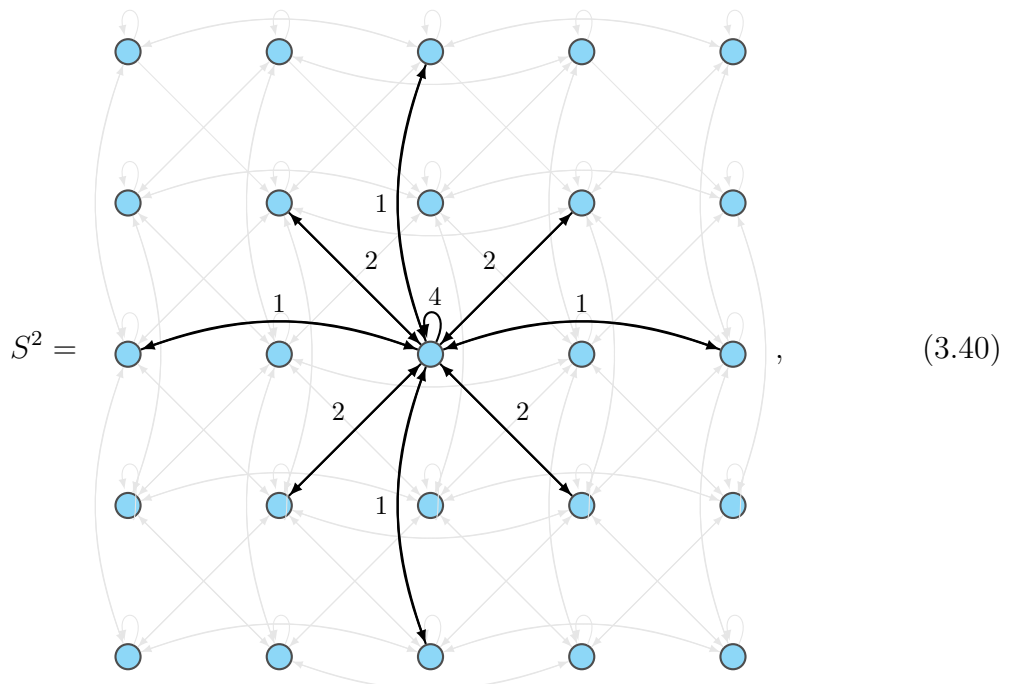
where the edges to and from a single site are emphasised and labelled for visual clarity, while translational symmetry applies and each site has the same configuration.

There are four walks of length 2 that return to the original vertex (up and down, down and up, left and right, right and left), and this results in a loop edge of weight 4. There is a single walk which ends two vertices to the right, so this results in an edge of unit weight; the same applies for two vertices to the left, upwards, and downwards. Diagonals have two paths; for example, walking upwards then to the right, and walking to the right then upwards.

Whilst the square lattice can be represented as a bipartite lattice, and thus its square is separable into two disjoint lattices, an elegant intepretation of S through polynomials is hindered by the diagonal edges: In their absence, S^2 would be separable into a set of four square lattices.

3.3.1 The Hofstadter Butterfly

When a quantum system is subject to a magnetic vector potential $\vec{A}$, the hopping amplitude between two sites is rotated in the complex plane by an angle determined by the line integral of $\vec{A}$ between them, through the Peierls substitution[28]

$$t_{a,b}(\vec{A}) = t_{a,b}(0) \exp\left(i \int_{r(a)}^{r(b)} \vec{A} \cdot d\vec{s} \right), \qquad (3.41)$$

where $r(a)$ and $r(b)$ are the physical positions of lattice sites represented by the vertices a, b, which we normalise such that neighbours are a unit distance apart. This transformation is commonly to as the Peierls substitution, and has two immediate implications: loop edges are left unchanged, and the phase applied to an edge from a node b to a node a is opposite to that applied to an edge from a to b; a hermitian system remains hermitian

under the influence a magnetic vector potential.

To describe a square lattice under the influence of a perpendicular magnetic field $\vec{B} = B\hat{z}$, where $\hat{z} \perp \hat{y}$, $\hat{z} \perp \hat{x}$, and $\hat{x} \perp \hat{y}$, and where $\hat{x}$ and $\hat{y}$ are the physical unit translations described by the translation graphs, we choose the transverse magnetic vector potential $\vec{A}(x,y) = Bx\hat{y}$, and modify our translation graphs according to the Peierls substitution. Let $T_x(0)$ and $T_y(0)$ refer to our earlier square lattice translation vectors, then we can describe the Peierls substitution through the graph $P(B)$ with

$$\text{walk}(P(B)) = \qquad\qquad\qquad\qquad\qquad\qquad\qquad\qquad\qquad\qquad$$
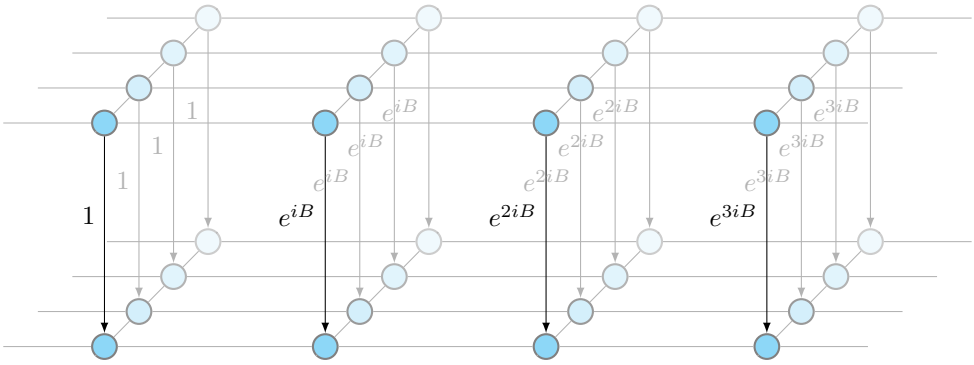
$$(3.42)$$

$$T_y(B) = T_y(0)P(B) \tag{3.43}$$

$$T_x(B) = T_x(0), \tag{3.44}$$

such that

$$S(B) = \tilde{G}^{\oplus\infty,\infty} + (T_x(B) + T_x(B)^{-1} + T_y(B) + T_y(B)^{-1})\tilde{C}^{\oplus\infty\infty} \tag{3.45}$$

Except for when B is an integer multiple of 2π, the translation graphs $T_x(B)$ and $T_y(B)$ do not commute. Instead,

$$T_y(B)T_x(B) = e^{iB}T_x(B)T_y(B) \tag{3.46}$$

Let us describe a more general commutator $(\cdot, \cdot | \cdot)$ with

$$(A, B | \mu) = AB - \exp(2\pi i \mu) BA, \tag{3.47}$$

such that, for $n \in \mathbb{Z}$,

$$(A, B | 2\pi n) = AB - BA = [A, B] \tag{3.48}$$

$$(A, B | 2\pi(n + {}^1\!/2)) = AB + BA = \{A, B\}. \tag{3.49}$$

Consider some A, B, μ that obey

$$(A, B | \mu) = 0 \tag{3.50}$$

then raising A to an integer power provides

$$A^n B = \exp(i\mu) A^{n-1} BA \tag{3.51}$$

$$= \exp(i\mu n) BA^n \tag{3.52}$$

by induction, and, by symmetry,

$$A^n B^m = \exp(i\mu nm) B^m A^n \tag{3.53}$$

thus

$$(A^n, B^m | \mu nm) = 0 \tag{3.54}$$

As a result, if μ is a rational multiple of 2π, such that $\mu = \frac{2\pi p}{q}, p \in \mathbb{Z}, q \in \mathbb{N}_+$, then any combination $n, m \in \mathbb{N}$ satisfying $nm = rq, r \in \mathbb{N}_+$ will result in

$$(A^n, B^m | \mu nm) = (A^n, B^m | 2\pi rp) \tag{3.55}$$

$$= [A^n, B^m] \tag{3.56}$$

We can now rewrite eq. (3.46) as

$$(T_y(B), T_x(B) | B) = 0, \tag{3.57}$$

and from eq. (3.56) we conclude that, for a rational magnetic field strength $B = \frac{2\pi p}{q}$,

$$[T_y(B)^{nq}, T_x(B)] = 0 \qquad\qquad n \in \mathcal{N}_+. \tag{3.58}$$

The only terms in $S(B)$ that do not commute with $T_y(B)$ are due to multiplications by $T_x(B)$ and $T_x(B)^{-1}$, and eq. (3.58) demonstrates that $T_y(B)^{nq}$ commutes with these terms. Thus, $T_y(B)^{nq}$ commutes with $S(B)$.

Let us return to the issue of the diagonal edges of $S(0)^2$. As we saw in section 3.2, destructive walks of length N between two vertices in a graph G eliminate an edge connecting them in G^N, and we have also seen how edges gain a phase due to a magnetic vector potential, and that a translation of q unit cell lengths in an orthogonal magnetic field of strength $B = \frac{2\pi p}{q}$ commutes with the square lattice $S(B)$. As it turns out, there is a polynomial of degree q that produces a graph that is separable into q^2 square graphs, each with unit edges.

Consider, for example, the case of $q = 2$,

$$S(\pi) = \qquad\qquad\qquad\qquad\qquad\qquad\qquad\qquad\qquad . \qquad\qquad (3.59)$$

with spectrum

$$\lambda_{\pm}(\theta_x, \theta_y) = \pm\sqrt{4\cos^2(2\pi\theta_y) + 2\cos(2\pi\theta_x) + 2} \qquad\qquad (3.60)$$

plotted in fig. 3.7.

In this case, the diagonal edges in $S(\pi)^2$ must vanish: there are two walks of equal and opposite weight of length 2 from each vertex at position (i, j) to each diagonal partner at position $(i \pm 1, j \pm 1)$. The loop edges in $S(\pi)^2$ are, like in $S(0)^2$, still of weight 4. Thus
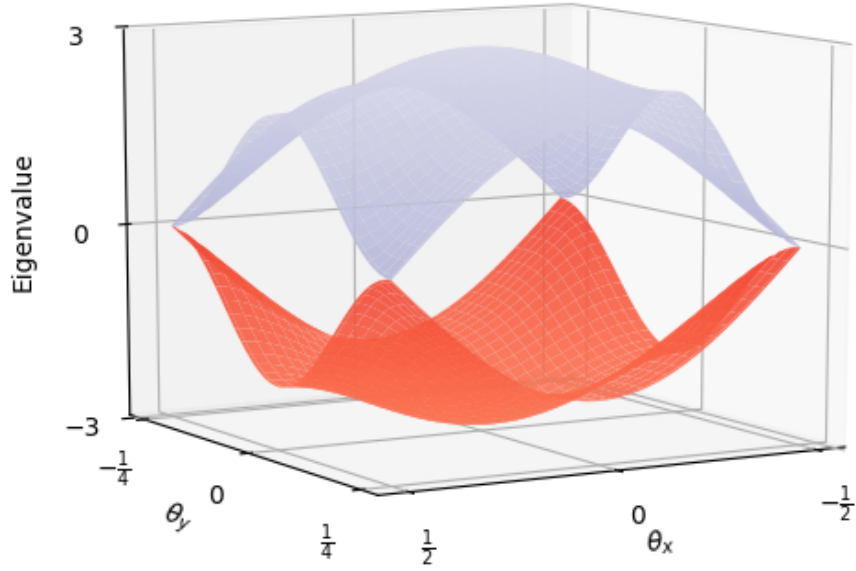
Figure 3.7:   The spectrum of a unit square lattice in the presence of an orthogonal magnetic field of strength π

$$S(\pi)^2 - 4 = \qquad \text{} \qquad , \qquad (3.61)$$
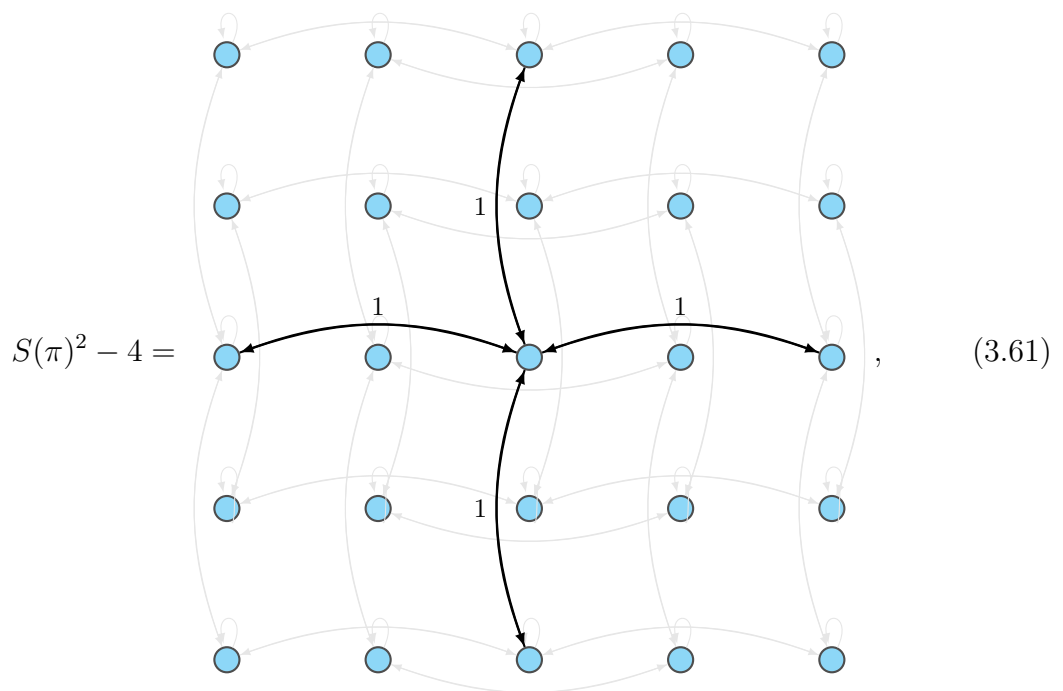
which corresponds to four separable square graphs with unit edges, without phases, and thus has the same spectrum as $S(0)$. Indeed, performing the polynomial $P(x) = x^2 - 4$ on the spectrum in fig. 3.7 produces fig. 3.6, albeit with appropriately scaled translation eigenvalues.

As it turns out, $S(2\pi p/q)^q$ removes all diagonal edges between vertices of distance q. This can be understood rather intuitively by considering the phases along each possible path. Consider the length-q walks from a vertex (a, b) to a vertex $(a + q - 1, b + 1)$: each necessarily involves a walk of length $q - 1$ in the x direction, which gains no phase, and a walk of length 1 from any vertex (c, b) to $(c, b + 1)$, $a \leq c \leq b$, thus gaining a phase $\exp\left(\frac{2\pi i c}{q}\right)$. The sum over all of these multiplicative walks is simply a sum over evenly distributed points on the unit circle in the complex plane, resulting in an edge of weight zero, or, equivalently, no edge.

The same logic applies to the walk from vertex (a, b) to vertex $(a + q - 2, b + 2)$, though this time the overall phase is

$$\sum_{n=0}^{q-2} \sum_{m=n}^{q-2} \exp\left(\frac{2\pi(n + m)}{q}\right) = 0, \tag{3.62}$$

and so on.

Removing other edges to result in a separable square graph can be achieved by adding terms of power less than q. Finding such polynomials is a non-trivial process: for $q \geq 4$, walks can be performed around full plaquettes, for $q \geq 6$ we must to take into account walks around rectangular formations of plaquettes, and for $q \geq 8$ we must consider terms corresponding to walks around the same a plaquette multiple times, larger squares, triangular block shapes, and walks surrounding non-neighbouring plaquettes. When a walk of length q ends at a vertex which could be reached in a shorter walk of length $\tilde{q}$, its

weight must be cancelled out by a term of power $\tilde{q}$, typically requiring trigonometric terms corresponding to the magnetic flux.

Let

$$\mathcal{B}(q, p) = 2 + 2\cos(\frac{2\pi p}{q}) \tag{3.63}$$

be modified Beraha constants. Then

$$P_{1,1} : x \to x \tag{3.64}$$

$$P_{2,1} : x \to x^2 - 4 \tag{3.65}$$

$$P_{3,1} : x \to x^3 - 6x \tag{3.66}$$

$$P_{4,1} : x \to x^4 - 8x^2 + 4(3 - \mathcal{B}(4, 1)) \tag{3.67}$$

$$P_{5,p} : x \to x^5 - 10x^3 + 5(5 - \mathcal{B}(5, p))\, x \tag{3.68}$$

$$P_{6,p} : x \to x^6 - 12x^4 + 6(7 - \mathcal{B}(6, p))\, x^2 - 6\left(\frac{2}{\mathcal{B}(6, p)}\right) \tag{3.69}$$

$$P_{7,p} : x \to x^7 - 14x^5 + 7(9 - \mathcal{B}(7, p))\, x^3 - 7\left(2 + \frac{2}{\mathcal{B}(7, p)}\right) x \tag{3.70}$$

$$P_{8,p} : x \to x^8 - 16x^6 + 8(11 - \mathcal{B}(8, p))\, x^4 - 8\left(4 + \frac{8}{\mathcal{B}(8, p)}\right) x^2 + 4 \tag{3.71}$$

are polynomials such that $P_{q,p}\left(S\left(\frac{2\pi p}{q}\right)\right)$ are graphs comprising q^2 separable square lattices, each of unit area q^2, and each with unit edges*.

As such graphs must also have the eigenspectrum $2\cos(2\pi\theta_x) + 2\cos(2\pi\theta_y)$, lying

---

*The polynomials $P_{q,p}$ were found recursively. Let $X = S(\frac{2\pi p}{q})$. Then identify the edge weight w from a point (a, b) to a point $(a + q - 2, b)$ in the graph X^q. Then identify the weight w_2 from a point (a, b) to a point $(a + q - 4, b)$ in the graph $X^q - wX^{q-2}$, and so on. An attempt at a general form of $P_{q,p}$ was made, but it requires the highly non-trivial task of identifying the multiplicative weight of all length-N walks between two points on a square lattice with position-dependent complex edges.
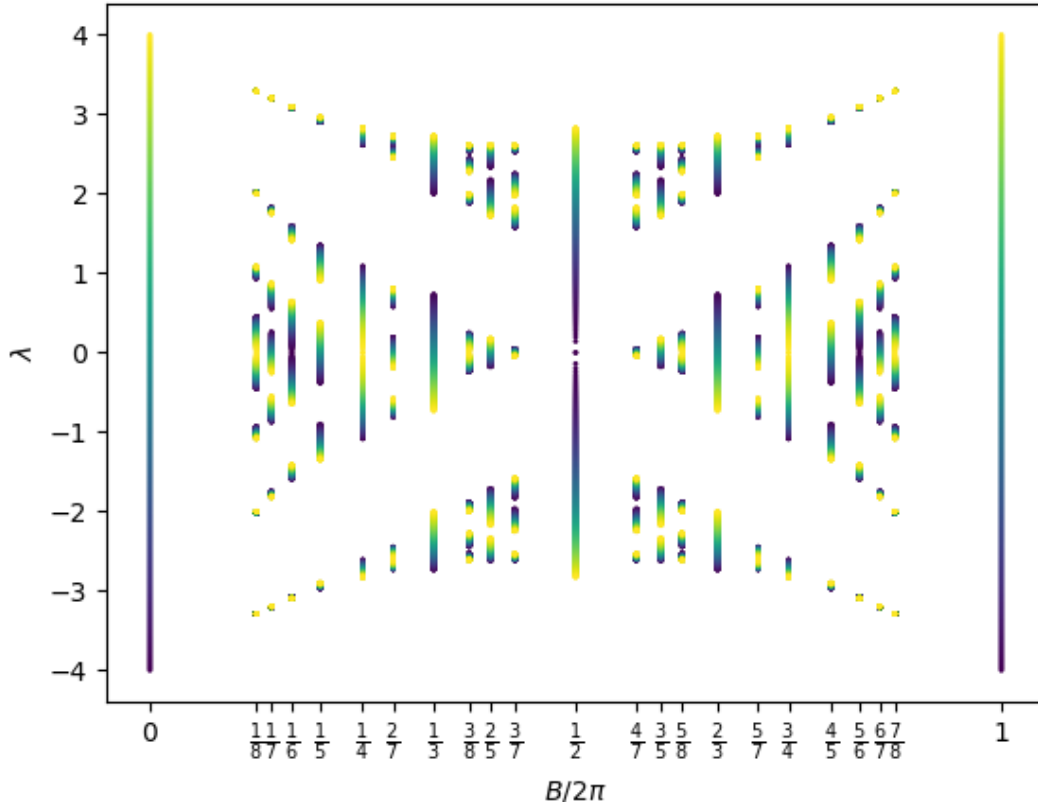
Figure 3.8: Hofstadter Butterfly, colour co-ordinated such that points of the a colour are solutions to the equation $P_{p,q}(x) = y$, where y has the same colour in the $B = 0$ line.

in the interval $(-4, 4)$, the values of λ satisfying $-4 \leq P_{q,p}(\lambda) \leq 4$ are eigenvalues of $S(\frac{2\pi p}{q})$. Such eigenvalues are plotted in fig. 3.8, forming the Hofstadter Butterfly[29]. This process is analogous to vanilla eigendecomposition: the polynomials are of the same degree as would be required to decompose a unit cell of q vertices, and we know that the eigenstates of such graphs must be superpositions of the eigenstates of the zero-flux square lattice graph, expanded to an area of q^2.

3.4 Honeycomb Strutures

The honeycomb structure has significant prevalence in modern condensed matter. The first significant theoretical analysis of the carbon layers of graphite in a tight-binding setting was conducted by P.R. Wallace in 1947[30], who identified an approximately linear energy dispersion around two distinct points in the Brillouin zone. These points were analysed by D. P. DiVincenzo and E.J. Mele in 1984[31], and the hamiltonian was brought into a form identical to a two-dimensional Dirac equation, replacing spin with a sublattice index. In 2004, A. Geim and K. Novoselov isolated individual layers of hexagonal carbon, known as Graphene. Their experimental confirmation of theoretical results, along with further groundbreaking research[32], resulted in them being awarded the 2010 Nobel Prize in Physics.

Monolayer Hexagonal Boron Nitride[33] (HBN) is another honeycomb material, with Boron and Nitrogen, rather than carbon, as the two sites in the unit cell rather than Carbon. As such, we can approximate the electronic properties of monolayer HBN by using two vertices with loop edges of different weights.

In this section, honeycomb structures will be analysed through the graph algebra. We will discover that a next-nearest neighbour tight binding model of the honeycomb is in fact a polynomial of the nearest-neighbour graph, and show that the tight binding model of monolayer HBN and that of graphene are be algebraic related using the microscopic graph algebra rules outlined in chapter 2.

3.4.1 Polynomials and next-nearest neighbours

Let the infinite honeycomb be described by the graph

$$G = \qquad\qquad\qquad\qquad\qquad\qquad\qquad\qquad (3.72)$$
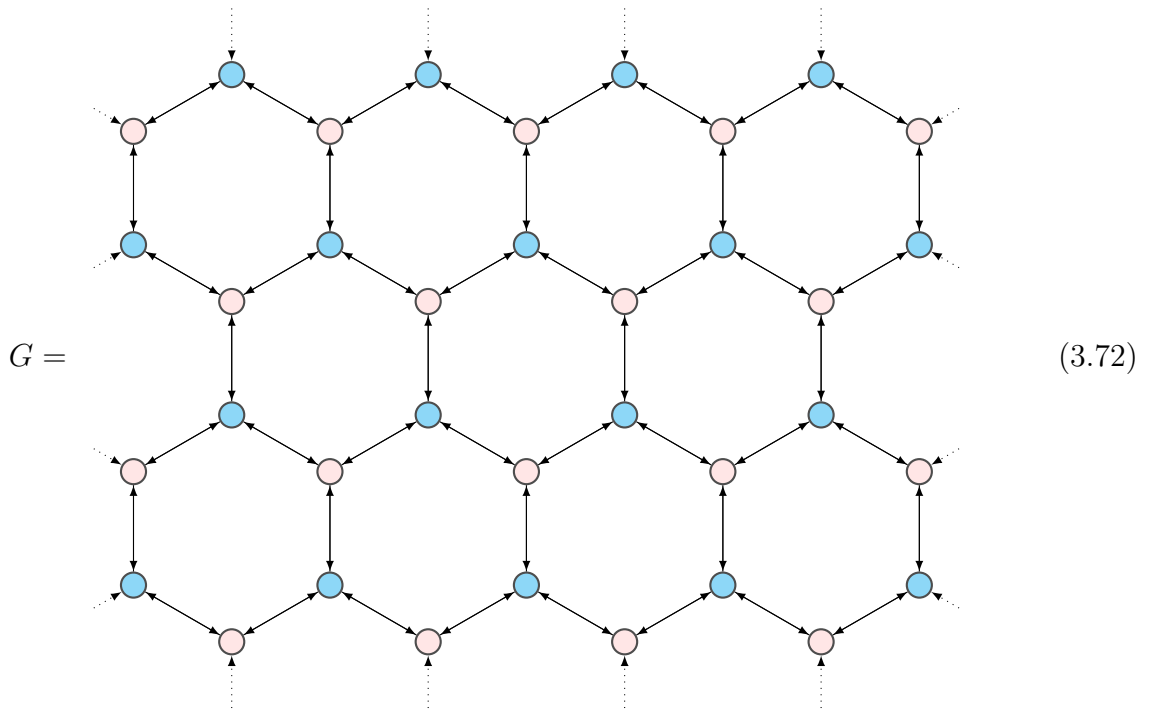
which can be broken down into

$$\tilde{G} = \qquad 1 \qquad \tilde{C}_{AB} = \qquad 1 \qquad \tilde{C}_{BA} = \qquad 1 \qquad (3.73)$$

$$T_A = \qquad\qquad\qquad\qquad\qquad\qquad\qquad\qquad (3.74)$$

95
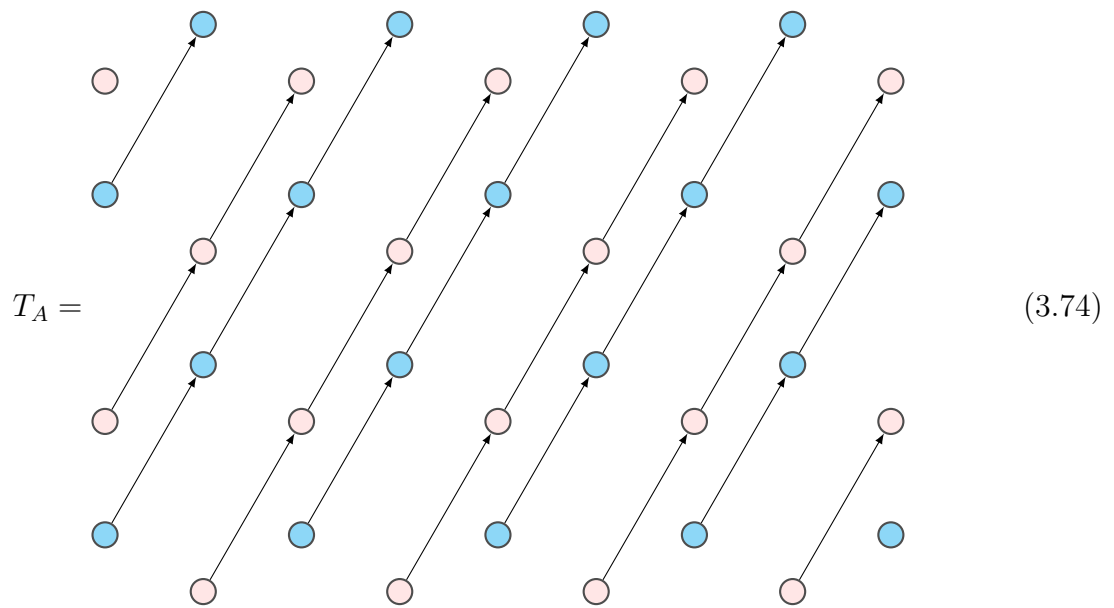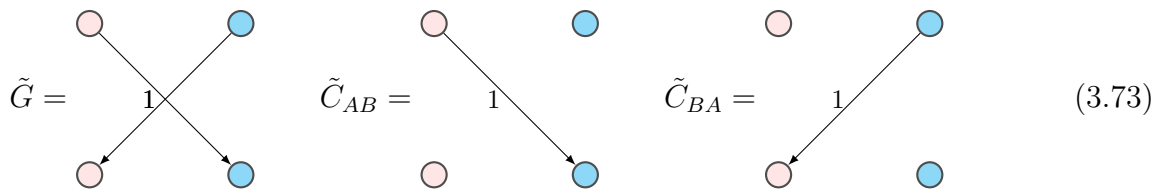
$$T_B = \qquad\qquad\qquad\qquad\qquad\qquad\qquad\qquad\qquad\qquad\qquad \text{(3.75)}$$

such that

$$G = \tilde{G}^{\oplus\infty,\infty} + (T_A + T_B)\,\tilde{C}_{AB}^{\oplus\infty,\infty} + \left(T_A^{-1} + T_B^{-1}\right)\tilde{C}_{BA}^{\oplus\infty,\infty} \qquad\qquad \text{(3.76)}$$

which is decomposable into translation eigenspaces of T_A and T_B as

$$\tilde{g}(\theta_1, \theta_2) = \tilde{G} + (\exp(2i\pi\theta_1) + \exp(2i\pi\theta_2))\,\tilde{C}_{AB}$$

$$+ (\exp(-2i\pi\theta_1) + \exp(-2i\pi\theta_2))\,\tilde{C}_{BA} \qquad\qquad \text{(3.77)}$$

where

$$\mathrm{adj}(\tilde{g}(\theta_1,\theta_2)) = \begin{pmatrix} 0 & 1 + \exp(2i\pi\theta_1) + \exp(2i\pi\theta_2) \\ 1 + \exp(-2i\pi\theta_1) + \exp(-2i\pi\theta_2) & 0 \end{pmatrix}.$$

$$\text{(3.78)}$$

The eigenspectrum of eq. (3.78) is given by

$$\lambda_\pm = \pm\sqrt{3 + 2\cos(2\pi\theta_1) + 2\cos(2\pi\theta_2) + 2\cos(2\pi(\theta_1 - \theta_2))} \qquad\qquad \text{(3.79)}$$
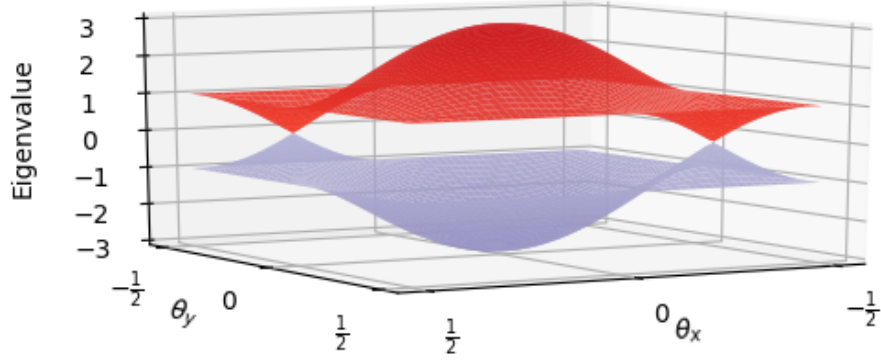
Figure 3.9: Eigenspectrum of the unit honeycomb

plotted in fig. 3.9. The two eigenvalues meet at the points

$$(\theta_1, \theta_2) = (n - \frac{1}{3}, n - \frac{1}{3}) \tag{3.80}$$

$$(\theta_1, \theta_2) = (n + \frac{1}{3}, n + \frac{1}{3}) \tag{3.81}$$

for all integers n.

In a condensed matter setting, θ_1 and θ_2 are transformed into inner products of a two-dimensional Bloch momentum vector with the position vectors corresponding to the translations,

$$\vec{T_A} = \left(\frac{\sqrt{3}}{2}, \frac{3}{2} \right) \qquad\qquad \vec{T_B} = \left(-\frac{\sqrt{3}}{2}, \frac{3}{2} \right) \tag{3.82}$$

$$\vec{k} \cdot T_A = \frac{3k_y + \sqrt{3}k_x}{2} \qquad\qquad \vec{k} \cdot T_B = \frac{3k_y - \sqrt{3}k_x}{2} \tag{3.83}$$

$$= \quad 2\pi\theta_1 \qquad\qquad\qquad = \quad 2\pi\theta_2 \tag{3.84}$$

$$\Rightarrow k_x = \frac{2\pi(\theta_1 - \theta_2)}{\sqrt{3}} \qquad\qquad k_y = \frac{2\pi(\theta_1 + \theta_2)}{3}. \tag{3.85}$$

97

The degenerate points are the so-called "Dirac points" described in this section's introduction.

The honeycomb eigenspectrum being positive and negative square roots, the next natural step is to look at G^2. We know that it must have the eigenspectrum

$$\lambda_\pm(\theta_1, \theta_2) = 3 + 2\cos(2\pi\theta_1) + 2\cos(2\pi\theta_2) + 2\cos(2\pi(\theta_1 - \theta_2)), \qquad (3.86)$$

which is simply a shifted spectrum of a triangular lattice. Indeed, the graph algebra allows us to separate the honeycomb into a direct sum of its two sublattices, each connected in a triangular lattice formation, and with loop edges of weight 3 on each vertex,

$$G^2 = \qquad\qquad\qquad\qquad\qquad\qquad\qquad\qquad\qquad (3.87)$$

$$= \qquad \oplus \qquad , \qquad (3.88)$$
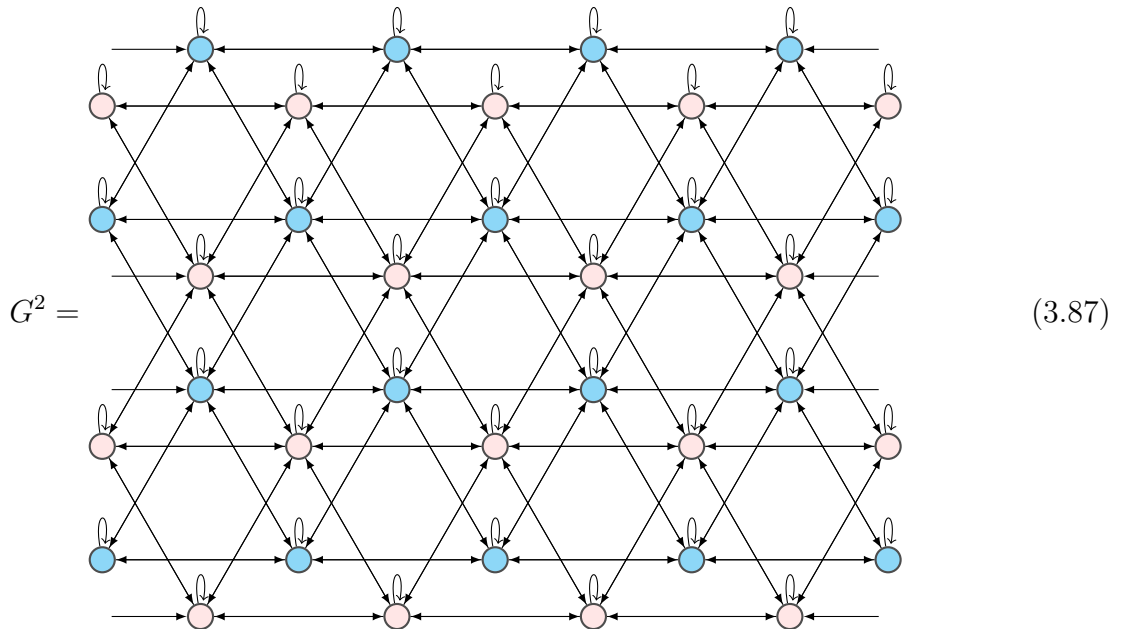
In the square lattice graph, there were two varieties of next-nearest neighbours. The geometrical next-nearest neighbours are those which are a physical distance $\sqrt{2}$ apart, at diagonals to one another. The topological next-nearest neighbours are simply those that can be reached in walks of length 2, including those of geometrical distance 2 apart, the geometrical next-nearest neighbours of distance $\sqrt{2}$ apart, both of unit weight, and the source sites themselves. From a physical standpoint, we expect a relationship between edge weight and distance, so polynomials of the square lattice do not aid an exploration into next-nearest neighbours.

In the honeycomb, this is not the case. The geometrical and topological next-nearest neighbours are the same, apart from the loop edges of weight 3 which can trivially be removed by a subtraction of the identity graph. As such, the polynomial

$$p_{t_1,t_2} : x \to t_1 x + t_2(x^2 - 3) \qquad (3.89)$$

can be applied to G to form a honeycomb with nearest neighbour edges of weight t_1 and next-nearest *geometrical* neighbour edges of weight t_2, the eigendecomposition of which being obtainable from the eigendecomposition of the nearest neighbour-only graph G through the usual approach: eigenstates are unchanged, and eigenvalues λ are transformed to $p_{t_1,t_2}(\lambda)$, as depicted in fig. 3.10.
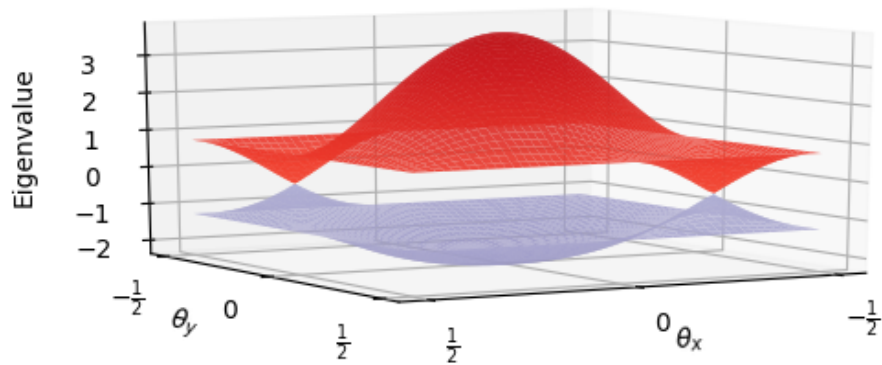
Figure 3.10: Eigenspectrum of the squared honeycomb lattice

3.4.2 Different self-loop weights

In the previous subsection, we described a honeycomb graph without loop edges, rendering the two vertices in the unit cell equivalent. Let us now consider a modification to G, providing loop edges of weight ϵ_A and ϵ_B to the vertices in the unit cell,

$$G(\epsilon_A, \epsilon_B) =$$

$$\tag{3.90}$$

As the loop edges modify the diagonal elements of $\mathrm{adj}(G)$, we can subtract the mean of their weights to result in a honeycomb with equal magnitude loop edges, alternating in sign, such that

$$\mu = \frac{\epsilon_A + \epsilon_B}{2} \tag{3.91}$$

$$\Delta = \frac{\epsilon_A - \epsilon_B}{2} \tag{3.92}$$

$$G(\epsilon_A, \epsilon_B) - \mu = G(\Delta, -\Delta) \tag{3.93}$$

As we saw in section 2.2, squaring such a graph separates the sublattices into two disjoint graphs. The result is the same as eq. (3.87), except that the loop edges on the vertices become $\Delta^2 + 3$. Thus,

$$\left(G(\epsilon_A, \epsilon_B) - \mu\right)^2 = G(0,0)^2 + \Delta^2, \tag{3.94}$$

the eigenspectrum for which is plotted in fig. 3.11. As the spectrum of the squared graph is lifted by Δ^2, we know that the positive and negative eigenvalue bands in $G(\epsilon_A, \epsilon_B) - \mu$ must symmetrically separate apart, such that the gap between the would-be degenerate points becomes Δ. To obtain the spectrum of $G(\epsilon_A, \epsilon_B)$, we shift the bands by μ, visually depicted in fig. 3.12.
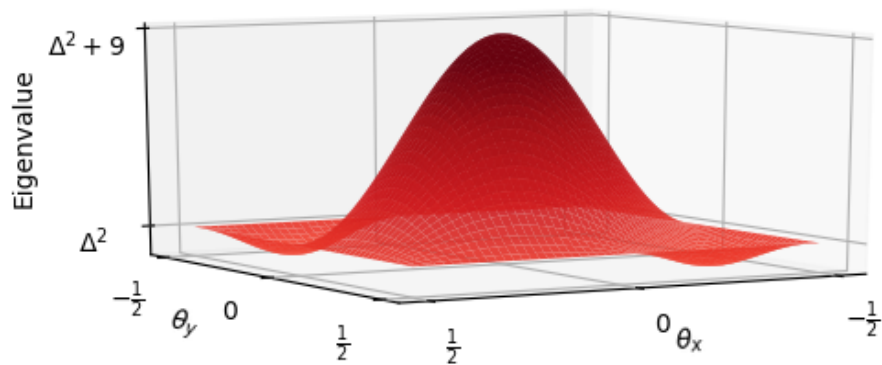
Figure 3.11: The eigenspectrum for $(G(\epsilon_A, \epsilon_B) - \mu)^2$, with extrema at Δ^2 and $\Delta^2 + 9$
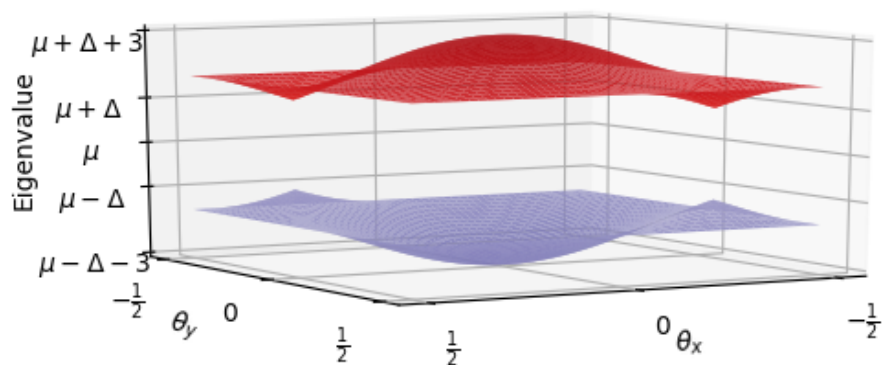
Figure 3.12: The eigenspectrum of $G(\epsilon_A, \epsilon_B)$, exhibiting a band splitting of 2Δ centred around μ.

3.5 Sibling systems

In section 2.3 we saw that squaring a parent graph can result in a child graph such that next-nearest neighbours of the parent are neighbours in the child. It follows that one can find a parent H of a graph G, such that $H^2 = G + b, b \in \mathbb{R}$, simply by bisecting each non-loop edge $e \in G$ with an additional vertex in H, carefully choosing the weights of the split edges in order to reproduce the edges of G upon squaring. The same approach can then be applied to loop edges, with weights chosen such that the weights of G's loop edges can be achieved with a constant offset b upon squaring.

Upon squaring our designed H, we will then obtain the direct sum of two graphs, $(G + b) \oplus (\tilde{G} + \tilde{b})$, where G is our target child graph offset by the constant b, $\tilde{G}$ is formed of the bisecting vertices we added to H, and $\tilde{b}$ is an arbitrary offset, included for consistency.

Let us illustrate this with the honeycomb G from eq. (3.72). As weights are all of unit weight, we can split each edge into two of unit weight, connecting them with a new vertex (coloured white).

$$H = \qquad\qquad\qquad\qquad\qquad\qquad\qquad\qquad \text{(3.95)}$$
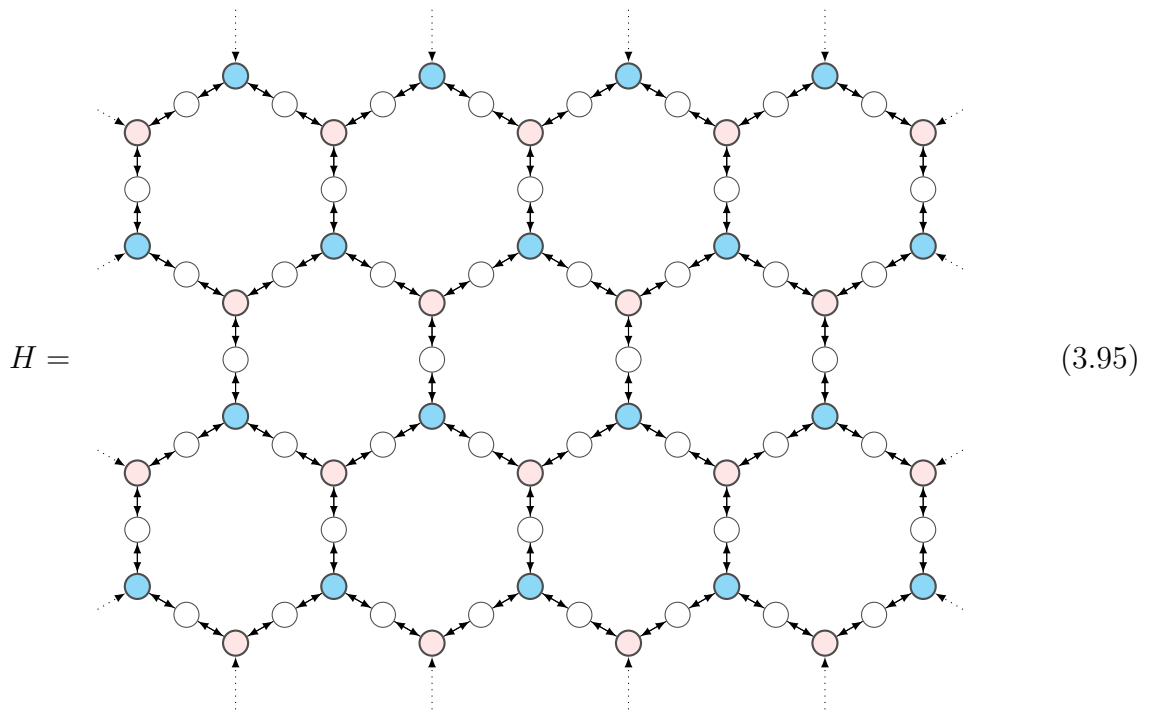
This system is, in itself, very interesting. Its eigenspectrum, plotted in fig. 3.13, reveals a flat band with eigenvalue zero across all momenta and, as we have learned to expect from previous results, there is an analogue of Dirac cones in the positive and negative energy spectra. Its square

$$H^2 = \qquad\qquad\qquad\qquad\qquad\qquad\qquad . \qquad \text{(3.96)}$$
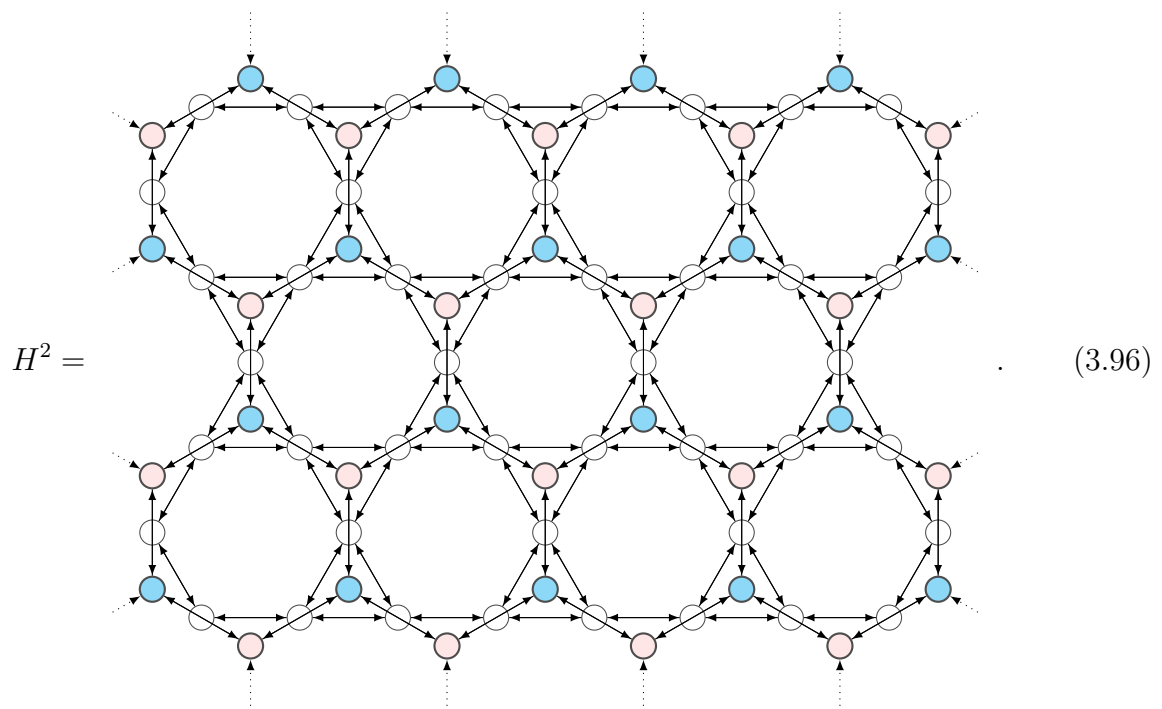
is indeed a disjoint graph comprising two subgraphs, one of which being the honeycomb $G + 3$ Note that loop edges are not displayed in eq. (3.96), for visual clarity. H^2 separates as

$$H^2 = (G + 3) \oplus (\tilde{G} + 2) \tag{3.97}$$

$$\tilde{G} = \tag{3.98}$$
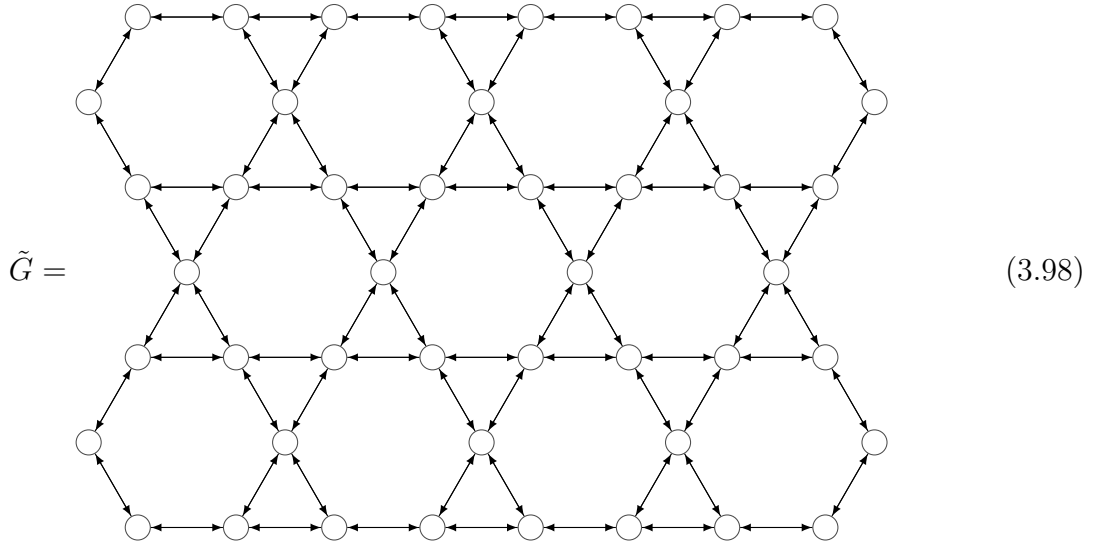
revealing the "sibling" lattice of the honeycomb to be the kagome lattice $\tilde{G} + 2$. The symmetry of the parent lattice's eigenspectrum around the zero eigenvalue demonstrates that H^2 comprises three sets of eigenvalue bands: one at zero energy, which corresponds to the kagome lattice's flat band at eigenvalue -2 (the full eigenspectrum of the kagome lattiice is shown in fig. 3.14), and two bands that are formed from the bands seen in both the honeycomb and kagome spectra, offset by $+3$ and $+2$ respectively.

We can recreate the honeycomb seen in section 3.4.2, with alternating loop edges on the A and B sublattices, by choosing the weights of edges from A vertices to the bisecting vertices to be α, and the edge weights from B vertices to the bisecting vertices to be α^{-1},

resulting in a system

$$F = \qquad\qquad\qquad\qquad\qquad\qquad\qquad\qquad (3.99)$$

$$F^2 = G(\alpha^2, \alpha^{-2}) + K \qquad\qquad\qquad\qquad (3.100)$$

$$K = \qquad\qquad\qquad\qquad\qquad\qquad\qquad\qquad (3.101)$$
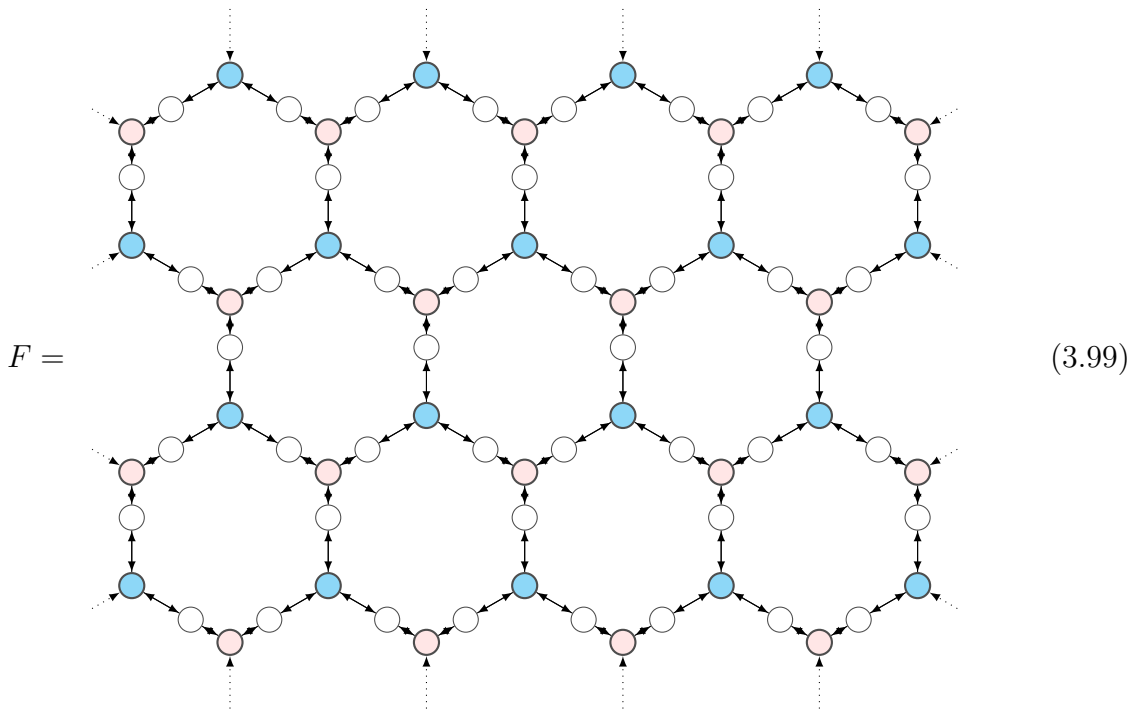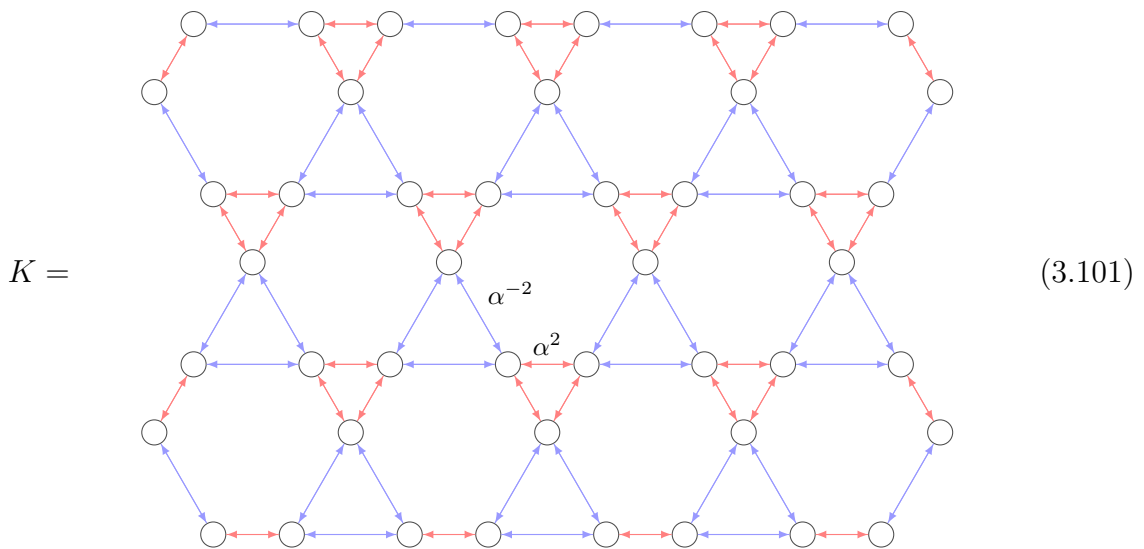
with eigenspectrum plotted in fig. 3.15. The square of this system is then a honeycomb with loop edges $3\alpha^2$ on A sites and $3\alpha^{-2}$ on B sites, and a kagome-like lattice with loop edges $(\alpha^2 + \alpha^{-2})$, edge weights α^2 between vertices surrounding a common A vertex, and edge weights α^{-2} between vertices separated by a B vertex.

This prescription can be applied to any lattice structure, and indeed any graph. It is
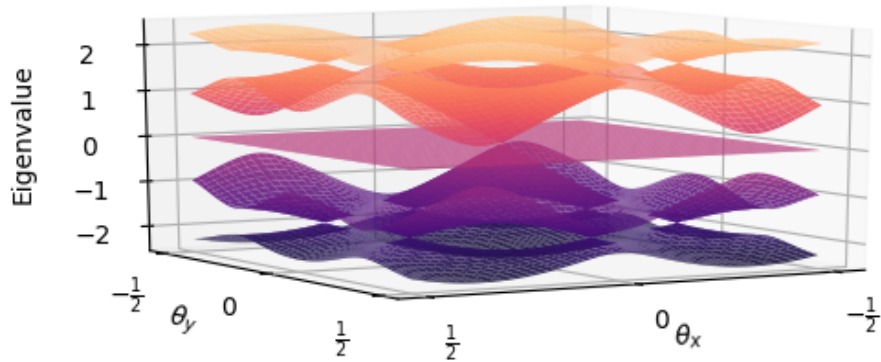
Figure 3.13: Eigenspectrum of the honeycomb's parent H

useful both as an exploratory tool and as a way of finding an ancestral relation between different systems.

3.6   Conclusion

In this chapter, we have looked at several well-known quantum systems through a new perspective using the graph algebra introduced in chapter 1. We have seen how different systems can be related to one another through polynomials, and how the solution of a parent system can be utilised to gain quantitative understanding about the behaviour of its child systems.

In section 3.1 we saw how homogeneous n^{th}-neighbour models of the monatomic chain can be solved indirectly, by taking polynomials of the unit nearest-neighbour version. We used this result to demonstrate several examples of distance-bond relationships.

We demonstrated the Aharonov-Bohm effect in a discrete system in section 3.2, describing how an injected state at one side of a system can be prevented from occupying a vertex at the other side due to destructive interference from its multiple paths. We then
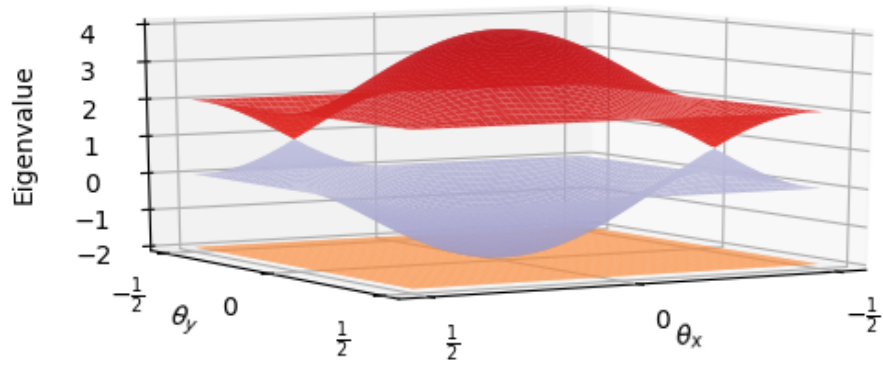
Figure 3.14: Eigenspectrum of the kagome lattice with unit edges and zero self-loop weights
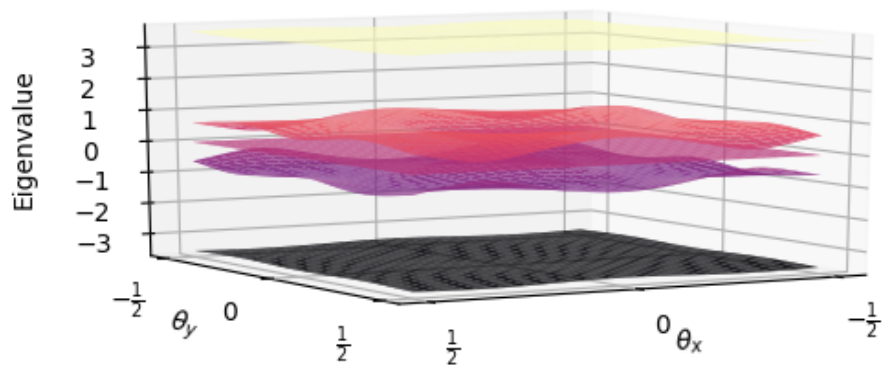
Figure 3.15: Eigenspectrum of the alternating honeycomb's parent F

showed how the time-dependent Schrödinger equation allows us to coerce a chain into performing a π rotation in the phase of the amplitude at a final site, simply by exploiting the odd and even powers of a lattice which squares to an Aharonov-Bohm loop.

In section 3.3 and section 3.4 we demonstrated the use of the graph algebra in two-dimensional systems. We noted the difference between topological and geometrical next-nearest neighbours, and explored how polynomials can introduce meaningful next-nearest neighbour edges when the topological and geometrical next-nearest neighbours are equivalent. In a system presenting different types of next-nearest neighbours are inequivalent, we have explored how a magnetic field may introduce a destructive interference to remove unwanted interactions in higher powers, and how the famous Hofstadter Butterfly results from the separation of a lattice into sublattices of larger area.

We also saw how two different systems can be related through polynomials, providing that they share a similar structure. Even when equivalence holds only when both sides of the equation involve polynomials, we can intuitively understand the behavioural differences between the two systems using the rules set out in chapter 2. When the child system is separable, the parent eigenspectrum can be recovered by solving equations of fewer sites. Indeed, knowing that the honeycomb has a symmetric eigenspectrum, a simulation of a finite honeycomb can be performed indirectly by decomposing a single sublattice of its squared representation and passing the resulting eigenvalues through a square root.

Although the systems we have covered in this chapter are simple, they serve as a useful platform from which to view tight-binding systems in a new light.

Chapter 4

Polynomial relationships of topological chains

Introduction

As the story goes, in 1927 Niels Bohr asked Paul Dirac "What are you working on Mr. Dirac?" to which Dirac replied "I'm trying to take the square root of something." Once Dirac achieved his goal, to identify the desired operator that squares to the Klein-Gordon equation, he had not only laid down a description of relativistic electrons replete with spin and antimatter [34, 35]. As it emerged later, Dirac's very same operator also plays a central role for topological considerations in differential geometry, where the Atiyah-Singer index theorem addresses its zero modes [36]. The zero modes in the topological materials considered today are a direct extension of this connection [37, 38]. Fundamental symmetries can guarantee that all positive-energy states are paired with negative-energy states, with the exception of a protected set of zero-energy states whose number $|\nu|$ is obtained from a topological invariant. These properties may follow from a charge-conjugation sym-

metry, as encountered in superconductors [39, 40], or from a chiral symmetry, as encountered for the Dirac operator [41, 42]; both operations anticommute with the Hamiltonian and therefore single out a spectral symmetry point.

In combination with possible invariance under time-reversal, these spectral symmetries determine a ten-fold system of universality classes [43, 40], which can be further extended by including aspects of dimensionality [44, 45] and the space group (i.e., crystal symmetries) [46]—for example, nonsymmorphic symmetries involving fractional lattice translations can replace fundamental symmetries normally associated with fermionic systems [47]. Depending on the universality class, the topological invariant may take the values $\nu \in \{0, 1\}$, leading to the notion of a $\mathbb{Z}_2$ invariant, or be any integer, leading to the notion of a $\mathbb{Z}$ invariant. These topological features are not present in the Klein-Gordon equation, from which Dirac had started to take the square-root of, a task which was non-trivial as it required him to introduce extra components and matrices.

In this chapter, we explore the properties of topological chains through the perspective of the graph algebra, forming relationships between some notable models. We see how the topological properties of such models can be directly related to trivial systems that result from taking polynomials, and how the inverse relationship describes the appearance of topological artifacts as a result of a "square root". These features arise because the square-root operation provides a way of inducing (typically nonsymmorphic) *spectral* symmetries at the expense of broken *crystal* symmetries.

4.1   The SSH Model

The Su-Schrieffer-Heeger (SSH) model of Polyacetylene[48] describes a chain with alternating edge weights, induced by a dimerisation known as the Peierls instability. Let us

denote the graph of this model by $S(\Delta)$, where the edge weights alternate as $1+\Delta$, $1-\Delta$. Then, if we represent edges of weight $1+\Delta$ by a solid line and edges of weight $1-\Delta$ with a dashed line,

$$S(\Delta) = \ldots \qquad \ldots \qquad (4.1)$$

$$\mathrm{walk}(S) = \ldots \qquad \ldots \qquad (4.2)$$

We can build this chain in the previous manner through the graphs

$$\mathrm{walk}(\tilde{G}(\Delta)) = \qquad \mathrm{adj}(\tilde{G}(\Delta)) = \begin{pmatrix} 0 & 1+\Delta \\ 1+\Delta & 0 \end{pmatrix} \qquad (4.3)$$

$$\mathrm{walk}(\tilde{L}(\Delta)) = \qquad \mathrm{adj}(\tilde{L}(\Delta)) = \begin{pmatrix} 0 & 0 \\ 1-\Delta & 0 \end{pmatrix} \qquad (4.4)$$

$$\mathrm{walk}(\tilde{R}(\Delta)) = \qquad \mathrm{adj}(\tilde{R}(\Delta)) = \begin{pmatrix} 0 & 1-\Delta \\ 0 & 0 \end{pmatrix} \qquad (4.5)$$

such that

$$S(\Delta) = \tilde{G}^{\oplus\infty} + T\tilde{R}^{\oplus\infty} + T^{-1}\tilde{L}^{\oplus\infty} \qquad (4.6)$$

Projecting into an eigenspace of translation eigenvalue $\exp(2\pi i \theta)$, we find

112

$$\tilde{s}(\Delta,\theta) = \begin{array}{c} (1+\Delta) \\ +e^{-2\pi i\theta}(1-\Delta) \end{array} \qquad \begin{array}{c} (1+\Delta) \\ +e^{2\pi i\theta}(1-\Delta) \end{array} \tag{4.7}$$

$$\mathrm{adj}(\tilde{s}(\Delta,\theta)) = \begin{pmatrix} 0 & (1+\Delta)+e^{2\pi i\theta}(1-\Delta) \\ (1+\Delta)+e^{-2\pi i\theta}(1-\Delta) & 0 \end{pmatrix} \tag{4.8}$$

with eigenspectrum

$$\lambda_\pm = \pm\sqrt{2(1+\Delta^2)+2(1-\Delta^2)\cos(2\pi\theta)}, \tag{4.9}$$

depicted visually in fig. 4.1. The spectrum is symmetric around zero for each choice of translation eigenvalue, with a gap of 4Δ at $\theta = \frac{1}{2}$. Thus the difference in the alternating edge weights is the root cause of the gap. At $\Delta = 1$, the inter-cell connection units become null and we represent an infinite set of connected pairs, each disconnected from its neighbouring pairs. As a result, the graph loses its dependence on the translation graphs and the bands become flat.

We apply the prescription that we are now very used to. Knowing that $\tilde{s}(\Delta,\theta)^2$ must have the eigenspectrum

$$\lambda_+^2 = 2(1+\Delta^2)+2(1-\Delta^2)\cos(2\pi\theta), \tag{4.10}$$

$$\lambda_-^2 = 2(1+\Delta^2)+2(1-\Delta^2)\cos(2\pi\theta), \tag{4.11}$$

plotted in fig. 4.2, we note some familiarity with a spectrum we have already seen. Indeed, λ_+^2 and λ_-^2 are polynomials of the eigenspectrum of the monatomic chain $\tilde{m}(\theta)$,

113
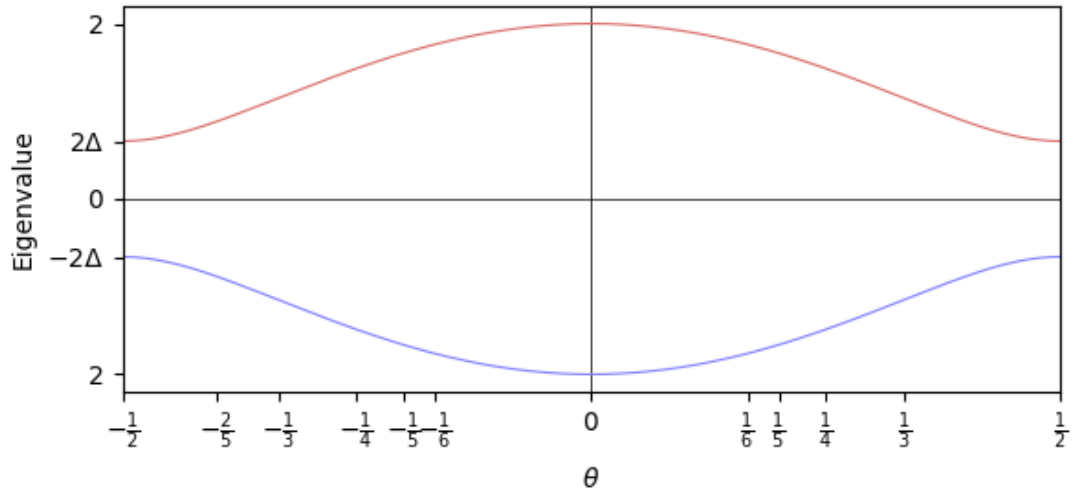
Figure 4.1: Eigenspectrum of the SSH chain with unit average edge weight
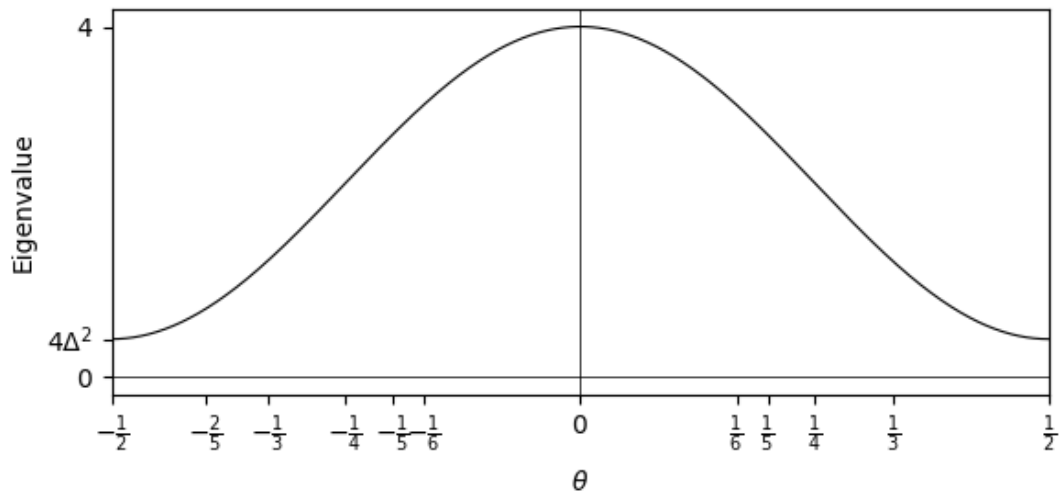
Figure 4.2: Eigenspectrum of the squared SSH chain

114

or a monatomic chains with modified nearest-neighbour edges and loop edges. As such, fig. 4.2 is related to fig. 3.1 through a linear transformation of scaling by $(1 - \Delta^2)$ and shifting by $2(1 + \Delta^2)$. Such a transformation is revealed through the graph algebra, in the projected graph with

$$\tilde{s}(\Delta, \theta)^2 = \qquad\qquad\qquad\qquad\qquad\qquad\qquad\qquad\qquad (4.12)$$

$$= \quad \begin{array}{c} 2(1 + \Delta^2) \\ +2(1 - \Delta^2)\cos(2\pi i\theta) \end{array} \qquad\qquad \begin{array}{c} 2(1 + \Delta^2) \\ +2(1 - \Delta^2)\cos(2\pi i\theta) \end{array} \qquad (4.13)$$

which is the polynomial

$$= \Big(2\big(1 + \Delta^2\big)\, p_0(\tilde{m}(\theta)) + \big(1 - \Delta^2\big)\, p_1(\tilde{m}(\theta)) \Big)^{\oplus 2}, \qquad (4.14)$$

and through the full graph with

$$\text{walk}(S(\Delta)^2) = \dots \qquad\qquad\qquad\qquad\qquad \dots \qquad (4.15)$$

$$= \dots \qquad \qquad \dots \qquad (4.16)$$

where, in eq. (4.16) the solid lines represent edges of weight $2(1+\Delta^2)$ and dotted lines represent edges of weight $2(1-\Delta^2)$. Thus

$$S(\Delta)^2 = \dots \qquad \qquad \dots \qquad (4.17)$$

or, equivalently

$$\frac{S(\Delta)^2 - 2(1+\Delta^2)}{1-\Delta^2} = \dots \qquad \qquad \dots \qquad (4.18)$$

$$= M \oplus M \qquad (4.19)$$

We have so far looked at infinite chains, particularly for their convenience: finite systems cannot commute with translation operators, and thus cannot be simplified into translation eigenspaces. However, the SSH chain provides a suitable setting for exploring the impact of restricting a system into a finite graph.

Let us consider a finite SSH chain of N cells, such that the total number of vertices remains even,

$$S' = \qquad \qquad (4.20)$$
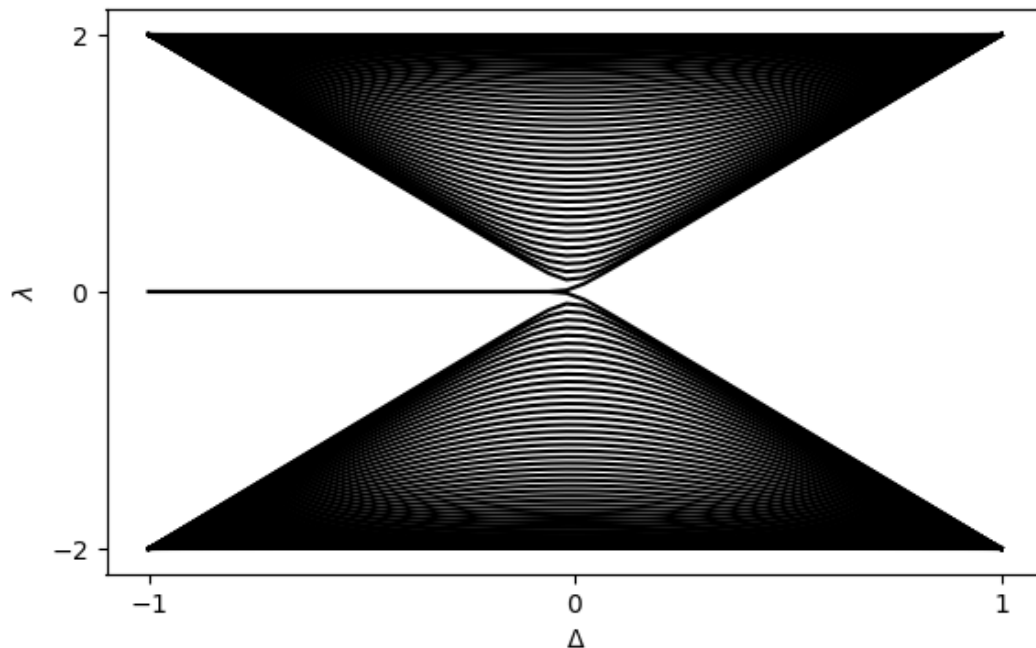
Figure 4.3: The eigenspectrum of a finite chain of 200 vertices, with alternating hoppings $1 + \Delta$ and $1 - \Delta$, with varying Δ.

The eigenspectrum is plotted in fig. 4.3, varying Δ from -1 to 1, the dimerisation limits. In the infinite system, as explained above, the dimerisation limits cause flat bands. For $\Delta = -1$, the vertices in the same unit cell become disconnected, and for $\Delta = 1$ the neighbouring cells become disconnected. These two cases are equivalent in the infinite system, each obtainable from the other by a translation of half of a unit cell, and thus the bands hold flat at eigenvalues 2 and -2 in both cases. In the finite system, the dimerisation limits are inequivalent: in the case of $\Delta = 1$, every vertex is paired with the other in its unit cell, but in the case of $\Delta = -1$, the vertices at each edge of the chain have no neighbouring cell to connect to, and become isolated. Having no loop edge, a state fully occupying them necessarily has an eigenvalue of zero.

Although we have a solid argument that the zero eigenvalue state must fully occupy one of the extreme vertices in the $\Delta = -1$ limit, we can explore the nature of the zero

117

eigenvalue states at other Δ by breaking down the eigenvalue equation into constituent parts. Let v be an eigenstate at eigenvalue λ, and consider the component v_n of this eigenvector corresponding to a vertex V_n, connected to a set $\{V_m\}$ of vertices with with bonds of weight $\{w_{n,m}\}$. The eigenvalue equation then demands

$$\lambda v_n = \sum_m w_{n,m} v_m \tag{4.21}$$

As such, let us consider an eigenstate v with eigenvalue $\lambda = 0$, with some real, positive-definite amplitude v_1 at the far left vertex. Then

$$0(v_1) = (1 + \Delta)v_2 \qquad\qquad \Rightarrow v_2 = 0 \tag{4.22}$$

$$0(v_2) = (1 + \Delta)v_1 + (1 - \Delta)v_3 \qquad\qquad \Rightarrow (\Delta + 1)v_1 = (\Delta - 1)v_3 \tag{4.23}$$

$$\Rightarrow v_3 = \left(\frac{\Delta + 1}{\Delta - 1}\right) v_1 \tag{4.24}$$

$$0(v_3) = (1 - \Delta)v_2 + (1 + \Delta)v_4 \qquad\qquad \Rightarrow v_4 = 0, \tag{4.25}$$

$$0(v_4) = (1 + \Delta)v_3 + (1 - \Delta)v_5 \qquad\qquad \Rightarrow (\Delta + 1)v_3 = (\Delta - 1)v_5 \tag{4.26}$$

$$\Rightarrow v_5 = \left(\frac{\Delta + 1}{\Delta - 1}\right) v_3, \tag{4.27}$$

and so on, such that

$$v_{2j+1} = \left(\frac{\Delta + 1}{\Delta - 1}\right) v_{2j-1} \qquad\qquad v_{2j} = 0 \qquad\qquad \forall j \in [1..N] \tag{4.28}$$

The resulting state is thus an evanescent mode decaying to the right, occupying a single sublattice, when $\Delta < 0$. Note here that we have relied upon a positive-definite v_1: at $\Delta > 0$, the amplitude of the state on successive odd-numbered vertices increases exponentially to the right according to the local parameter Δ, which is unphysical unless we had set $v_1 = 0$. As well as this "zero mode" decaying to the right, there is another

such mode decaying to the left from the right edge of the system, symmetrically following the same principle as equations eq. (4.22) to eq. (4.27), using the even-indexed vertices. These modes are sublattice-polarised for all negative Δ; these modes are thus *topologically-protected* against local perturbations within the limit $\Delta < 0$.

Let us now look at the impact of the hard boundary on the squared system. The loop edges of the vertices in the monatomic child of the SSH chain are determined by length-2 walks that return to the original vertex. In the case of the finite SSH chain, the vertices at the boundaries of the chain thus have a modified weight compared with the rest of the chain.

$$S'(\Delta)^2 = \qquad\qquad\qquad\qquad\qquad\qquad\qquad\qquad (4.29)$$

Remarkably, this configuration of a monatomic chain is sufficient to create these zero modes, demonstrated in the spectum plotted in fig. 4.4; this is a property that would be difficult to interpret without the graph algebra.

We can introduce a defect in the SSH chain by breaking the alternating pattern of the edge weights, such that one site has edges of equal weight either side, as in

$$S'(\Delta) = \qquad\qquad\qquad\qquad\qquad\qquad\qquad\qquad (4.30)$$

we can observe the impact on the squared system by looking at the local impact on the system,
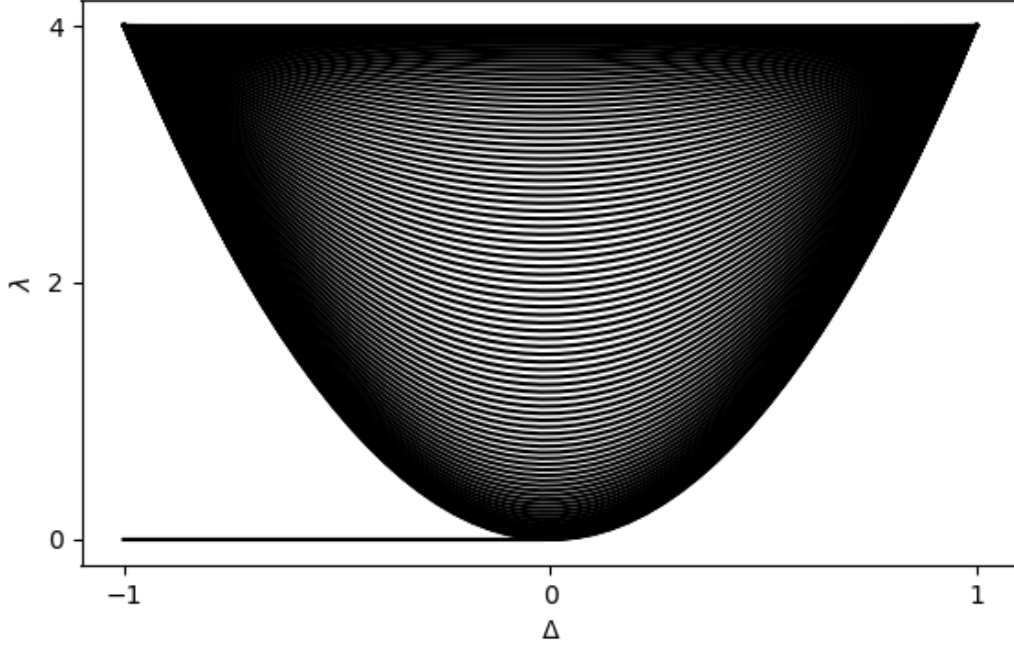
Figure 4.4: The eigenspectrum of a single monatomic chain in $S'(\Delta)^2$, demonstrating the appearance of the zero mode for negative Δ.

$$S'(\Delta)^2 = \qquad\qquad\qquad\qquad\qquad . \qquad (4.31)$$

The loop edge weight at the defect site in $S'(\Delta)^2$ transforms from $2(1+\Delta^2)$ to $2(1+\Delta)^2$, and the edge passing through it, from the vertex to the left to the vertex to that on the right, is transformed from $(1-\Delta^2)$ to $(1+\Delta)^2$. Thus, the defect modifies a vertex in one of the separated graphs of $S'(\Delta)^2$, and modifies an edge in the other separated graphs.

As the defect is connected to by edges of the same weight, it too can become isolated in one of the dimerised limits, forming a triplet in the other, and thus contributes a zero-eigenvalue at both dimerisation limits as in fig. 4.5.

120
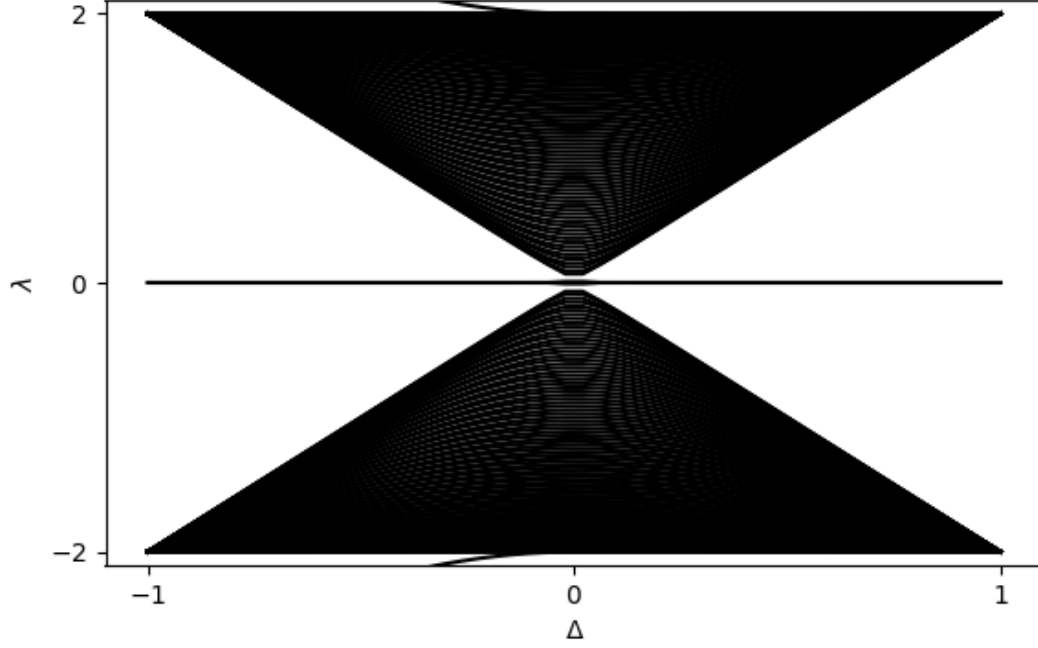
Figure 4.5: Eigenspectrum of a finite SSH chain of 200 vertices, with a defect in the centre, with varying Δ.

The SSH chain anticommutes with a chiral operator[49] C corresponding to the σ_z Pauli matrix

$$\text{König}(\sigma_z) = \quad \begin{array}{c} 1 \end{array} \quad \begin{array}{c} -1 \end{array} \, , \tag{4.32}$$

$$C = \text{graph}(\sigma_z)^{\oplus \infty, \infty} \tag{4.33}$$

such that

$$CS(\Delta)C = -S(\Delta) \tag{4.34}$$

and, for the infinite case,

$$\text{graph}(\sigma_z) \, \tilde{s}(\Delta, \theta) \, \text{graph}(\sigma_z) = -\tilde{s}(\Delta, \theta), \tag{4.35}$$

described as chiral symmetry (in a condensed matter setting). As such, positive and

negative eigenvalues are related through the σ_z operator. We can thus decompose the polynomial form of S as a monoatomic chain, and add the components from each sublattice deterministically to create the positive and negative eigenstates of S. If we add or remove a vertex from the finite SSH chain, the number of eigenstates becomes odd, such that there exists a state for which there is no partner state which has an eigenvalue of the opposite sign: it must obey this relationship with itself. As a result, it must commute with the chiral symmetry operator, and thus exist solely on one sublattice, and have an eigenvalue of zero.

4.2 The Rice-Mele model

The Rice-Mele model[50] is a system proposed to describe conjugated polymers. It extends the idea of the SSH chain by equipping vertices with loop edges of equal magnitude δ, but alternating sign, as in

$$R = \qquad\qquad\qquad\qquad\qquad\qquad\qquad\qquad\qquad\qquad (4.36)$$

As we have already seen in section 3.4, this results in a pseudo-bipartite system with very similar properties to the SSH chain, except that each eigenvalue λ of the SSH chain becomes $\sqrt{\lambda^2 + \delta^2}$, as in fig. 4.6. This result is trivially derived from the polynomial relationship

$$R^2 = S^2 + \delta^2 \qquad\qquad\qquad\qquad\qquad\qquad\qquad (4.37)$$

In the case of the finite Rice-Mele model, the zero-eigenvalue states from the finite SSH chain become separated, as shown in fig. 4.7. The sublattice occupied by each such
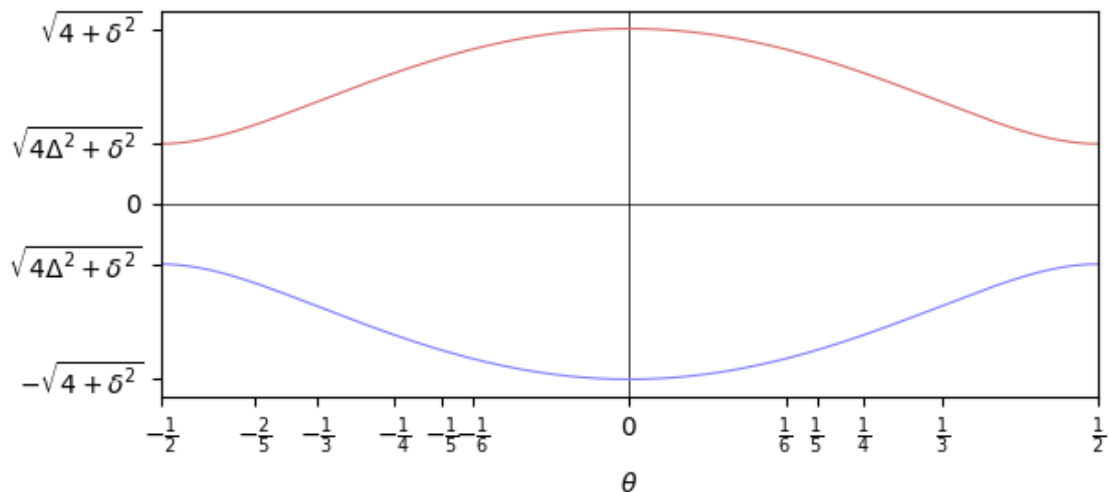
Figure 4.6: Eigenspectrum of an infinite Rice-Mele chain with varying translation eigenvalue

eigenstate is trivial to identify in the dimerisation limit, and as eq. (4.21) takes into account the loop edges, the transfer approach used in Equations 4.22 to 4.27 also apply to the Rice-Mele model.

However, while the SSH chain anticommutes with the chiral symmetry graph, rendering it topologically-nontrivial, this is not the case with the Rice Mele model with $\delta \neq 0$, because the loop edges return to their original signs after multiplication on the left and right with $\text{graph}(\sigma_z)$. Thus the Rice Mele model is topologically trivial.

In the SSH chain we looked at how a defect formed by breaking the alternating pattern of edges strengths can introduce a pair of zero-eigenvalue bands that result from the isolation of a vertex. In the Rice-Mele model, we can introduce a defect by breaking the alternating pattern of the loop edges. As we are aware, the alternating sign of the loop edges maintains the separability of the squared system into monatomic chains, and thus we expect that breaking this pattern will render the squared system unseparable.

Indeed, if
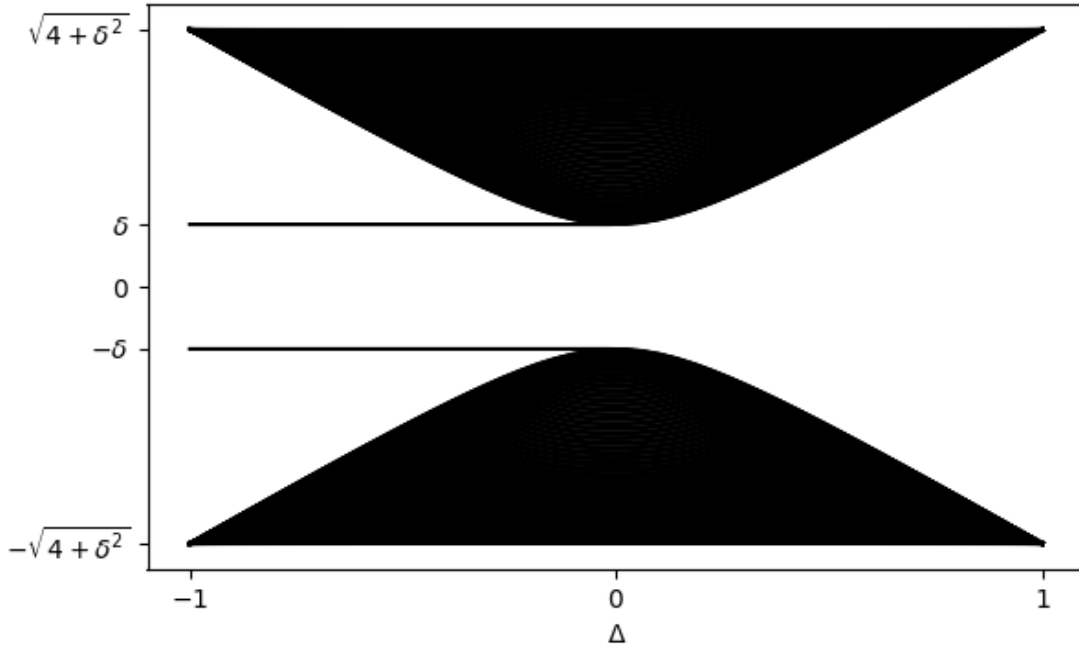
Figure 4.7: Eigenspectrum of a finite Rice-Mele chain of 200 vertices

$$R' = \ldots \qquad \qquad \ldots \qquad (4.38)$$

then

$$(R')^2 = \ldots \qquad \qquad \ldots, \qquad (4.39)$$

and if

$$R' = \ldots \qquad \qquad \ldots \qquad (4.40)$$

124

then

$$(R')^2 = \ldots \qquad\qquad\qquad\qquad\qquad\qquad\qquad\qquad\qquad \ldots,$$

(4.41)

4.3 The bowtie chain

We shall now look at an extension of the Rice-Mele model with remarkable topological properties, linked to its squared representation as a two-legged ladder. Although our original research began from the opposite direction, starting from the two-legged ladder and discovering the bowtie chain as a square root through symmetry arguments, we shall here present the reverse of this process in order to maintain the pedagogical manner of writing. A more detailed explanation of how we arrived at the bowtie chain model, along with a proposal for a photonic experimental realisation, can be found at [12], upon which this section is based, and the reader is encouraged to explore the subsequent work inspired in part by this research at [51, 52, 53, 54, 55, 56, 57, 58], and the realisation of the photonic system at [59].

Introduction

The bowtie chain is a chain with loop edges alternating as $(\beta, \beta, -\beta, -\beta, \ldots)$ and nearest neighbour edges alternating as $(\kappa, \gamma, -\kappa, -\gamma, \ldots)$,

$$B = \quad \text{(4.42)}$$

which can be represented with the translation method, in the usual manner, through the graphs

$$\tilde{G} = \quad \text{(4.43)}$$

$$\text{walk}(\tilde{L}) = \quad \text{(4.44)}$$

$$\text{walk}(\tilde{R}) = $$

$$B = \tilde{G}^{\oplus\infty} + T_L\tilde{L}^{\oplus\infty} + T_R\tilde{R}^{\oplus\infty} \quad \text{(4.45)}$$

which we can project to the translation eigenspace and obtain

$$\text{adj}(\tilde{b}(\theta)) = \begin{pmatrix} \beta & \kappa & 0 & -\gamma e^{-2\pi i\theta} \\ \kappa & \beta & \gamma e^{2\pi i\theta} & 0 \\ 0 & \gamma e^{-2\pi i\theta} & -\beta & -\kappa \\ -\gamma e^{2\pi i\theta} & 0 & -\kappa & -\beta \end{pmatrix} \quad \text{(4.46)}$$

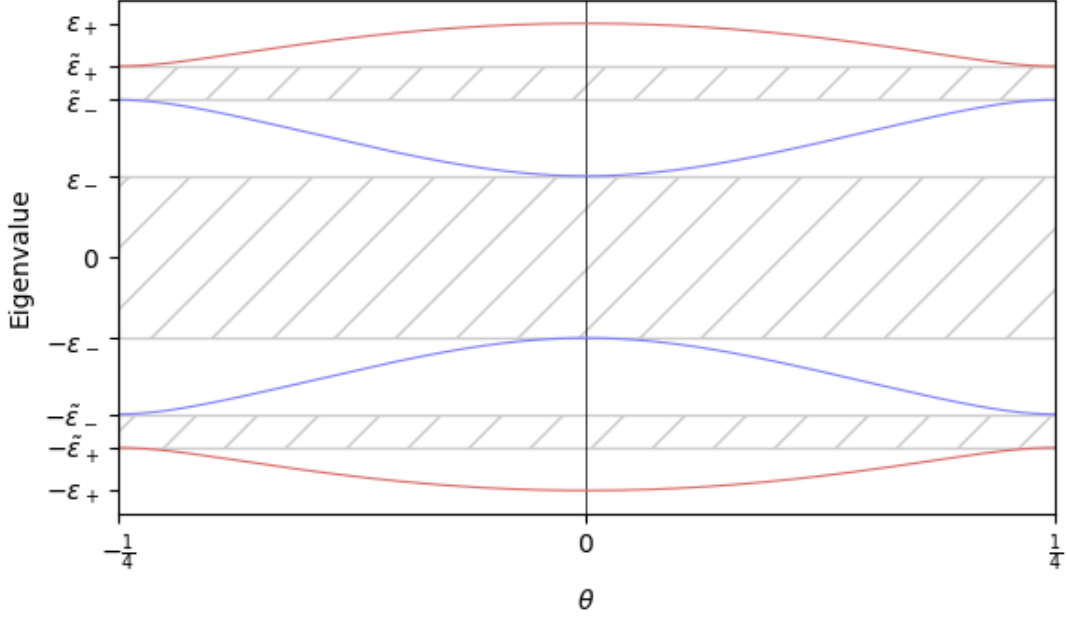with the four eigenvalues, plotted in fig. 4.8,

Figure 4.8: The spectrum of the bowtie chain, demonstrating the band edges at the ε and $\tilde{\varepsilon}$ described in eq. (4.48) in the phase $(\xi, \tilde{\xi}) = (1, 1)$, described in eq. (4.111). Other phases change the order of the band edges.

$$\lambda_{\mu,\eta}(\theta) = \eta\sqrt{\beta^2 + \gamma^2 + \kappa^2 + 2\mu\kappa\sqrt{\beta^2 + \gamma^2 \cos^2(2\pi\theta)}}, \qquad (4.47)$$

where the label $\eta = \pm 1$ selects between positive and negative eigenvalues, and the label $\mu = \pm 1$ selects between higher and lower magnitude eigenvalues. The four bands thus come in two pairs, with edges

$$\varepsilon_\pm = \sqrt{\beta^2 + \gamma^2} \pm \kappa, \qquad\qquad \tilde{\varepsilon}_\pm = \sqrt{\gamma^2 + (\beta \pm \kappa)^2}. \qquad (4.48)$$

The square of the bowtie chain adopts the remarkable form of a two-legged ladder with an effective π magnetic flux,

127

$$B^2 = \qquad \qquad \qquad ,$$

(4.49)
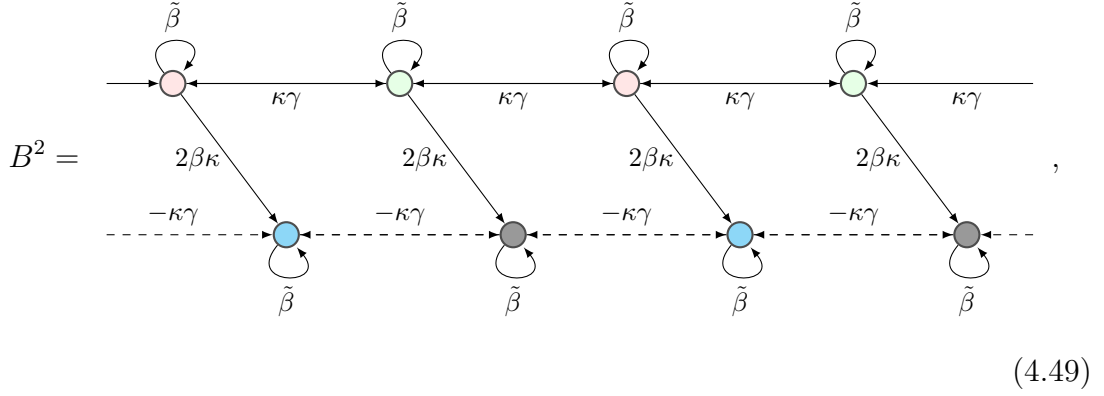
$$\text{adj}(\tilde{b}^2(\theta)) = \begin{pmatrix} \tilde{\beta} & 2\beta\kappa & \kappa\gamma(1 + e^{-2\pi i\theta}) & 0 \\ 2\beta\kappa & \tilde{\beta} & 0 & -\kappa\gamma(1 + e^{-2\pi i\theta}) \\ \kappa\gamma(1 + e^{2\pi i\theta}) & 0 & \tilde{\beta} & 2\beta\kappa \\ 0 & -\kappa\gamma(1 + e^{2\pi i\theta}) & 2\beta\kappa & \tilde{\beta} \end{pmatrix}$$

(4.50)

where $\tilde{\beta} = \beta^2 + \kappa^2 + \gamma^2$. The eigenspectrum of this graph is plotted in fig. 4.9.

B possesses a *nonsymmorphic* symmetry in the form of a fractional lattice translation[60]. Let T' be a translation by half of a unit cell, then

$$T'B = -B'T.$$

(4.51)

As we saw in section 3.3, such an anticommuting relationship between B and T' manifests itself as a commuting relationship between B and $(T')^2$, which we know as the translational symmetry of B, and as a commuting relationship between B^2 and T'. Indeed, B^2 is invariant under the translation T', and we can project B^2 into the eigenspaces of T', with eigenvalues $\exp(2\pi i\theta') = \exp(4\pi i\theta)$, in the simpler form

$$\text{adj}(\tilde{l}(\theta')) = \begin{pmatrix} \tilde{\beta} + 2\kappa\gamma\cos(2\pi\theta') & 2\beta\kappa \\ 2\beta\kappa & \tilde{\beta} - 2\kappa\gamma\cos(2\pi\theta') \end{pmatrix},$$

(4.52)

which we can describe with periodic graphs as

$$\tilde{H} = \quad \tilde{L} = \quad \tilde{R} = \tag{4.53}$$

with

$$B^2 = \tilde{H}^{\oplus\infty} + T'_L\tilde{L}^{\oplus\infty} + T'_R\tilde{R}^{\oplus\infty} \tag{4.54}$$

Due to the effective π-flux of the two-legged ladder B^2, we can obtain further decoupling by taking another polynomial. Indeed, $B^2 - \tilde{\beta}$ itself squares to a set of four independent monatomic chains with edge weight $(\kappa\gamma)^2$ and loop edges of weight $\alpha = 2\kappa^2(2\beta^2 + \gamma^2)$,

$$(B^2 - \tilde{\beta})^2 - \alpha = \tag{4.55}$$

4.3.1 Symmetries and the 10 fold way

The Atland-Zirnbauer symmetry classes categorise quantum systems by their time-reversal, charge-conjugation, and chiral symmetry operations. We represent these symmetries with the operators $\mathcal{T}$, $\mathcal{C}$, and $\mathcal{X}$ respectively, and operate upon a hamiltonian $H(\theta)$ as

$$\mathcal{T}H(\theta)\mathcal{T}^{-1} = +H(-\theta) \tag{4.56}$$
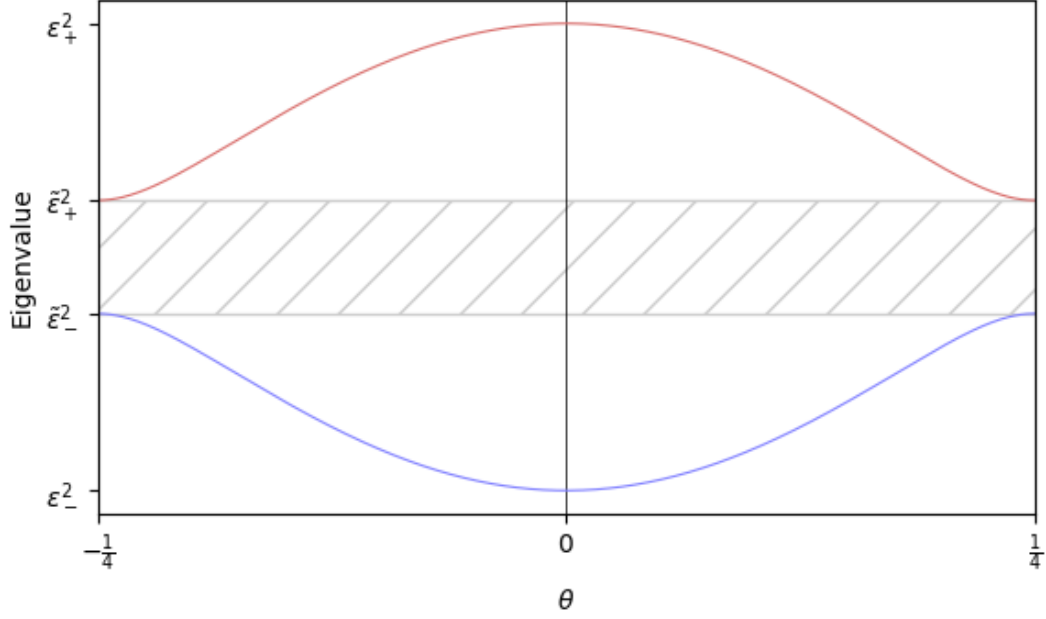
Figure 4.9: The eigenspectrum of the squared bowtie chain, demonstrating the band edges at the

ε *and* $\tilde{\varepsilon}$ *described in eq.* (4.48)

$$\mathcal{C}H(\theta)\mathcal{C}^{-1} = -H(-\theta) \tag{4.57}$$

$$\mathcal{X}H(\theta)\mathcal{X}^{-1} = -H(+\theta) \tag{4.58}$$

For any hamiltonian with periodicity in N dimensions, there may or may not exist an operator $\mathcal{T}$ satisfying eq. (4.56). If one does exist, it may square to either the unit matrix in N dimensions, or it may square to negative the unit matrix. Thus there are three classes of system corresponding to time reversal. Consider some eigenstate $|\psi(\theta)\rangle$ of $H(\theta)$ with eigenvalue $\lambda_\psi(\theta)$. Then, if a time reversal symmetry exists in H,

$$H(-\theta)\mathcal{T}|\psi(\theta)\rangle = \mathcal{T}H(\theta)|\psi(\theta)\rangle \tag{4.59}$$

$$= \lambda_\psi(\theta)\mathcal{T}|\psi(\theta)\rangle, \tag{4.60}$$

which enforces that, for each such eigenstate $|\psi(\theta)\rangle$ of $H(\theta)$, there is an eigenstate $\mathcal{T}|\psi(\theta)\rangle$ of $H(-\theta)$ with the same eigenvalue: the eigenspectrum is thus symmetric around the line

130

$\theta = 0$.

Likewise, there may or may not exist an operator $\mathcal{C}$ satisfying eq. (4.57), and, if one does exist, it may square either to the unit matrix or negative the unit matrix. Thus there are three classes of system corresponding to charge-conjugation. The existence of such a $\mathcal{T}$ is independent from the existence of a $\mathcal{C}$ operation, and so there are 9 possible classes of system corresponding to the combination of these two symmetries. Consider again the state $|\psi(\theta)\rangle$ of some $H(\theta)$ which possesses charge-conjugation symmetry. Then

$$H(-\theta)\mathcal{C}|\psi(\theta)\rangle = -\mathcal{C}H(\theta)|\psi(\theta)\rangle \tag{4.61}$$

$$= -\lambda_\psi(\theta)\mathcal{C}|\psi(\theta)\rangle, \tag{4.62}$$

which enforces that, for each eigenstate $|\psi(\theta)\rangle$ of $H(\theta)$, there is an eigenstate $\mathcal{C}|\psi(\theta)\rangle$ of $H(-\theta)$ with an eigenvalue of the same magnitude but opposite sign.

The existence of both a time reversal operator and a charge conjugation operator implies the existence of the chiral symmetry by choosing $\mathcal{X} = \exp(i\omega)\mathcal{T}\mathcal{C}$ for some $\omega \in \mathbb{R}$. If only one of either the time reversal symmetry or the charge conjugation symmetry is present, there is no chiral symmetry[10]. Finally, if neither time reversal symmetry nor charge conjugation symmetry are found, then there may or may not be a chiral symmetry. Considering again the state $|\psi(\theta)\rangle$ of some $H(\theta)$ which possesses chiral symmetry,

$$H(\theta)\mathcal{X}|\psi(\theta)\rangle = -\mathcal{X}H(\theta)|\psi(\theta)\rangle \tag{4.63}$$

$$= -\lambda_\psi(\theta)\mathcal{X}|\psi(\theta)\rangle, \tag{4.64}$$

Such that each such eigenstate $|\psi(\theta)\rangle$ of $H(\theta)$ is accompanied by an eigenstate $\mathcal{X}|\psi(\theta)\rangle$, also of $H(\theta)$, with the opposite eigenvalue. If an odd number of eigenstates are present, then there necessarily exists an eigenstate at eigenvalue $\lambda = 0$, which is invariant under

$\mathcal{X}$ up to a phase.

Taking all combinations of time-reversal, charge-conjugation, and chiral symmetry into account, there are 10 possible symmetry classes, provided in table 4.1. For any hamiltonian with an infinite translational symmetry, the nature of possible topological phases can be determined by identifying the existence of such symmetries and cross-referencing against the number N of dimensions of infinite translational symmetry.

For the bowtie chain, with hamiltonian $\tilde{b}(\theta)$, a time reversal graph $\mathcal{T}$ exists in the form

$$\text{walk}(\mathcal{T}) = \quad\quad\quad \text{adj}(\mathcal{T}) = \begin{pmatrix} 0 & 1 & 0 & 0 \\ 1 & 0 & 0 & 0 \\ 0 & 0 & 0 & -1 \\ 0 & 0 & -1 & 0 \end{pmatrix},$$

(4.65)

where

$$\mathcal{T}\tilde{b}(\theta)\mathcal{T} = \tilde{b}(-\theta), \tag{4.66}$$

$$\mathcal{T}\tilde{b}^2(\theta)\mathcal{T} = \tilde{b}^2(\theta), \tag{4.67}$$

$$\mathcal{T}^2 = 1. \tag{4.68}$$

There exists the charge conjugation symmetry in the form

$$\mathcal{C} = \quad\quad\quad \text{adj}(\mathcal{C}) = \begin{pmatrix} 0 & 0 & 0 & i \\ 0 & 0 & i & 0 \\ 0 & -i & 0 & 0 \\ -i & 0 & 0 & 0 \end{pmatrix}, \tag{4.69}$$

	Symmetry			Dimension							
Class	$\mathcal{T}$	$\mathcal{C}$	$\mathcal{X}$	1	2	3	4	5	6	7	8
A	0	0	0	0	$\mathbb{Z}$	0	$\mathbb{Z}$	0	$\mathbb{Z}$	0	$\mathbb{Z}$
AIII	0	0	1	$\mathbb{Z}$	0	$\mathbb{Z}$	0	$\mathbb{Z}$	0	$\mathbb{Z}$	0
AI	$+1$	0	0	0	0	0	$\mathbb{Z}$	0	$\mathbb{Z}_2$	$\mathbb{Z}_2$	$\mathbb{Z}$
BDI	$+1$	$+1$	1	$\mathbb{Z}$	0	0	0	$\mathbb{Z}$	0	$\mathbb{Z}_2$	$\mathbb{Z}_2$
D	0	$+1$	0	$\mathbb{Z}_2$	$\mathbb{Z}$	0	0	0	$\mathbb{Z}$	0	$\mathbb{Z}_2$
DIII	-1	$+1$	1	$\mathbb{Z}_2$	$\mathbb{Z}_2$	$\mathbb{Z}$	0	0	0	$\mathbb{Z}$	0
AII	-1	0	0	0	$\mathbb{Z}_2$	$\mathbb{Z}_2$	$\mathbb{Z}$	0	0	0	$\mathbb{Z}$
CII	-1	-1	1	$\mathbb{Z}$	0	$\mathbb{Z}_2$	$\mathbb{Z}_2$	$\mathbb{Z}$	0	0	0
C	0	-1	0	0	$\mathbb{Z}$	0	$\mathbb{Z}_2$	$\mathbb{Z}_2$	$\mathbb{Z}$	0	0
CI	$+1$	-1	1	0	0	$\mathbb{Z}$	0	$\mathbb{Z}_2$	$\mathbb{Z}_2$	$\mathbb{Z}$	0

Table 4.1: *The 10 Atland-Zirnbauer symmetry classes, categorised by symmetries and dimensions. We denote the symmetries as $\mathcal{T}$ for time-reversal symmetry, $\mathcal{C}$ for charge-conjugation symmetry and $\mathcal{X}$ for chiral symmetry. In the symmetries section, cells are allocated 1 if the corresponding operator squares to the unit matrix, -1 if it squares to negative the unit matrix, and 0 if the symmetry doesn't hold. Cells in the Dimension section are allocated $\mathbb{Z}_2$ if the phases of the respective symmetry class are characterised by a $\mathbb{Z}_2$ (binary) invariant in the respective dimension, $\mathbb{Z}$ if the phases are characterised by a $\mathbb{Z}$ (integer) invariant, or 0 if the phases are topologically trivial. Adapted from Ref. [10].*

under which

$$\mathcal{C}\tilde{b}(\theta)\mathcal{C} = -\tilde{b}^*(\theta), \tag{4.70}$$

$$\mathcal{C}^2 = 1. \tag{4.71}$$

We also have a chiral symmetry,

$$\mathrm{walk}(\mathcal{X}) = \qquad\qquad \mathrm{adj}(\mathcal{X}) = \begin{pmatrix} 0 & 0 & 1 & 0 \\ 0 & 0 & 0 & 1 \\ 1 & 0 & 0 & 0 \\ 0 & 1 & 0 & 0 \end{pmatrix}, \tag{4.72}$$

$$\tag{4.73}$$

under which

$$\left\{\mathcal{X}, \tilde{b}(\theta)\right\} = 0, \tag{4.74}$$

$$\left[\mathcal{X}, \tilde{b}^2(\theta)\right] = 0, \tag{4.75}$$

$$\mathcal{X}^2 = 1, \tag{4.76}$$

where, as in the case of the half-translation, eq. (4.75) naturally extends from eq. (4.74) due to eq. (3.54).

As such, in accordance with table 4.1, we establish that the bowtie chain belongs to the BDI symmetry group. As there is a single dimension of infinite periodicity, the bowtie chain is thus characterised by a $\mathbb{Z}$ topological invariant.

Finally, we note a symmetry $\tilde{\chi}$, where

$$\text{walk}(\tilde{\mathcal{X}}) = \qquad\qquad \text{adj}(\tilde{\mathcal{X}}) = \begin{pmatrix} 1 & 0 & 0 & 0 \\ 0 & -1 & 0 & 0 \\ 0 & 0 & -1 & 0 \\ 0 & 0 & 0 & 1 \end{pmatrix}.$$

$$\tag{4.77}$$

$$\sigma_y = \qquad\qquad \text{adj}(\sigma_y) = \begin{pmatrix} 0 & -i \\ i & 0 \end{pmatrix} \tag{4.78}$$

These graphs obey the relationships

$$\tilde{\mathcal{X}}\tilde{b}^2(\theta)\tilde{\mathcal{X}} = 2\tilde{\beta} - \tilde{b}^2(\theta) \tag{4.79}$$

$$\sigma_y \tilde{l}(\theta')\sigma_y = 2\beta - \tilde{l}(\theta') \tag{4.80}$$

where it is clear that $\tilde{\chi}$ operates on $\tilde{b}^2(\theta)$ in eq. (4.79) in a manner equivalent to σ_y on $l(\theta')$ in eq. (4.80). From this unconventional symmetry, we know that the eigenspectrum of the bowtie chain has a spectral symmetry

$$\lambda_{-,\eta}^2(\theta) = 2\tilde{\beta} - \lambda_{+,\eta}^2(\theta) \tag{4.81}$$

of the squared bands about $\lambda^2 = \tilde{\beta}$, which is a property of the bowtie chain that would be difficult to interpret without knowledge that it squares to a two-legged ladder, which in turn may be passed through the polynomial $p' : \tilde{l} \rightarrow \left(\tilde{l} - \tilde{\beta}\right)^2$ resulting in a set of monatomic chains.

135

4.3.2 Finite bowtie chain polynomials

To restrict the bowtie chain to a finite chain, we have a choice of terminating at any of the four vertices in the unit cell. In order to further understand the topological distinction between these systems, we can employ our graph algebra and analyse the impact of the termination upon the polynomials B^2 and $p(B) = (B^2 - \tilde{\beta})^2 - \alpha$, describing the two-legged ladder and separated monatomic chain child systems respectively.

Let B_i be a bowtie chain terminated at vertex i of the unit cell. Then

$$B_1 = \qquad\qquad\qquad\qquad\qquad\qquad\qquad\qquad\qquad\qquad\qquad\qquad\qquad\qquad (4.82)$$

$$B_2 = \qquad\qquad\qquad\qquad\qquad\qquad\qquad\qquad\qquad\qquad\qquad\qquad\qquad\qquad (4.83)$$

$$B_3 = \qquad\qquad\qquad\qquad\qquad\qquad\qquad\qquad\qquad\qquad\qquad\qquad\qquad\qquad (4.84)$$

$$B_4 = \qquad\qquad\qquad\qquad\qquad\qquad\qquad\qquad\qquad\qquad\qquad\qquad\qquad\quad. \quad (4.85)$$

These graphs have the squared representations as the two-legged ladders

$$B_1^2 = \qquad\qquad\qquad\qquad\qquad\qquad\qquad\qquad\qquad\qquad\qquad (4.86)$$

$$B_2^2 = \qquad\qquad\qquad\qquad\qquad\qquad\qquad\qquad\qquad\qquad\qquad (4.87)$$

$$B_3^2 = \qquad\qquad\qquad\qquad\qquad\qquad\qquad\qquad\qquad\qquad\qquad (4.88)$$

$$B_4^2 = \qquad\qquad\qquad\qquad\qquad\qquad\qquad\qquad\qquad\qquad , \quad (4.89)$$
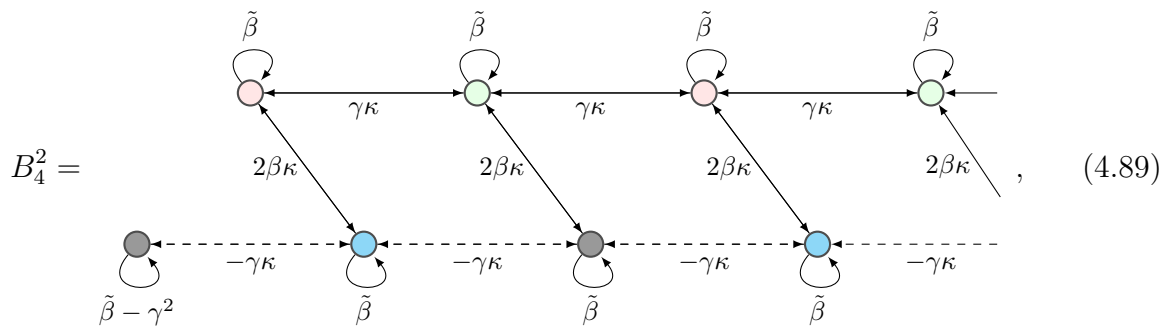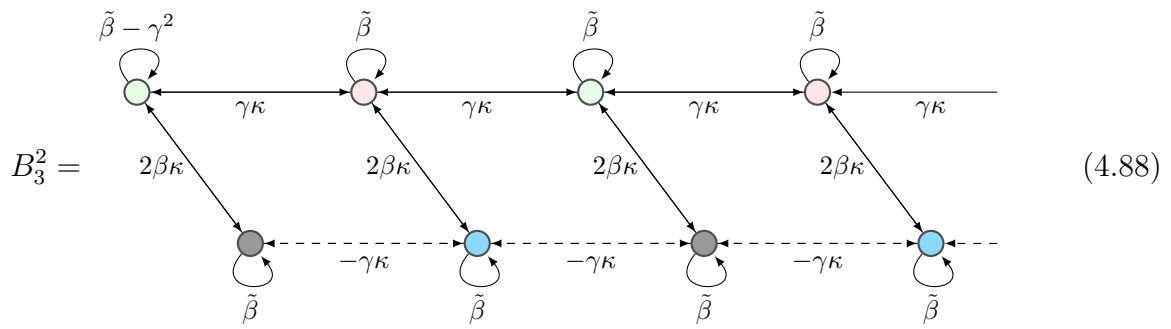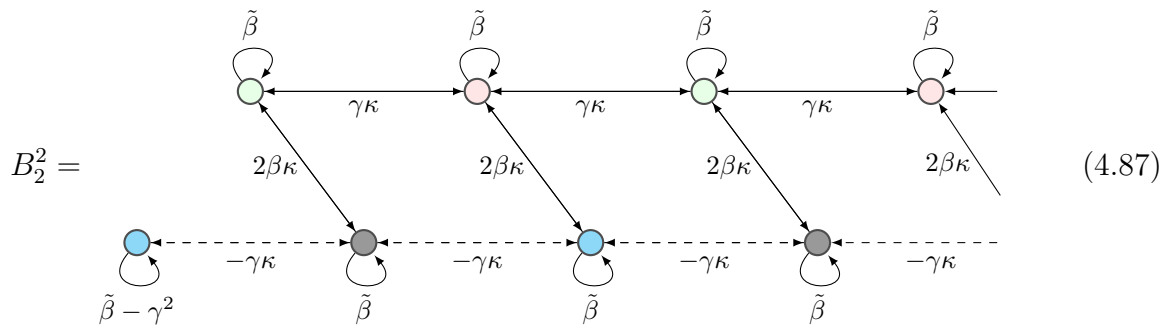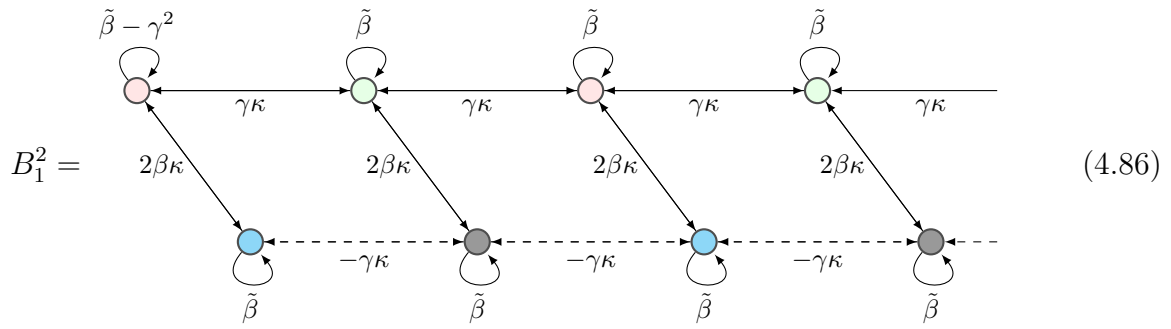
from which we can already see a striking structural difference emerging between the

137

even and odd site termination, and we can note that the B_1^2 and B_3^2 graphs are structurally identical, as are B_2^2 and B_4^2. This is due to the fact that $B_i = -B_{i+2}$, as per eq. (4.79), hence $B_i^2 = B_{i+2}^2$.

Further structural impacts of the termination are found in the 4th order polynomial grandchild graphs $p(B_i)$,

$$p(B_1) = \qquad\qquad (4.90)$$

$$p(B_2) = \qquad\qquad (4.91)$$
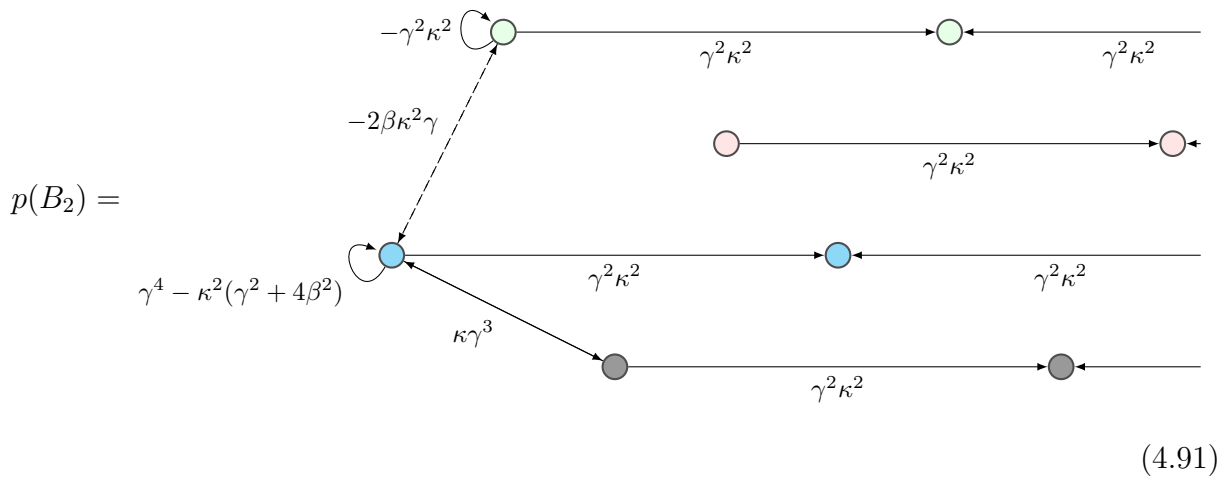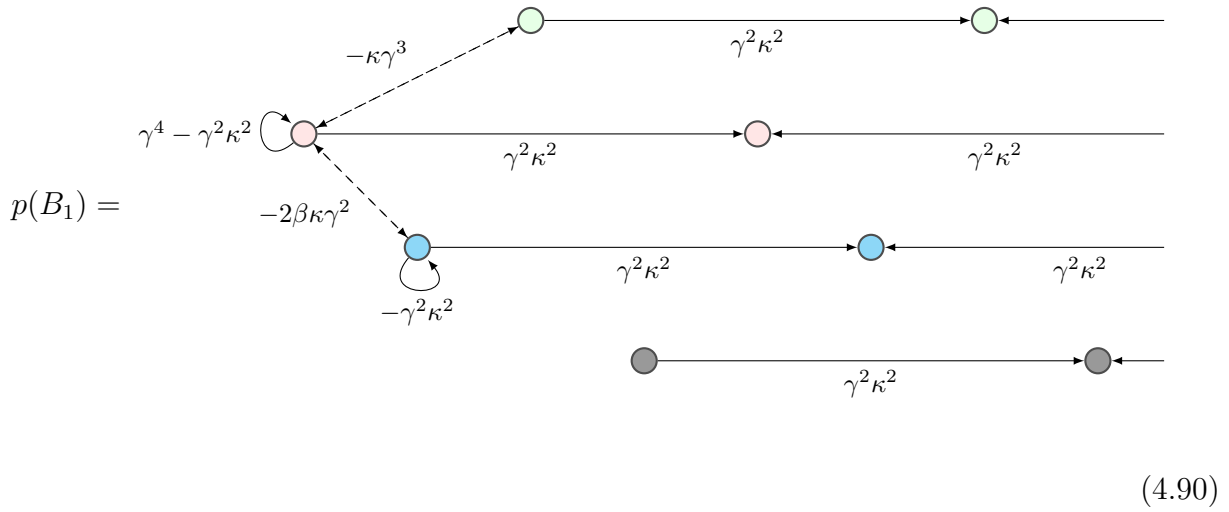
$$p(B_3) = \qquad$$

$$(4.92)$$

$$p(B_4) = \qquad$$

$$(4.93)$$

Unlike in the case of the SSH chain, the child graphs of the bowtie chain undergo a structural change at the termination vertex. For even i, B_i^2 is no longer a closed ladder, but has a hanging vertex. This is a significant result: all other vertices being paired up in the ladder formation, we thus expect a *single* midgap state to emerge from these configurations, while for odd i we expect any midgap states to arrive in pairs.

This is a particularly interesting feature of the bowtie chain. As the gap in B^2 corresponds to the finite-eigenvalue gaps in the bowtie chain, and as a consequence of both the singular nature of the midgap state in B_{2i}^2 and the relationship $B_i = -B_{i+2}$, we then conclude that if B_i exhibits a defect state in the positive gap, then B_{i+2} exhibits a de-

fect state in the negative gap. This is indeed the case, demonstrated in the eigenspectra

plotted in fig. 4.10.
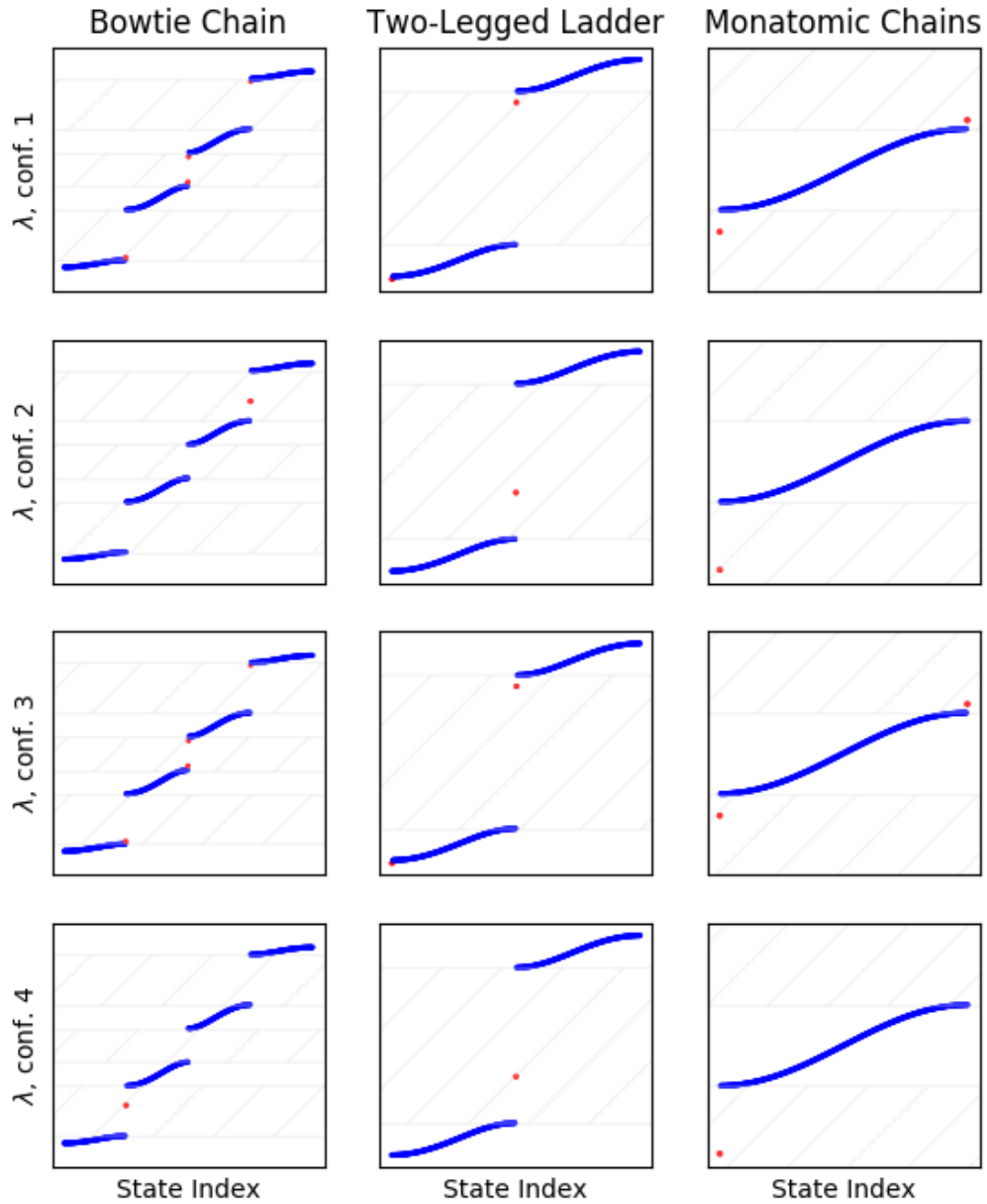
*Figure 4.10: The eigenspectra of finite bowtie chains and their polynomial child systems, terminated at sites 1 (**conf. 1**), 2 (**conf. 2**), 3 (**conf. 3**) and 4 (**conf. 4**), demonstrating the presence of the midgap states of the bowtie chain (coloured red) in the child systems.*

4.3.3 Topological phases

Each band n can be associated with a Zak phase[61], the one-dimensional analogue of the Berry phase[62], calculated by integrating the associated wavefunction $|n, \theta\rangle$ across the Brillouin zone,

$$\mathcal{Z}_n = \frac{i}{\pi} \oint_{\text{BZ}} \langle n, \theta| \frac{d}{d\theta} |n, \theta\rangle d\theta. \tag{4.94}$$

This requires $|n, \theta\rangle$ to evolve smoothly with θ, and as eigendecomposition provides eigenstates multiplied by an arbitrary phase, we must fix the eigenstates with a gauge choice. We choose that the first component of $|n, \theta\rangle$ is real and positive. In systems exhibiting topological characteristics, the phase is quantized, giving rise to an integer index $\mathcal{Z}_n$ for each band n, while in non-topological systems the phase can take any value [49].

As we have seen, states appear in the gaps between bands when the system is finite. Thus our interest lies not just within the bands, but also in the gaps between them. In order to investigate such phenomena, we must take a short step away from what we may call the Bloch question, which fundamentally asks which *energies* exist at specified *momenta*, and step into the scattering question, where we may ask which *momenta* are present at specified *energies*. We choose the transfer matrix approach[63, 64, 65, 66, 67, 12], utilised on a simple level in eq. (4.22).

As the bowtie chain exhibits only nearest-neighbour edges, and as each site has at most two nearest neighbours, the Schrödinger equation allows us to relate any single component of a consecutive triplet of eigenstate components to the other two.

Let v be an eigenstate with eigenvalue λ, and let the component $v_{n,m}$ describe the state component at the vertex n in the mth unit cell, indexed such that vertices 1 and 2 have the positive weighted loop edges β. Then

$$(\lambda - \beta)v_{n,1} = -\gamma v_{(n-1),4} + \kappa v_{n,2}, \qquad (4.95)$$

$$(\lambda - \beta)v_{n,2} = \kappa v_{n,1} + \gamma v_{n,3}, \qquad (4.96)$$

$$(\lambda + \beta)v_{n,3} = \gamma v_{n,2} - \kappa v_{n,4}, \text{and} \qquad (4.97)$$

$$(\lambda + \beta)v_{n,4} = -\kappa v_{n,3} - \gamma v_{(n+1),1}. \qquad (4.98)$$

We can write these linear equations using the *transfer matrices*

$$\tilde{M}_1(\lambda) = \begin{pmatrix} 0 & 1 \\ -\kappa/\gamma & (\lambda - \beta)/\gamma \end{pmatrix}, \qquad (4.99)$$

$$\tilde{M}_2(\lambda) = \begin{pmatrix} 0 & 1 \\ \gamma/\kappa & -(\lambda + \beta)/\kappa \end{pmatrix}, \qquad (4.100)$$

$$\tilde{M}_3(\lambda) = \begin{pmatrix} 0 & 1 \\ -\kappa/\gamma & -(\lambda + \beta)/\gamma \end{pmatrix}, \qquad (4.101)$$

$$\tilde{M}_4(\lambda) = \begin{pmatrix} 0 & 1 \\ \gamma/\kappa & (\lambda - \beta)/\kappa \end{pmatrix}. \qquad (4.102)$$

such that

$$\begin{pmatrix} v_{n,2} \\ v_{n,3} \end{pmatrix} = \tilde{M}_1 \begin{pmatrix} v_{n,1} \\ v_{n,2} \end{pmatrix} \qquad \begin{pmatrix} v_{n,3} \\ v_{n,4} \end{pmatrix} = \tilde{M}_2 \begin{pmatrix} v_{n,2} \\ v_{n,3} \end{pmatrix}$$

$$\begin{pmatrix} v_{n,4} \\ v_{n+1,1} \end{pmatrix} = \tilde{M}_3 \begin{pmatrix} v_{n,3} \\ v_{n,4} \end{pmatrix} \qquad \begin{pmatrix} v_{n+1,1} \\ v_{n+1,2} \end{pmatrix} = \tilde{M}_4 \begin{pmatrix} v_{n,4} \\ v_{n+1,1} \end{pmatrix}. \qquad (4.103)$$

Eigenstates of $\tilde{b}(\theta)$ are simultaneously eigenstates of the translation operator with eigenvalue $\exp(2\pi i\theta)$, and must then obey

$$\begin{pmatrix} v_{n,1} \\ v_{n,2} \end{pmatrix} = \exp(2\pi i\theta) \begin{pmatrix} v_{n-1,1} \\ v_{n-1,2} \end{pmatrix} \tag{4.104}$$

and are thus also eigenstates of the product

$$\mathbf{M}(\lambda) = \tilde{M}_4(\lambda)\tilde{M}_3(\lambda)\tilde{M}_2(\lambda)\tilde{M}_1(\lambda) \tag{4.105}$$

with eigenvalue $\exp(2\pi i\theta)$. As such, the two eigenstates $\phi_\pm$ with eigenvalues $\Lambda = \exp(2\pi i\theta_\pm)$ of $\mathbf{M}(\lambda)$ can be used to fully describe the eigenstates of B with eigenvalue λ and translation eigenvalues $\theta_\pm$. Within the bands, $\theta_\pm$ are real, thus their eigenvalues lie on the unit circle in the complex plane. In the band gaps, the effective momentum is imaginary, and the eigenvalues Λ are real valued. At the band edges, which form a boundary between bands and gaps, the translation eigenvalues are thus necessarily ± 1. This is illustrated in fig. 4.11. We choose the sign of $\theta = i\omega(\lambda)$ according to $\mathrm{Re}\,\omega > 0$, such that $|\Lambda_+(\lambda)| < 1$ describes an evanescent state ϕ_+ that decays to the right, while $|\Lambda_-(\lambda)| > 1$ describes an evanescent state ϕ_- that decays to the left.

We exemplify this in fig. 4.12 with plots of the midgap states in the finite bowtie chain of configuration B_1, which has four gap states. Lying in the bandgap of the infinite chain, they decay exponentially from one of the boundaries towards the other.

From the eigenvectors $\phi_\pm(\lambda)$ of the transfer matrix, we may describe a reflection coefficient[12]

$$r(\lambda) = \frac{\phi_{+,1}(\lambda) + i\phi_{+,2}(\lambda)}{\phi_{+,2}(\lambda) + i\phi_{+,1}(\lambda)}, \tag{4.106}$$

due to a plane wave entering the system being of the form $\propto (\exp(ik) + r(\lambda)\exp(-ik))$.

Recall our gauge choice: the first eigenstate component is real and positive, and the
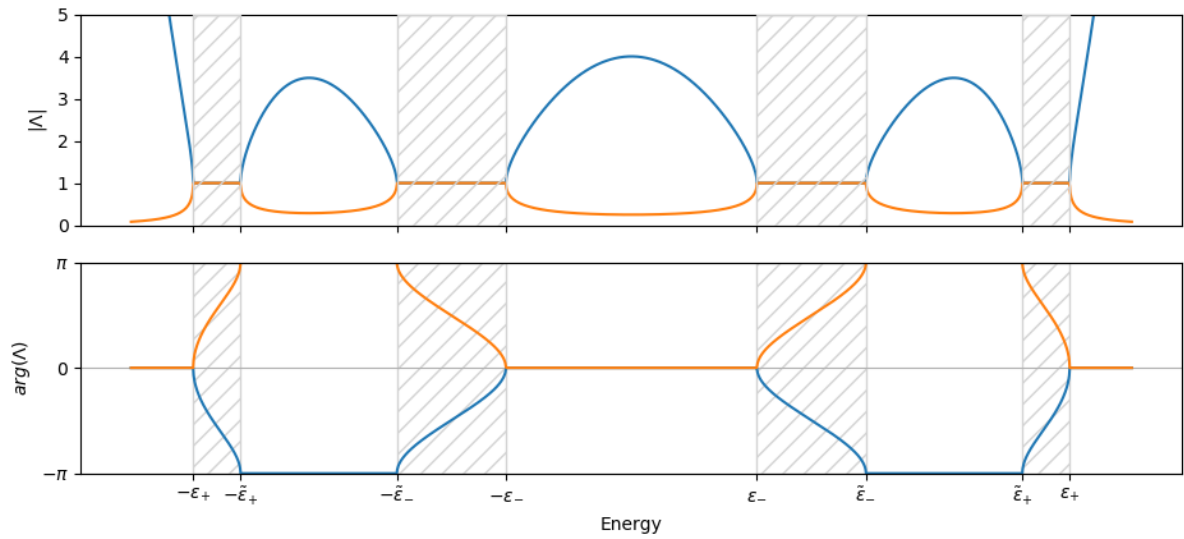
Figure 4.11: Magnitude and angle of the eigenvalues of the transfer matrix $\mathbf{M}(\lambda)$ for a range of energies λ encompassing the bands and gaps of the bowtie chain with $\beta = 0.5, \kappa = 0.75, \gamma = 0.5$. Within the bands, signified with a hatched background, the eigenvalues are of unit magnitude and each half way around the unit circle. Outside of energy bands, solutions to the transfer matrix are real valued, with values above and below 1 describing exponentially increasing and decreasing amplitudes respectively.
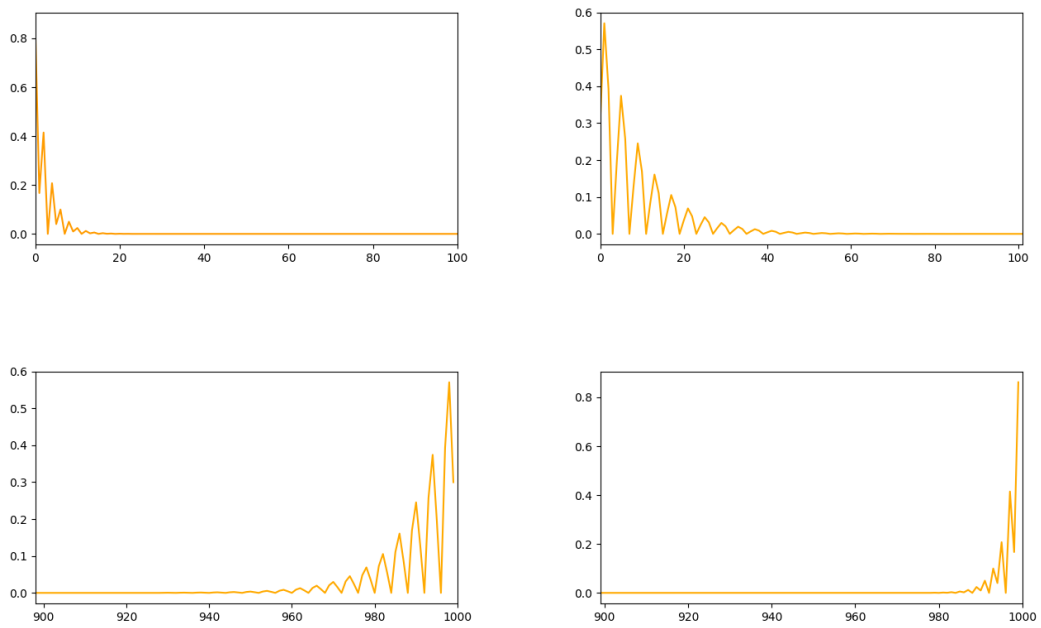
*Figure 4.12: Absolute values of the amplitudes of the midgap eigenstates along vertices in the finite bowtie chain B_1, arranged as **Top left**: lowest eigenvalue, **Top right**: second lowest eigenvalue **Bottom left**: second highest eigenvalue **Bottom Right**: highest midgap eigenvalue.*

other components scale accordingly. Thus in eq. (4.106), we can enforce $\phi_{+,1}(\lambda) = 1$ and obtain the Zak phase by integrating over eigenstates propagating in each direction through the nth band's energy minimum to its maximum,[12]

$$\mathcal{Z}_n = \frac{1}{\pi} \int_{\lambda_{\min}(n)}^{\lambda_{\max}(n)} d\lambda \, \phi_{+,2}(\lambda) \frac{d}{d\lambda} \phi_{+,2}(\lambda) \tag{4.107}$$

$$= \frac{1}{\pi} \int_{\lambda_{\min}(n)}^{\lambda_{\max}(n)} d\lambda \frac{1}{1 + r(\lambda)^2} \frac{d}{d\lambda} r(\lambda) \tag{4.108}$$

$$= \frac{2}{\pi} \left[\arctan r(\lambda_{\min}(n)) - \arctan r(\lambda_{\max}(n)) \right] \tag{4.109}$$

In the band gaps, including the band edges, waves are totally reflected, so that $|r(\lambda)| = 1$, as demonstrated in fig. 4.14. At the band edges, translation eigenstates from the bands must match up with evanescent states found in the gaps, enforcing $r(\lambda) = \pm 1$. As $\arctan(\pm 1) = \pm \pi/4$,

$$\mathcal{Z}_n = \frac{1}{2} \left[r(\lambda_{\min}(n)) - r(\lambda_{\max}(n)) \right] \tag{4.110}$$

As $r(\lambda_{\min}(n))$ and $r(\lambda_{\max}(n))$ adopt the values ± 1, the Zak phase for each band is indeed quantized.

Before we are ready to assign a Zak phase to each band, however, we must address an important assumption that has been implicit in our exploration so far: We must ensure that there is indeed a gap between each band, thus avoiding degeneracies in the bowtie chain eigenspectrum. Gaps close if $\beta = 0$, when the bowtie chain becomes the SSH model with a single central gap, or if $\beta^2 + \gamma^2 = \kappa^2$. As such we can separate four topologically distinct regions in the bowtie chain parameter space, identified by the parameters $(\xi, \tilde{\xi})$, where

$$\xi = \text{sgn} \left(\beta^2 + \gamma^2 - \kappa^2 \right) \qquad \tilde{\xi} = \text{sgn} \, \beta, \tag{4.111}$$
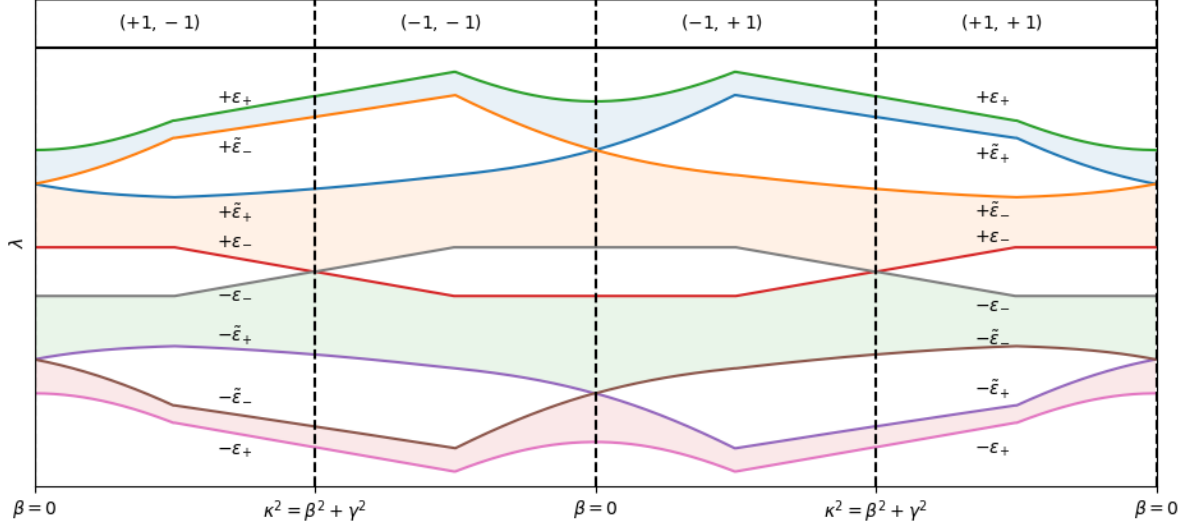
Figure 4.13:   Locations of the band edges (eq. (4.47)) as the bowtie chain is deformed through different topological sectors $(\xi, \tilde{\xi})$ described in eq. (4.111) and illustrated in fig. 4.15. The range of energies λ available in each band is coloured for clarity. At a boundary between topological sectors, band edges are exchanged. Iff $\kappa^2 = \beta^2 + \gamma^2$, the central bands touch and there is a degenerate point in the spectrum at $\lambda = 0$. Either side of this topological boundary, $\tilde{\varepsilon}$ has a different sign, and behaves as the central upper band minimum or the central lower band minimum when it is positive or negative, respectively. Iff $\beta = 0$, the same phenomenon happens between the upper and central upper bands, and between the lower and central lower bands.
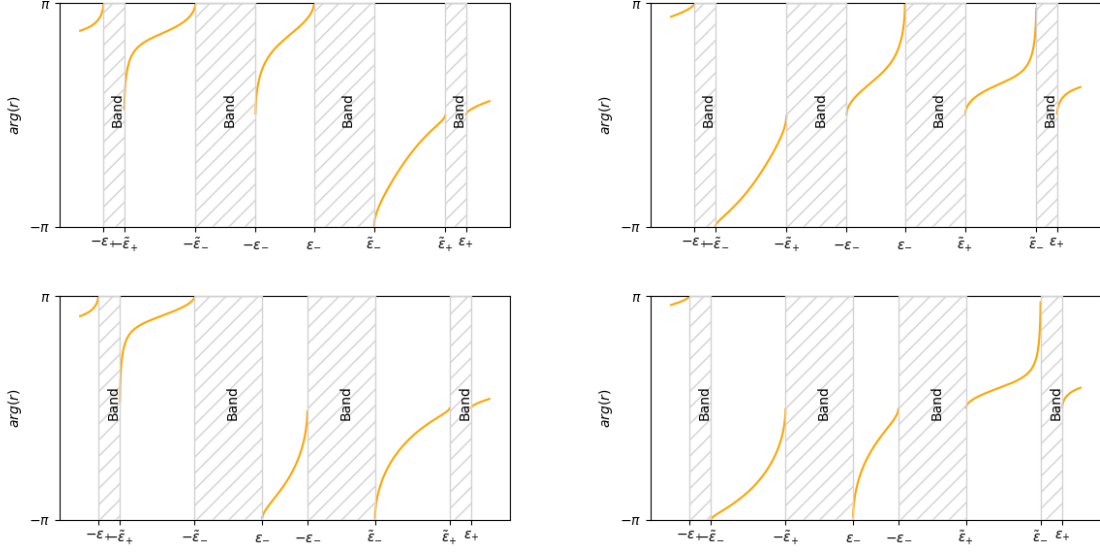
Figure 4.14: *Clockwise winding of the reflection coefficient of the bowtie chain in topological phases* **Top Left:** $(\xi = 1, \tilde{\xi}1)$, **Top Right:** $(\xi = 1, \tilde{\xi} = -1)$, **Bottom Left:** $(\xi = -1, \tilde{\xi} = 1)$, **Bottom Right:** $(\xi = -1, \tilde{\xi} = -1)$.

such that ξ changes sign when the central gap closes, while parameters are steered through an inversion of the inner bands, and $\tilde{\xi}$ changes sign in a band inversion in which the finite-eigenvalue gaps close. Starting with fixed γ and allowing variable β and κ, we obtain the phase diagram provided in fig. 4.15.

Although the lowest energy band's minimum is $-\varepsilon_+$ and the highest energy band's maximum is $+\varepsilon_+$ in all topological phases, the other band extrema $\pm\tilde{\varepsilon}_-, \pm\tilde{\varepsilon}_+, \pm\varepsilon_-$ depend on the topological phase, demonstrated in fig. 4.13. Specifically, the lowest energy band's maximum and the centre-low band's minimum are $-\tilde{\varepsilon}_{\tilde{\xi}}$ and $-\tilde{\varepsilon}_{-\tilde{\xi}}$ respectively, and ξ thus determines which of these band edges belong to which band. By symmetry, the highest energy band's minimum and the centre-high energy band's maximum are $+\tilde{\varepsilon}_{\tilde{\xi}}$ and $+\tilde{\varepsilon}_{-\tilde{\xi}}$. Finally, the centre-low band's maximum and the centre-high band's minimum are $\xi\varepsilon_-$ and $-\xi\varepsilon_+$ respectively, such that a sign flip of ξ exchanges the central gap edges.
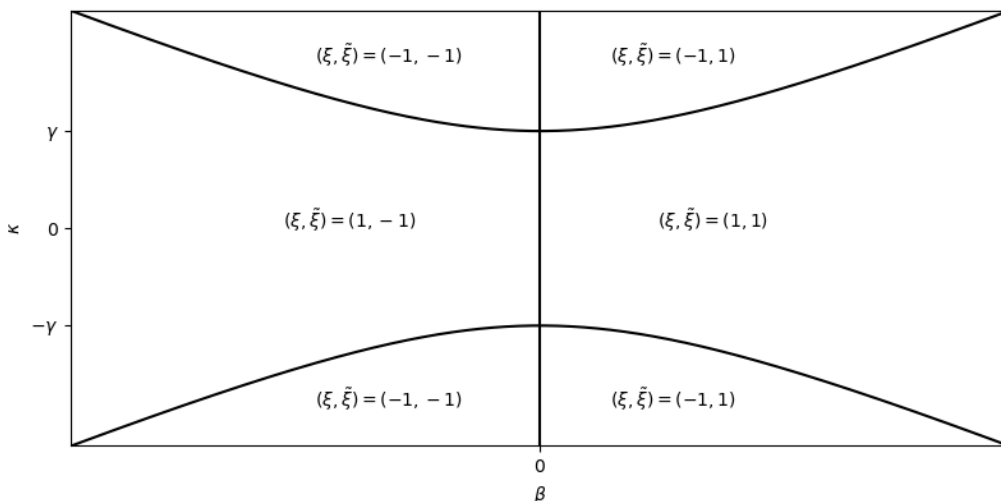
Figure 4.15: Phase diagram of the bowtie chain with constant γ. Each phase corresponds to an ordering of band edges according to $\varepsilon_\pm$ and $\tilde{\varepsilon}_\pm$ in eq. (4.48).

To calculate the Zak phases of the bands in each topological phase, all we require is the reflection coefficients of the band edges, given in table 4.2. From these we simply apply eq. (4.110) to each band according to the edges assigned as above. The resulting Zak phases are provided in table 4.3.

Similarly, we can associate a topological phase to each *gap*. This can normally done, e.g., via the Witten index [68], which here relates to the reflection phase at a spectral symmetry point [69, 70, 71]. In the finite-eigenvalue gaps, this information is instead encoded in the winding of the reflection coefficient as λ increases from the lower band maximum to the upper band minimum. Crossing a gap, $r(\lambda)$ necessarily winds clockwise[72] along the unit circle, from ± 1 to ∓ 1, encoding topological information along the way. For example, if the reflection coefficient starts at $r = 1$, it needs to pass $r = -i$ along the way to $r = -1$, and the Witten index $\mathcal{W}$ is $+1$. Alternatively, if the reflection coefficient starts at $r = -1$, it needs to pass through $r = i$ before reaching $r = 1$, and this gives $\mathcal{W} = -1$. As with the Zak phase, we can utilise the reflection coefficients at the band

Energy	Transfer Eigenvalue	Transfer Eigenvector	Reflection Coefficient
λ	Λ_+	ϕ_+	$r(\lambda)$
$-\varepsilon_+$	$+1$	$(1,-1)$	-1
$-\tilde{\varepsilon}_+$	-1	$(1,+1)$	$+1$
$-\tilde{\varepsilon}_-$	-1	$(1,-1)$	-1
$-\varepsilon_-$	$+1$	$(1,-1)$	$+1$
$+\varepsilon_-$	$+1$	$(1,-1)$	-1
$+\tilde{\varepsilon}_-$	-1	$(1,-1)$	-1
$+\tilde{\varepsilon}_+$	-1	$(1,+1)$	$+1$
$+\varepsilon_+$	$+1$	$(1,+1)$	$+1$

Table 4.2: Transfer eigenvalues and eigenvectors at the band edges provided in eq. (4.47) alongside the reflection coefficient $r(\lambda)$ defined in eq. (4.106).

Phase		Lowest Band			Centre Low Band			Centre High Band			Highest Band		
ξ	$\tilde{\xi}$	$\lambda_{\min}$	$\lambda_{\max}$	$\mathcal{Z}$	$\lambda_{\min}$	$\lambda_{\max}$	$\mathcal{Z}$	$\lambda_{\min}$	$\lambda_{\max}$	$\mathcal{Z}$	$\lambda_{\min}$	$\lambda_{\max}$	$\mathcal{Z}$
1	1	$-\varepsilon_+$	$-\tilde{\varepsilon}_+$	-1	$-\tilde{\varepsilon}_-$	$-\varepsilon_-$	-1	$+\varepsilon_-$	$+\tilde{\varepsilon}_-$	0	$+\tilde{\varepsilon}_+$	$+\varepsilon_+$	0
1	-1	$-\varepsilon_+$	$-\tilde{\varepsilon}_-$	0	$-\tilde{\varepsilon}_+$	$-\varepsilon_-$	0	$+\varepsilon_-$	$+\tilde{\varepsilon}_+$	-1	$+\tilde{\varepsilon}_-$	$+\varepsilon_+$	-1
-1	1	$-\varepsilon_+$	$-\tilde{\varepsilon}_+$	-1	$-\tilde{\varepsilon}_-$	$+\varepsilon_-$	0	$-\varepsilon_-$	$+\tilde{\varepsilon}_-$	1	$+\tilde{\varepsilon}_+$	$+\varepsilon_+$	0
-1	-1	$-\varepsilon_+$	$-\tilde{\varepsilon}_-$	0	$-\tilde{\varepsilon}_+$	$+\varepsilon_-$	1	$-\varepsilon_-$	$+\tilde{\varepsilon}_+$	0	$+\tilde{\varepsilon}_-$	$+\varepsilon_+$	-1

Table 4.3: Zak phases of each band in each topological phase $(\xi, \tilde{\xi})$. For each band, the energy minimum and maximum are given in reference to the band edges eq. (4.47), and the Zak phase $\mathcal{Z} = (r(\lambda_{min}) - r(\lambda_{max}))/2$ is calculated with the reflection coefficients provided in table 4.2. Though calculated through the reflection coefficients, the values present a relationship between the topological phase and the Zak phase for each band. The lowest energy band's Zak phase depends only on $\tilde{\xi}$, and takes the value $-(\tilde{\xi} + 1)/2$. The highest energy band has similar form $(\tilde{\xi} - 1)/2$. The central low energy band has Zak phase equal to $-(\tilde{\xi} + \xi)/2$, and the central high energy band has Zak phase $(\tilde{\xi} - \xi)/2$.

Phase		Negative Energy Bandgap			Central Bandgap			Positive Energy Bandgap		
ξ	$\tilde{\xi}$	$\lambda_{\min}$	$\lambda_{\max}$	$\mathcal{W}$	$\lambda_{\min}$	$\lambda_{\max}$	$\mathcal{W}$	$\lambda_{\min}$	$\lambda_{\max}$	$\mathcal{W}$
1	1	$-\tilde{\varepsilon}_+$	$-\tilde{\varepsilon}_-$	1	$-\varepsilon_-$	$+\varepsilon_-$	1	$+\tilde{\varepsilon}_-$	$+\tilde{\varepsilon}_+$	-1
1	-1	$-\tilde{\varepsilon}_-$	$-\tilde{\varepsilon}_+$	-1	$-\varepsilon_-$	$+\varepsilon_-$	1	$+\tilde{\varepsilon}_+$	$+\tilde{\varepsilon}_-$	1
-1	1	$-\tilde{\varepsilon}_+$	$-\tilde{\varepsilon}_-$	1	$+\varepsilon_-$	$-\varepsilon_-$	-1	$+\tilde{\varepsilon}_-$	$+\tilde{\varepsilon}_+$	-1
-1	-1	$-\tilde{\varepsilon}_-$	$-\tilde{\varepsilon}_+$	-1	$+\varepsilon_-$	$-\varepsilon_-$	-1	$+\tilde{\varepsilon}_+$	$+\tilde{\varepsilon}_-$	1

Table 4.4: *Witten phases of each bandgap in each topological phase $(\xi, \tilde{\xi})$. For each bandgap, the energy minimum and maximum are given in reference to the band edges eq. (4.47), and the Witten phase $\mathcal{W} = (r(\lambda_{min}) - r(\lambda_{max}))/2$ is calculated with the reflection coefficients provided in table 4.2. The Witten index for the negative bandgaps equal $\tilde{\xi}$, those in the positive bandgaps equal $-\tilde{\xi}$, while the central bandgap has a Witten index equal to ξ.*

edges to calculate band gap Witten indices for each topological phase of the bowtie chain, for which we have provided the results in table 4.4.

4.4 Conclusion

This chapter explored some of the interesting topological features that can arise from when one considers a lattice which adopts the form of a square root of a more trivial structure.

In section 4.1 we looked at the SSH chain, observing that it squares to a monoatomic chain, and identified the structure of the zero-eigenvalue defect state from basic principles which were later formalised into the language of transfer matrices in section 4.3. We observed how the defects can be directly linked to edge states of the monatomic chains that were modified as a result of the SSH chain termination.

We extended the model to the Rice-Mele model in section 4.2 and found a polynomial connection with the SSH chain, algebraically formulating the splitting behaviour of the defect state We also looked at a different form of defect, created by breaking the alternating pattern of loop edges, and had a first glimpse of how a modification to a parent system can form connections between otherwise separable chains in a child system.

Exploiting this behaviour, we extended the Rice-Mele model by changing the behaviour of the alternating loop edges and nearest-neighbour edges, resulting in the bowtie chain in section 4.3. Here, we took a closer look at the rich topological properties that emerged as a result of nonsymmorphic symmetries that become symmomorphic in the child two-legged ladder, including the emergence of states in the different spectral gaps when the bowtie chain is restricted to a semi-infinite system. The topological sectors, separated by configurations with degenerate states, were identified, and the properties of each sector

154

were explored using an energy integral form of the Zak phase, allowing us to also extend the topological characterisation to the band gaps through the Witten index. The Zak phases and Witten indices of the bowtie chain's bands and bandgaps are stable across a topological sector, changing only upon transition from one sector into another. This is indeed the fundamental concept of topological features: they are stable to perturbations of the underlying system, including thermal fluctuations[73] and can relate to experimentally observable[74][59] characteristics.

Chapter 5

Concluding remarks

In this thesis, we have utilised König digraphs to present the concept of polynomials of graphs. This representation allows us to describe the concepts of more general matrices. Indeed, any $N \times M$ matrix may be represented through a walk graph with M input vertices and M output vertices. We make particular use of this by defining vectors and scalars, which have no direct representation in conventional graph theory.

In section 1.5 we showed that the eigendecomposition of any "parent" graph G is deeply related to that of a "child" graph $p(G)$, namely that the eigenstates of G are eigenstates of $p(G)$ and each eigenvalue λ of G takes the eigenvalue $p(\lambda)$ in the child graph. This provides motivation for further exploration of the algebra, particularly in a condensed matter setting where, through the Schrödinger equation, the eigendecomposition of G provides the stable wavefunctions of a system, along with their corresponding energies.

With this motivation in mind, we moved on to describe the microscopic behaviour of graph polynomials, i.e. the way that a local set of edges transform as a result of the polynomial, in chapter 2. This allowed us to describe the impact upon loop edges on isolated vertices, which are modified directly by the polynomial. We extended this by

looking at the behaviour of edges that connect a set of vertices, describing the methods by which a polynomial can cancel out such edges in the child system, either by direct cancellation or by destructive interference. We also described an approach analogous to Bloch's theorem, allowing us to remain within the graph-theoretical framework for the remainder of the thesis.

We moved on to discuss concrete models in a condensed matter setting in chapter 3. Although the models under discussion were simple, our new approach enabled us to view them in an entirely new way. We derived the properties of arbitrary-neighbour homogeneous monatomic bonds using polynomials derived from cycle graphs, found a square root of an Aharonov-Bohm loop, used destructive interference to view a square lattice under the influence of a rational magnetic field as a root of a set of larger, separable square lattices, and derived the properties of honeycomb systems, using only structural arguments and the eigendecomposition of the unit honeycomb.

Finally, chapter 4 explored the properties of topological chains, revealing their topological properties as an artifact of a non-trivial square root of more trivial child chain systems. We examined the impact of termination of a parent system on its child systems, and demonstrated that the resulting modifications have physical ramifications in the parent system. This was particularly useful in the case of the bowtie chain, where we related graph-theoretic arguments to the results of explicit topological invariant calculations.

The methods introduced by this thesis have a direct application in condensed matter systems. Not only can parent topological systems be described through simpler child systems, but they can also be derived from them; this was the case with our research on the bowtie chain, although this thesis presents the reverse of this process in order to obtain continuity with with previous sections. Even outside of the context of topological systems,

a lot can be learned about a quantum system simply by squaring it, or by attempting to obtain a square root system.

We finally remark that our algebra also provides an intuitive mechanism by which to explore any abstract entity that can be modelled as a graph, particularly when their adjacency matrix eigendecomposition plays an important role.

List of Figures

Bibliography

[1] M. Born and P. Jordan, "Zur quantenmechanik," *Zeitschrift für Physik*, vol. 34, pp. 858–888, Dec 1925.

[2] B. Van der Waerden, *Sources of Quantum Mechanics.* Elsevier, 1967.

[3] W. Heisenberg, "Über quantentheoretische Umdeutung kinematischer und mechanischer Beziehungen.," *Zeitschrift fur Physik*, vol. 33, pp. 879–893, Dec. 1925.

[4] M. Born, W. Heisenberg, and P. Jordan, "Zur quantenmechanik. ii.," *Zeitschrift für Physik*, vol. 35, pp. 557–615, Aug 1926.

[5] P. A. M. Dirac, "The fundamental equations of quantum mechanics," *Proc. Roy. Soc. Lond.*, vol. A109, pp. 642–653, 1925.

[6] P. A. M. Dirac, "Quantum mechanics and a preliminary investigation of the hydrogen atom," *Proc. Roy. Soc. Lond.*, vol. A110, pp. 561–579, 1926.

[7] W. Pauli, "Über das Wasserstoffspektrum vom Standpunkt der neuen Quantenmechanik," *Zeitschrift fur Physik*, vol. 36, pp. 336–363, May 1926.

[8] F. Bloch, "Über die quantenmechanik der elektronen in kristallgittern," *Zeitschrift für physik*, vol. 52, no. 7-8, pp. 555–600, 1929.

[9] A. Kitaev, "Anyons in an exactly solved model and beyond," *Annals of Physics*, vol. 321, no. 1, pp. 2–111, 2006.

[10] K. Shiozaki and M. Sato, "Topology of crystalline insulators and superconductors," *Phys. Rev. B*, vol. 90, no. 165114, 2014.

[11] M. Doob, "Applications of graph theory in linear algebra," *Mathematics Magazine*, vol. 57, no. 2, pp. 67–76, 1984.

[12] J. Arkinstall, M. Teimourpour, L. Feng, R. El-Ganainy, and H. Schomerus, "Topological tight-binding models from nontrivial square roots," *Physical Review B*, vol. 95, no. 16, p. 165109, 2017.

[13] R. Bapat, D. Kalita, and S. Pati, "On weighted directed graphs," *Linear Algebra and its Applications*, vol. 436, no. 1, pp. 99–111, 2012.

[14] C. Adiga, B. Rakshith, and W. So, "On the mixed adjacency matrix of a mixed graph," *Linear Algebra and its Applications*, vol. 495, pp. 223 – 241, 2016.

[15] S. Kirchhoff, "Ueber den durchgang eines elektrischen stromes durch eine ebene, insbesondere durch eine kreisförmige," *Annalen der Physik*, vol. 140, no. 4, pp. 497–514, 1845.

[16] G. Strang, "Graphs, matrices, and subspaces," *The College Mathematics Journal*, vol. 24, no. 1, pp. 20–28, 1993.

[17] X. Ouvrard, J.-M. L. Goff, and S. Marchand-Maillet, "Adjacency and tensor representation in general hypergraphs part 1: e-adjacency tensor uniformisation using homogeneous polynomials," *arXiv preprint arXiv:1712.08189*, 2017.

[18] B. Mohar, Y. Alavi, G. Chartrand, and O. Oellermann, "The laplacian spectrum of graphs," *Graph theory, combinatorics, and applications*, vol. 2, no. 871-898, p. 12, 1991.

[19] A. Agaskar and Y. M. Lu, "A spectral graph uncertainty principle," *IEEE Transactions on Information Theory*, vol. 59, no. 7, pp. 4338–4356, 2013.

[20] U. Murty and A. Bondy, *Graph Theory (Graduate Texts in Mathematics 244)*. Springer, 2008.

[21] A. Cayley, "Ii. a memoir on the theory of matrices," *Philosophical Transactions of the Royal Society of London*, vol. 148, pp. 17–37, 1858.

[22] J. Mason and D. Handscomb, *Chebyshev Polynomials*. CRC Press, 2002.

[23] B. Mohar and W. Woess, "A survey on spectra of infinite graphs," *Bulletin of the London Mathematical Society*, vol. 21, no. 3, pp. 209–234, 1989.

[24] M. S. of Japan, K. Itō, and N. Sūgakkai, *Encyclopedic Dictionary of Mathematics*, p. 997. No. v. 1 in Encyclopedic Dictionary of Mathematics, MIT Press, 1993.

[25] A. Yariv, "Coupled-mode theory for guided-wave optics," *IEEE Journal of Quantum Electronics*, vol. 9, no. 9, pp. 919–933, 1973.

[26] Y. Aharonov and D. Bohm, "Significance of electromagnetic potentials in the quantum theory," *Physical Review*, vol. 115, no. 3, p. 485, 1959.

[27] R. Keil, C. Poli, M. Heinrich, J. Arkinstall, G. Weihs, H. Schomerus, and A. Szameit, "Universal sign control of coupling in tight-binding lattices," *Phys. Rev. Lett.*, vol. 116, no. 213901, 2016.

[28] R. Peierls, "Zur theorie des diamagnetismus von leitungselektronen," *Zeitschrift für Physik*, vol. 80, pp. 763–791, Nov 1933.

[29] D. R. Hofstadter, "Energy levels and wave functions of bloch electrons in rational and irrational magnetic fields," *Physical review B*, vol. 14, no. 6, p. 2239, 1976.

[30] P. R. Wallace, "The band theory of graphite," *Physical Review*, vol. 71, no. 9, p. 622, 1947.

[31] D. DiVincenzo and E. Mele, "Self-consistent effective-mass theory for intralayer screening in graphite intercalation compounds," *Physical Review B*, vol. 29, no. 4, p. 1685, 1984.

[32] A. K. Geim and K. S. Novoselov, "The rise of graphene," in *Nanoscience and Technology: A Collection of Reviews from Nature Journals*, pp. 11–19, World Scientific, 2010.

[33] J. Wang, F. Ma, and M. Sun, "Graphene, hexagonal boron nitride, and their heterostructures: properties and applications," *RSC Advances*, vol. 7, no. 27, pp. 16801–16822, 2017.

[34] P. A. M. Dirac, "The quantum theory of the electron," *Proc. R. Soc. A*, vol. 117, no. 610, 1928.

[35] P. Dirac and J. Polkinghorne, "The principles of quantum mechanics," *Physics Today*, vol. 11, p. 32, 1958.

[36] M. F. Atiyah and I. M. Singer, "The index of elliptic operators on compact manifolds," *Bull. Amer. Math. Soc.*, vol. 69, no. 422, 1963.

[37] Z. M. Hasan and C. L. Kane, "Colloquium: Topological insulators," *Rev. Mod. Phys.*, vol. 82, no. 3045, 2010.

[38] X.-L. Qi and S.-C. Zhang, "Topological insulators and superconductors," *Reviews of Modern Physics*, vol. 83, no. 4, p. 1057, 2011.

[39] A. Altland and M. R. Zirnbauer, "Nonstandard symmetry classes in mesoscopic normal-superconducting hybrid structures," *Phys. Rev. B*, vol. 55, no. 1142, 1997.

[40] C. W. J. Beenakker, "Random-matrix theory of majorana fermions and topological superconductors," *Rev. Mod. Phys.*, vol. 87, no. 1037, 2015.

[41] J. J. M. Verbaarschot and I. Zahed, "Spectral density of the qcd dirac operator near zero virtuality," *Phys. Rev. Lett.*, vol. 70, no. 3852, 1993.

[42] J. J. M. Verbaarschot and T. Wettig, "Random matrix theory and chiral symmetry in qcd," *Ann. Rev. Nucl. Part. Sci.*, vol. 50, no. 343, 2000.

[43] M. R. Zirnbauer, *Symmetry classes.* Oxford University Press, 2011.

[44] S. Ryu, A. P. Schnyder, A. Furusaki, and A. W. W. Ludwig, "Topological insulators and superconductors: Ten-fold way and dimensional hierarchy," *New J. Phys.*, vol. 12, no. 065010, 2010.

[45] J. C. Y. Teo and C. L. Kane, "Topological defects and gapless modes in insulators and superconductors," *Phys. Rev. B*, vol. 82, no. 115120, 2010.

[46] C.-K. Chiu, J. C. Teo, A. P. Schnyder, and S. Ryu, "Classification of topological quantum matter with symmetries," *Reviews of Modern Physics*, vol. 88, no. 3, p. 035005, 2016.

[47] L. Lu, C. Fang, L. Fu, S. G. Johnson, J. D. Joannopoulos, and M. M. Soljačić, "Symmetry-protected topological photonic crystal in three dimensions," *Nat. Phys.*, vol. 12, no. 337, 2016.

[48] W. P. Su, J. R. Schrieffer, and A. J. Heeger, "Solitons in polyacetylene," *Phys. Rev. Lett.*, vol. 42, no. 1698, 1979.

[49] S. Ryu and Y. Hatsugai, "Topological origin of zero-energy edge states in particle-hole symmetric systems," *Phys. Rev. Lett.*, vol. 89, no. 077002, 2002.

[50] M. J. Rice and E. J. Mele, "Elementary excitations of a linearly conjugated diatomic polymer," *Phys. Rev. Lett.*, vol. 49, no. 1455, 1982.

[51] J. Attig and S. Trebst, "Classical spin spirals in frustrated magnets from free-fermion band topology," *Physical Review B*, vol. 96, no. 8, p. 085145, 2017.

[52] E. S. G. Naz, I. C. Fulga, L. Ma, O. G. Schmidt, and J. v. d. Brink, "Topological phase transition in a stretchable photonic crystal," *arXiv preprint arXiv:1712.01678*, 2017.

[53] M. Kremer, I. Petrides, E. Meyer, M. Heinrich, O. Zilberberg, and A. Szameit, "Non-quantized square-root topological insulators: a realization in photonic aharonov-bohm cages," *arXiv preprint arXiv:1805.05209*, 2018.

[54] Y.-L. Zhang, R. P. Wu, A. Kumar, T. Si, and K. H. Fung, "Nonsymmorphic symmetry-protected topological modes in plasmonic nanoribbon lattices," *Physical Review B*, vol. 97, no. 14, p. 144203, 2018.

[55] C. W. Duncan, P. Öhberg, and M. Valiente, "Exact edge, bulk, and bound states of finite topological systems," *Physical Review B*, vol. 97, no. 19, p. 195439, 2018.

[56] E. Makri, R. Thomas, and T. Kottos, "Reflective limiters based on self-induced violation of c t symmetry," *Physical Review A*, vol. 97, no. 4, p. 043864, 2018.

[57] B. Midya, W. Walasik, N. M. Litchinitser, and L. Feng, "Supercharge optical arrays," *arXiv preprint arXiv:1809.05756*, 2018.

[58] Z. Zhang, M. Teimourpour, J. Arkinstall, M. Pan, P. Miao, H. Schomerus, R. El-Ganainy, and L. Feng, "Edge-state dynamics in a one-dimensional topological photonic lattice of multiple quantum numbers," in *CLEO: QELS_Fundamental Science*, pp. FM3Q–1, Optical Society of America, 2018.

[59] Z. Zhang, M. H. Teimourpour, J. Arkinstall, M. Pan, P. Miao, H. Schomerus, R. El-Ganainy, and L. Feng, "Experimental realization of multiple topological edge states in a 1d photonic lattice," *Laser & Photonics Reviews*, vol. 13, no. 2, p. 1800202, 2019.

[60] C.-X. Liu, R.-X. Zhang, and B. K. VanLeeuwen, "Topological nonsymmorphic crystalline insulators," *Physical Review B*, vol. 90, no. 8, p. 085304, 2014.

[61] J. Zak, "Berry's phase for energy bands in solids," *Phys. Rev. Lett.*, vol. 62, no. 2747, 1989.

[62] M. V. Berry, "Quantal phase factors accompanying adiabatic changes," *Proceedings of the Royal Society of London A: Mathematical, Physical and Engineering Sciences*, vol. 392, no. 1802, pp. 45–57, 1984.

[63] D. Meidan, T. Micklitz, and P. W. Brouwer, "Topological classification of adiabatic processes," *Physical Review B*, vol. 84, no. 19, p. 195410, 2011.

[64] I. C. Fulga, F. Hassler, and A. R. Akhmerov, "Scattering theory of topological insulators and superconductors," *Phys. Rev. B*, vol. 85, no. 165409, 2012.

[65] M. Xiao, Z.-Q. Zhang, and C.-T. Chan, "Surface impedance and bulk band geometric phases in one-dimensional systems," *Phys. Rev. X*, vol. 4, no. 021017, 2014.

[66] A. V. Poshakinskiy, A. N. Poddubny, and M. Hafezi, "Phase spectroscopy of topological invariants in photonic crystals," *Phys. Rev. A*, vol. 91, no. 043830, 2015.

[67] X. Shi, C. Xue, H. Jiang, and H. Chen, "Topological description for gaps of one-dimensional symmetric all-dielectric photonic crystals," *Opt. Express*, vol. 24, no. 18580, 2016.

[68] E. Witten, "Constraints on supersymmetry breaking," *Nucl. Phys. B*, vol. 202, no. 253, 1982.

[69] A. J. Niemi and G. W. Semenoff, "Fermion number fractionization in quantum field theory," *Phys. Rep.*, vol. 135, no. 100, 1986.

[70] D. Bollé, F. Gesztesy, H. Grosse, W. Schweiger, and B. Simon, "Witten index, axial anomaly, and krein's spectral shift function in supersymmetric quantum mechanics," *J. Math. Phys.*, vol. 28, no. 1512, 1987.

[71] N. Borisov, W. Müller, and R. Schrader, "Relative index theorems and supersymmetric scattering theory," *Communications in mathematical physics*, vol. 114, no. 3, pp. 475–513, 1988.

[72] C. A. A. de Carvalho and H. M. Nussenzveig, "Time delay," *Phys. Rep.*, vol. 364, no. 83, 2002.

[73] O. Viyuela, A. Rivas, and M. Martin-Delgado, "Symmetry-protected topological phases at finite temperature," *2D Materials*, vol. 2, no. 3, p. 034006, 2015.

[74] F. Cardano, A. D'Errico, A. Dauphin, M. Maffei, B. Piccirillo, C. de Lisio, G. De Filippis, V. Cataudella, E. Santamato, L. Marrucci, *et al.*, "Detection of zak phases and topological invariants in a chiral quantum walk of twisted photons," *Nature communications*, vol. 8, p. 15516, 2017.